Wayne State University Dissertations

1-1-2017

Actuation Of Droplets Using Transparent Graphene Electrodes For Tunable Lenses And Biomedical Applications

Ali Shahini
Wayne State University,

ACTUATION OF DROPLETS USING TRANSPARENT GRAPHENE ELECTRODES FOR TUNABLE LENSES AND BIOMEDICAL APPLICATIONS

by

ALI SHAHINI

DISSERTATION

Submitted to the Graduate School

of Wayne State University,

Detroit, Michigan

in partial fulfillment of the requirements

for the degree of

DOCTOR OF PHILOSOPHY

2016

MAJOR: ELECTRICAL ENGINEERING

Approved By:

_____
Advisor   Date

_____

_____

DEDICATION

To my family

ACKNOWLEDGMENTS

Firstly, I would like to express my sincere gratitude to my advisor, Professor Mark Cheng, who was always supportive and taught me a lot during my Ph.D Program. He gave me the opportunity to work with him in his highly equipped laboratories where I could implement science into application. I was always inspired by his hard work, deep knowledge, motivations and the time that he dedicated to his students. I really appreciate all the time he spent with me during this program and all the constructive advices. Professor Cheng gave me freedom to choose my direction in my research while encouraging me to grow as a scientist. He provided almost everything that I needed in my research and I was really lucky that I did my Ph.D under his supervision. He has been a tremendous mentor for me.

Besides my advisor, I would like to thank the rest of my committee: Professor Yong Xu, Professor Amar Basu and Professor Zhixian Zhou for their support and constructive advices during this program. Dr. Xu and his lab members, especially Dr. Eric Kim, were always helpful by sharing knowledge, experiences and some resources in microfabrication. Dr. Basu and his former Ph.D candidate, Dr. Razieh Kebriaei, whom were helpful in COMSOL simulation and sharing equipment that were substantial in my research progress. Dr. Zhou and his former Ph.D candidate, Dr. Hsun-Jen Chuang whom were helping me in some of my experiments especially using semiconductor parameter analyzer system.

In addition, I would like to thank Dr. Yang Zhao and Dr. Pai-Yen Chen for all the help and company that I received from them. Dr. Zhao always gave me great suggestions

TABLE OF CONTENTS

LIST OF TABLES

LIST OF FIGURES

CHAPTER 1 REVIEW OF EWOD AND OPTICAL LENSES

1.1 EWOD background and literature review

1.1.1 Droplet actuation from Electrocapillarity to EWOD

The physical properties of the materials can be changed using applied electrical field since Gabriel Lippmann has demonstrated electrocapillary effect experiment for the first time [1]. Researchers have developed techniques that use this effect to manipulate small droplet at microscale [2, 3] for applications such as optical displays [4, 5], electrical switches [6], optical lenses [7] and etc. This techniques have been developed in last decades thanks to Micro-electromechanical systems (MEMS) method for fabrication of sub-millimeter devices.

Electrowetting which is based on electrocapillary can describe the droplet actuation by application of an electric field which spreads the droplet on top of a solid surface [3, 8]. Researchers have used Lippmann's demonstrated capillary action to alter the curvature of a meniscus between a liquid metal and an electrolyte using electric field [9]. Before the term electrowetting become common, electrocapillary was used to describe electrowetting [10].

1.1.1.1 Electrowetting equation

In order to obtain the electrowetting equation, interfacial energy concept of electrocapillarity can be used. The interfacial energy between solid-liquid interface decreases by application of an electric field which accumulate charges at Electrical Double Layer (EDL). Thus, the electrical energy added to the system $(C_H \frac{V^2}{2})$ can be observed in apparent reduction of contact angle of the droplet due to decrease in

interfacial tension between solid and liquid. The electrowetting equation can be driven by thermodynamic principle of Gibbs free energy as follow [11]:

$$C_H = \frac{\partial \rho s}{\partial V} \qquad 1.1$$

Where C_H represents the Helmholtz capacitance per unit area of solid-liquid interface and the density of charge at the solid-liquid interface, ρs is defined as:

$$-\rho s = \frac{\partial \gamma}{\partial V}|\mu \qquad 1.2$$

Where γ is the interfacial energy (tension), V the applied potential and μ chemical potential.

$$\gamma_{sl}(V) = \gamma_{sl}(0) - \frac{C_H V^2}{2} \qquad 1.3$$

Young equation: $\gamma cos\theta = \gamma_{sf} - \gamma_{sl}$ \qquad 1.4

Where γ_{sf} is the solid-fluid interfacial energy and γ_{sl} is the solid-liquid interfacial energy. Finally, the electrowetting equation can be obtained.

$$Cos\theta = Cos\theta_0 + \frac{C_H V^2}{2\gamma} \qquad 1.5$$

In order to obtain equation 1.3 (voltage dependent interfacial tension), the equation 1.2 is integrated using a constant number for equation 1.1. Then, young equation is combined with this equation to obtain electrowetting equation. Electrowetting equation can also be used to drive an equation for EWOD by replacing the Helmholtz capacitance with insulator layer capacitance and V with an external applied voltage [12, 13]. In EWOD equation the EDL capacitor can be ignored compare to the insulator capacitor. The electrowetting can be divided into three concepts, direct electrowetting, continuous electrowetting and electrowetting on dielectric [14]. When electrowetting occurs between

an electrolyte and a solid surface the term is direct electrowetting. The continuous electrowetting is realized when the electrowetting occurs at the interface of two conducting liquids. In electrowetting, the direct contact between electrolyte and the electrode cause electrolysis and bubble formation that can degrade the electrodes. Electrowetting on dielectric is realized when a thin insulator is applied on the electrode to prevent electrolysis.

1.1.1.2 Electrowetting on Dielectric (EWOD)

Electrowetting on dielectric is a special configuration of electrowetting in which a thin dielectric layer is used between the liquid and the electrodes [5, 12, 15]. Despite electrowetting in which a high voltage (e.g., 100 volts in early days [16] and 15-20 volts in present days) is needed for droplet actuation, EWOD force is high enough even at voltages around 2 V to move the droplet. One important issue in traditional direct electrowetting on conductor is electrolysis that occur in low voltages which degrade the electrodes. The thin dielectric layer in EWOD acts as guard to prevent electrolysis and allows much higher electric field before breakdown (figure 3 at [13]). Also, in EWOD a thin hydrophobic layer can be applied on top of the insulator to improve the droplet movement and decrease the contact angle hysteresis. Researchers have used different combination of liquid-medium such as water in oil [17], water in air [18], oil in air [18] and etc, due to these attributes.

The physical properties and also the thickness of the insulating layer play an important role in EWOD due to large voltage drop on this layer. In order to understand the EWOD phenomenon in more depth, several key points should be considered:

- Although the droplet in common EWOD devices (figure 1.1a) is electrically neutral during actuation due to insulating layer that separate it from the electrodes, the surface in contact with solid acquire a net charge [19]. In contrast, the sessile droplet which is in direct contact with the electrode in common spreading EWOD devices (figure 1.1b) acquire a net charge [11].

- Application of a voltage generates an electric field in the droplet that depends on the frequency of the voltage. So the electric field distribution changes at different frequency in the droplet where at high frequency this internal field is high and mostly distributed along the liquid-fluid interface and at low frequency the low electric field is localized to the contact line.

- There is a resistance force in EWOD devices that prevent the droplet from actuation. Thus, a minimum voltage (minimum force) is always required for droplet actuation which depends on this resistance force that has been thought as a static friction. One way to increase the minimum EWOD force or to decrease the resistance force is to use a solid surface with low energy such as Teflon or Cytop that can reduce the contact angle hysteresis.

- Dielectric charging, leakage current and satellite droplet ejection are some dissipation mechanism that limits the electrowetting force and are not fully understood yet.
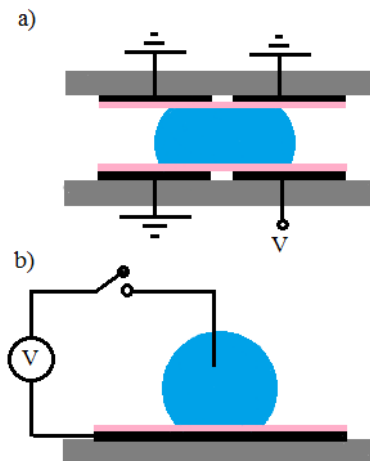
Figure 1.1 Schematic of (a) common EWOD device without contact between droplet and electrode, (b) EWOD with direct contact between droplet and electrode.

1.1.2 Basic physics of EWOD

1.1.2.1 Theoretical background

A droplet in microscale will form a spherical shape on a solid surface due to intermolecular force between the molecules of the droplet. For the molecules within a droplet, the net intermolecular force is zero due to equal force in all direction. But the story is different for the molecules close to the surface of a droplet where there is no molecule on top of them and they are attracted just by the inner neighbor molecules and the net charge is not zero. The intermolecular force between molecules close to the surface of a droplet generates surface tension. Surface tension can be described as amount of energy that is required to enlarge a surface by one surface unit and is measured as energy per unit area. From surface tension point of view, wetting can be described as ability of a liquid in contact with solid to maintain the contact line due to intermolecular interactions and the force balance between cohesive and adhesive forces [20].

The contact angle between a droplet on top of an ideal solid has demonstrated for the first time by young at 1805 [21]. In microscale the behavior of a droplet can be described by surface tension. T. Young demonstrated that the mechanical equilibrium of a droplet under action of three surface energy defines the contact angle of the droplet on top of solid as:

$$\gamma_{lv}cos\theta = \gamma_{sv} - \gamma_{sl} \qquad\qquad 1.6$$
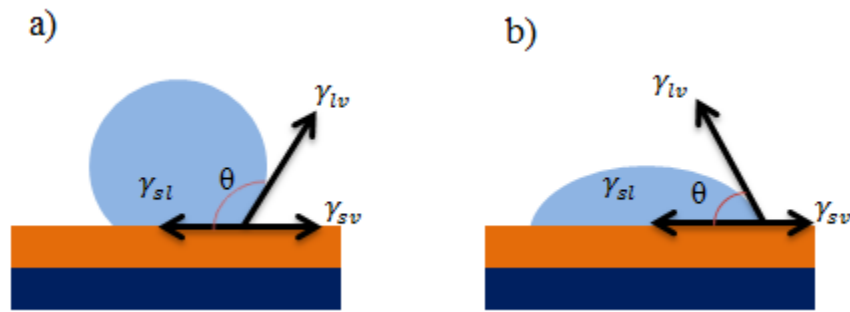
Figure 1.2 Contact angle of a droplet on a (a) hydrophobic surface (large contact angle), (b) Hydrophilic surface (small contact angle).

where γ_{lv}, γ_{sv} and γ_{sl} represent the liquid-vapor, solid-vapor and solid-liquid interfacial tension, respectively (figure 1.2). According to young's equation, a surface is completely wet when the contact angle is zero. As it is mentioned before, G. Lippmann was first demonstrated the relation between physical and electrical parameters in electrowetting phenomenon [1]. The principle of Lippmann's theory is based on electrocapillarity that is demonstrated in his experiment. The electrowetting effect has described for the first time by Beni and Hackwood at 1981 [3]. They demonstrated a system consists of a conducting solid, an electrolyte liquid and a fluid. They observed that the contact angle of the liquid on the solid surface could be changed by applying voltage. The term electrowetting was

illustrated for the first time after this experiment and they also emphasized that this is similar to but distinct from electrocapillary, figure 1.3 [22]. In both electrocapillay and electrowetting, electrolysis occurs at low voltages due to chemical reaction between electrode and electrolyte which cause an irreversible change. This irreversible change limits the systems in wide range of application.
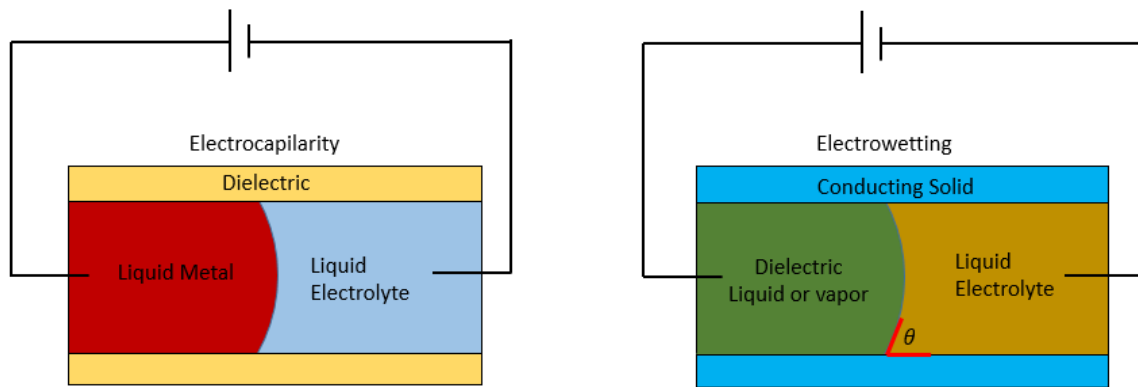
Figure 1.3 Electrocapillarity and electrowetting configuration.

The EWOD was born in 1993 when Berg added a thin layer of dielectric material to solve the electrolysis problem [23]. A general configuration of an EWOD system consists of a substrate with electrode on top which is covered with a thin dielectric material and a sessile droplet that is mounted on top of the insulator layer (figure 1.4). Application of a voltage between the conducting liquid (through an electric probe) and the electrode will accumulate the charges at the solid-liquid interface that generate electromechanical force to pull the droplet to its further wetting. In other words, the hydrophobic surface become hydrophilic and the contact angle at the solid-liquid interface decrease from its highest value (Young's angle, figure 1.4a) to smaller angle (figure 1.4b). Thus, a reversible EWOD can be achieved upon removal of voltage and the contact angle goes to its initial

value. In order to analyze behavior of a droplet the ratio between gravity and surface tension which considered as a bond number β is always considered.

$$\beta = \frac{\Delta\rho g R^2}{\gamma_{li}} \qquad\qquad 1.7$$

In this equation $\Delta\rho$ is the density difference between droplet and the surrounding media, g corresponds to gravitational acceleration, R is the characteristic length of the droplet and γ_{li} represents the interfacial tension between liquid and insulator. The surface tension dominates gravity in EWOD system under typical conditions and so, the bond number is less than unity [1]. In the absence of electric field (figure 1.4a) the contact angle of a droplet in contact with solid can be determined by young's equation (equation 1.6). When a voltage is applied (figure 1.4b) the charges will accumulate in liquid-insulator interface. The force per unit length far away from the surface of the droplet in droplet-insulator interface is vertical which is compensated by elastic stress.

However, edge effect introduces the surface charges at the three phase contact line which create additional horizontal electrostatic force (per unit length).

$$F = \frac{\varepsilon_0 \varepsilon_r V^2}{2d} \qquad\qquad 1.8$$

In this equation ε_0, ε_r, V and d correspond to permittivity of vacuum, relative permittivity of dielectric material, applied voltage and dielectric thickness, respectively.

Young equation can be rewritten by projecting the force balances onto horizontal line:

$$\gamma_{lv}cos\theta_V + \gamma_{ld} = \gamma_{vd} + F \qquad\qquad 1.9$$

Where γ_{lv} corresponds liquid-vapor interfacial tension, γ_{ld} represents liquid-dielectric interfacial tension, θ_V is the electrowetted angle and γ_{vd} is vapor-dielectric interfacial

tension. Finally by combining equation 1.6, 1.8 and 1.9 The Young-Lippmann equation that describes the electrowetting system can be achieved.

$$cos\theta_V = cos\theta + \frac{\varepsilon_0 \varepsilon_r V^2}{2d\gamma_{lv}} \qquad\qquad 1.10$$
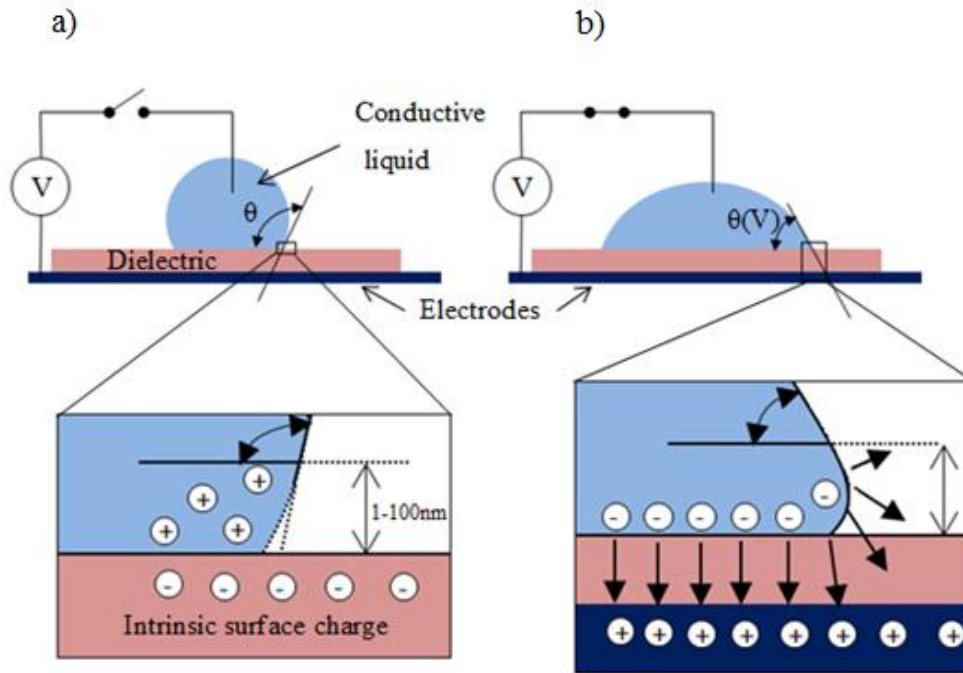
Figure 1.4 EWOD configurations (a) with no voltage, (b) with applied voltage.

1.1.2.2 Reversibility issues of contact angle

The surface property of a solid defines the shape of a droplet on top of it. The term contact angle refers to the angle of a droplet on a solid surface at the three phase contact line. The contact angle that measures the surface wettability is called static contact angle and the dynamic contact angle is used for contact line in motion. The Young equation can be used to determine the static contact angle. In EWOD system, contact angle changes by applying voltage between the droplet and electrodes.

According to Young-Lippmann's equation, one can assume that a complete wetting (zero contact angle) is possible when the voltage is increased. However, the EWOD experiments show no complete wetting even at high voltages. In EWOD experiments, the contact angle decreases by increasing the voltage to a certain value and then it doesn't change by further increasing the voltage and it saturate. The contact angle saturation phenomenon has not been investigated exactly and it has puzzled researchers [24]. Researchers have explained this phenomenon by several hypothesis such as dielectric charging (figure 1.5a), insulating fluid charging (figure 1.5b), micro droplet ejection (figure 1.5c), zero interfacial tension and so on [25]. Mugele et al has summarized several theories that explain contact angle saturation [26]. Verheijen and Prins reported that dielectric charging (charge trapping) occur after contact angle saturation [27]. They assumed that the charges trap in the dielectric layer that screen a part of electric field and keep the surface wet after removing the voltage. Vallet et al suggested that the contact angle saturation could be due to the ionization of air at the contact line [28]. Although several theories are trying to explain contact angle saturation but there are still debates about the exact phenomenon.
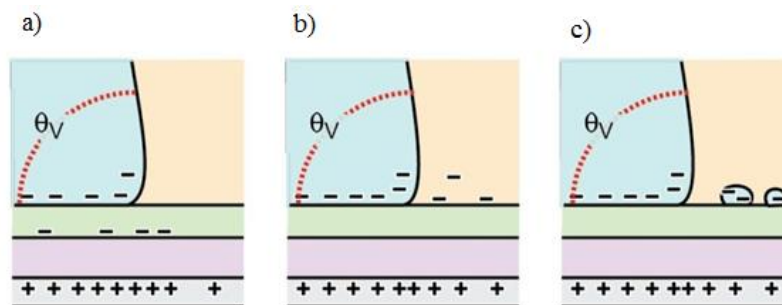
Figure 1.5 Contact angle saturation due to (a) dielectric charging, (b) fluid charging an (c) microdroplet ejection [22].

1.1.3 Applications of EWOD

Electrowetting or EWOD is an indispensable and easy way to manipulate a droplet. Due to easy fabrication process and wide range of application such as Lab-on-a-chip devices [29, 30], tunable lenses [31] and display technology [4], EWOD is being developed very fast.

1.1.3.1 Lab-on-a-chip

EWOD phenomenon was mainly exploited for Lab-on-a-chip applications by Richard Fair at Duke University and Kim at UCLA [30, 32]. An array of electrodes with a sequence design which allow the droplet to move in appropriate pass is the main idea for this application. The small droplets can be moved and combined together or extracted for different chemical reactions [29, 33]. In a common EWOD system a wire need to be inserted in the drop which is not practical in lab-on-a-chip application. Therefore, two parallel electrodes design that sandwiches the droplet is a necessary design that can solve this problem (figure 1.6). The size of the electrodes determines the smallest size of the droplet that needs to overlap on adjacent electrode to have reliable movement. Berge and Peseux have reported a zigzag design to improve the reliability of the droplet movement [17]. Furthermore, the droplet evaporation is prevented using oil environment in EWOD lab-on-a-chip devices [28].
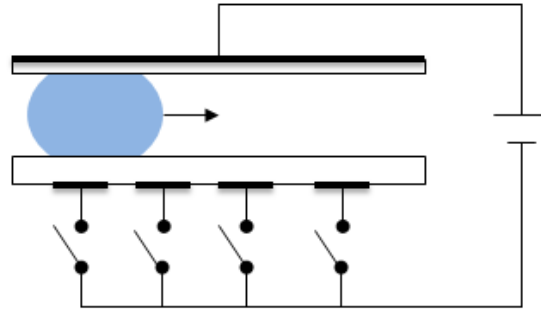
Figure 1.6 EWOD configuration with two parallel electrodes for lab-on-a-chip application.

Biological application of EWOD devices is the next step after establishing the basic manipulation techniques, which needs biocompatible materials and techniques. Hydrophobic surface in EWOD devices adsorb the biomolecules that makes the device irreversible [34]. Yoon and Garrell have used DNA and protein solution in EWOD devices with air fluid and they found that the adsorption of the molecules to the surface is due to both electrostatic and hydrophobic interactions [35]. Adsorption of biomolecules can be suppressed by using oil as surrounding medium which is due to thin oil that prevent the molecule from direct contact to the hydrophobic surface [32].

Another application of EWOD in terms of biotechnology is handling a small amount of droplet. Conventional technique to produce array of DNA or protein solution was photolithography and the more recent technique is the inkjet technique. Dip-pen nanolithography is a new technique to produce a tiny spot size around 1 μm [36]. Blaubre et al have demonstrated an electrowetting based dip-pen nanolithography design to better control of the amount of the liquid in the pen reservoir [37].

EWOD has also been used to control the flow in channel of a microfluidic device with two phase flow by activating the electrodes that control the pass of flow [38]. An EWOD-actuated micro-valve has been designed inside a microchannel by Cheng and Hsiung to control the flow [39]. The channel is coated with Teflon to provide a hydrophobic barrier that moves by activating the electrodes embedded in the active area.

1.1.3.2 Optical applications

1.1.3.2.1 Liquid lenses

The focal length of a liquid lens can be tuned by changing the curvature that changes the shape of the droplet. Tunable focal length lenses have wide range of application in camera, Medical instruments and consumer electronics. The tunability of liquid lenses can be achieved by changing the contact angle of the droplet on a solid surface using EWOD phenomenon. Peseux and Berge have demonstrated an electrowetting-driven liquid lens with variable focal length for the first time [9]. They have designed a chamber with two immiscible liquid, an oil inside a salt solution. They have matched the density of the two liquid to reduce the effect of gravity. In order to center the droplet in optical axis a dielectric layer with variable thickness has been designed (figure 1.7). Application of a voltage changes the shape of a droplet resulting to focal length change. A similar system with patterned electrodes has been reported by krupenkin et al with low activation voltage around 10 V [40]. Another configuration of EWOD lens has been introduced at [41] with ring electrodes and water droplet that works at low voltages around 40 V. Figure 1.8 shows the focusing ability of this lens that can be shifted from 2.5 cm to infinity. Polymers can also be used for liquid lenses. Im et al have fabricated an array of

lenses based on EWOD using PDMS with Parylens as dielectric layer and a thin Teflon layer as a hydrophobic surface [42]. Figure 1.9 Show their lens array with embedded electrode in which the contact angle reduces to 63° at 250 V.
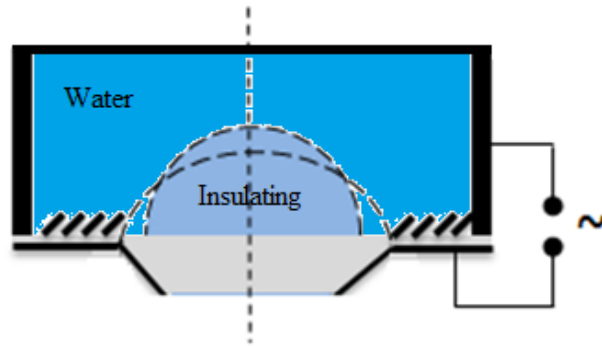
Figure 1.7 Liquid lens with two immiscible liquids and variable dielectric thickness.
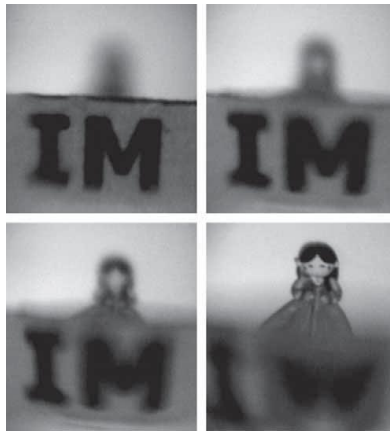
Figure 1.8 Focusing ability of an EWOD lens at different voltages [41].
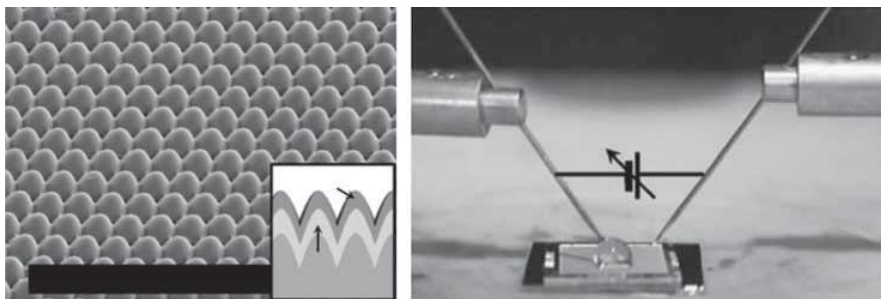
Figure 1.9 SEM image of a polymer microlens array [42].

1.1.3.2.2 Display technology

Display devices are output devices that present the information in visual or tactile form. These devices have been developed in recent years on flexible substrate due to several parameters such as light weight, low cost, easy processing, mechanical flexibility and etc. An EWOD-based reflective display system has been reported by Feenstra and Hayes that can be used in electronic paper [4]. Their system consists of a transparent electrode coated by hydrophobic layer on a white substrate with oil droplet containing dissolved dye, figure 1.10. At zero voltage, the oil droplet which is covered by a salt solution wets the whole hydrophobic pixel and the incoming light will strongly absorbed by dye. Application of a voltage contracts the oil droplet to a specified predefined patterned area at the corner of the pixel. At this step the dye is confined in a small part of the pixel that increases the reflectivity from 2.5% at zero volt to 35% at 20 volts. The thickness and viscosity of oil and also the pixel size and some other geometric parameters define the reversibility switching speed of a display device [43]. Feenstra and Hayes have also designed a color display that generate arbitrary colors by splitting each pixel into three subpixels [4]. They have used color filter on top of two oil layers with different dyes and they demonstrated that the reflectivity of this system is four times stronger than liquid crystal displays. An EWOD display fabricated on a flexible substrate consist of polymers, paper and metal have been demonstrated by You and Steckl [44]. They have designed an array of droplet on a flexible plastic substrate that is able to switch reversibility using EWOD phenomenon (figure 1.11). Their device is operational even on

mechanical bending which is promising for future flexible EWOD on mobile and other devices.
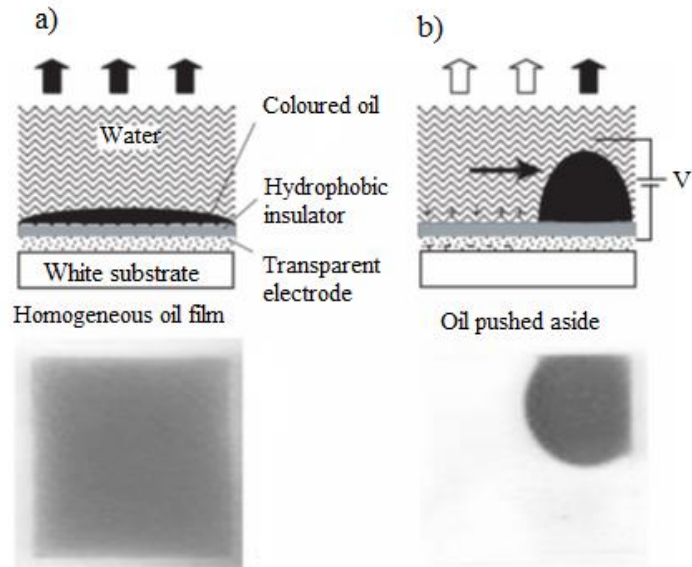
Figure 1.10 Diagram and photograph of an electrowetting display with (a) no voltage applied and (b) DC voltage applied [4].
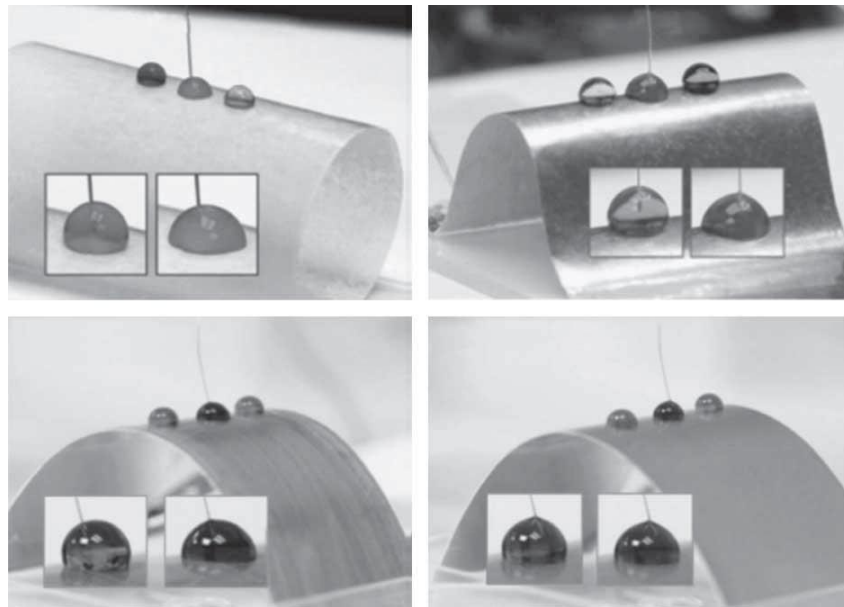
Figure 1.11 EWOD display on flexible substrate with an array of droplets [44].

1.2 Optical lenses and their actuation mechanism

1.2.1 Lens

A lens is an optical instrument that can be used to focus on objects at different distances. The most common lenses are made of glass which transmit the light and refract it based on its refractive index. The transmitted light can be diverged or converged depend on the lens geometry. Since the surface of glass is not elastic, it's not easy to change the curvature of the glass lens to get different focal length. One type of matter that can transmit the light and has elastic surface is liquid which can be an excellent candidate to replace glass. A drop of liquid with definite volume but no fixed shape can be manipulated to function as a lens. Surface tension can define the shape of the elastic membrane of a droplet to create contact angle. Contact angle is the angle between droplet and the solid surface at the three phase contact line which can be controlled by surface tension. This property of liquid can be utilized to make a lens with tunable focal length.

Variable focal length liquid microlenses are the next candidate for a wide variety of applications. Optical lenses with tunable focal length and wide field of view without moving parts are essential components for the next generation consumer products such as mobile phones, security cameras, surveillance systems, optical diagnostic devices, vertical scanners, and optical data storage devices [45-47]. These lenses can also be used to correct some eye diseases like presbyopia in which eye is not able to adjust the focal length or disorder of the eye [48].

Driving mechanism of the liquid lenses can be categorized into mechanical and electrical actuation. Many optical systems allow the focus and magnification to be

mechanically adjustable. The focusing mechanisms of conventional optical systems with lenses and mirrors as optical elements with fixed focal length is complicated due to using many moving parts such as motors, sliders and gears [49, 50].

1.2.2 Microlenses

Micro-electromechanical systems (MEMS) represent a technology of very small size that connects electrical and mechanical systems to create new devices. There has been a lot of progress in MEMS technology and numerous micro scale devices have been developed in recent years. Liquid lenses are one of the recent components in MEMS area that attract a lot of researcher's attention. A microlens can be defined as a very small-sized lens with a diameter ranging from several microns to less than a millimeter. Depending on the aperture of a microlens, it can be either a single lens with one aperture or a microlens array with multiple apertures (figure 1.12) [51, 52].
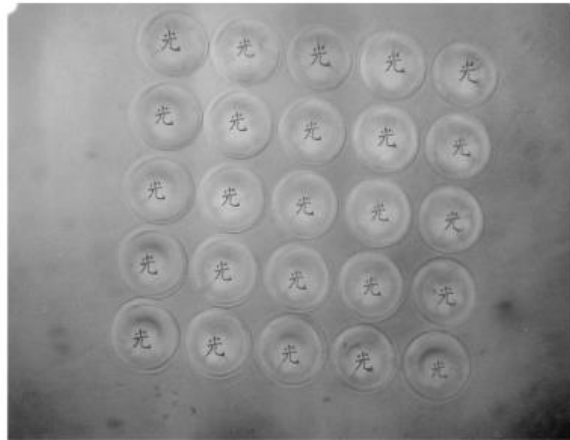
Figure 1.12 An array of microlenses [51].

Imaging and optical guiding are two important function of a lens in microsystem. Optical signals can be intensified using microlenses in optical imaging systems. On the

other hands, light beam splitting [53] and optical switching [54, 55] can be facilitated by application of a microlens in optical guiding. Based on focal length microlenses can be generally either fixed focal length or tunable focal length.

1.2.2.1 Fixed focal length microlens

In microlenses with fixed focal length, lens has a fixed aperture with single angular field of view. Researcher have been reported various fixed focal length microlens [56, 57] and array of microlenses [58, 59] for optical application in microsystems. The microlens array can be made by using some polymers or photoresist. The lens shape in these lenses can be achieved after some fabrication process and reflow of polymers through the microchannel [60]. Fixed focal length lenses are being used to guide some signals or light in optical communication. The fabrication process for these lenses is easy with low cost due to their simple structure.

1.2.2.2 Variable focal liquid lenses

In most conventional lenses the variation of the focal length could be obtained by displacement of components which is problematic in terms of fabrication, integration cost and etc. One solution to this problem is to miniaturize these optical systems. however, miniaturization has its own issues such as microfabrication and the manipulation of small elements [31]. Furthermore, downscaled moving and actuating parts are not easy to determine since scaling effect of forces such as mechanical friction [61] is more significant in microscale domain. Recently, human eye has inspired researchers to think about changing shape instead of mechanical displacement to get variable focal length.

1.2.2.2.1 Tunability with lens liquid

One way to change the focal length of an optical lens is to manipulate the refractive index of the liquid. The refractive index of a liquid can be adjusted by applying some forces such as acoustic, electric and temperature field or mechanical strain [62]. Microfluidic techniques enable control of lens liquid injection and adjusting of the fluid composition [63]. Table 1.1 compares the different tuning techniques and their relative refractive index change [62]. According to this table, micro-optofluidic tuning can give us the largest change in refractive index with slow microfluidic manipulation.

Table 1.1 Comparison between optofluidic tuning and other optical tuning techniques. $O(\Delta n/n)$: order of magnitude of the relative changes in refractive index n, $O(\tau)$ order of magnitude of time response [62].

Tuning techniques	$O(\Delta n/n)$	$O(\tau)$ s
Optofluidics	1	10^{-3}
Liquid crystal	10^{-1}	10^{-3}
Injection current	10^{-2}	10^{-9}
Temperature	10^{-2}	1
Photorefractive	10^{-3}	$10^{-1} - 10^{-5}$
Electro-optic (10 kV/cm)	10^{-3}	10^{-12}
Photoelastic/acusto-optic (10 W)	10^{-4}	$10^{-6} - 10^{-7}$

Some common liquids that can be used in micro-optofluidic are summarized in table 1.2. The refractive index of PDMS can be used as the reference to find the right liquid for lens due to large application of PDMS in microfluidic devices. The refractive index matching plays an important role in minimization of scattering effect in solid/liquid

interface. It is desirable to use liquid with lower refractive index than PDMS such as
water to design a liquid lens due to less health hazards. Other properties of a liquid as an
optical material such as diffusion of species, concentration distribution, mixture of liquids
and etc can also be manipulated to get tunability [64].

Table 1.2 Common liquids in micro-optofluidic. N: refractive index, μ: dynamic viscosity, ρ: density, σ surface tension, CAS: chemical abstract service, (parameters are at 25 °C, 100 kPa) [64].

Liquid	CAS code	n	μ (mPa s)	ρ (kg/m3)	σ (mN/m)
Trifluoroethanol	75-89-8	1.291	1.24	1382	20
DI-water	7732-18-5	1.33	0.89	997	73
Isopropanol	67-63-5	1.33	1.96	786	23
Methanol	67-561	1.33	0.59	787	23
Ethanol	64-17-5	1.36	1.04	789	22
Silicone oil	63148-62-9	1.375-1.405	0.494-976	760-976	16-22
Cured PDMS	-	1.412	-	-	-
73.5% ethylene glycerol, 26.5% ethanol	-	1.412	9.80	915	33
60% gelycerol, 40% water	-	1.412	8.99	1151	56
Ethylen glycon	107-21-1	1.43	16.1	960	47.3
5 M CaCl2 solution	-	1.44-1.46	9.00	1396	-
Benzyl alcohol	100-51-6	1.54	8.00	1044	39
Cinnamaldehyde	104-55-2	1.62	5.70	1050	36
Benzothiazole	95-16-9	1.64	-	1272	54

1.2.2.2.2 Tunability with lens shape

Solid lenses based on glass or crystal substrate have been developed more than 2000 years ago. These lenses can be used in variety applications such as microscopes, cameras, telescopes and etc. However, the development of devices that can be operational in consumer products are needed not only in handheld cameras but also in cell phones and laptops and so on. Miniaturization of the solid lenses with moving parts will limit the performance and complicate the fabrication process. Liquid lenses with tunable focal length have been demonstrated by getting advantage of the interface between two immiscible liquids with different refractive indices. These liquid lenses are highly adaptive and scalable. Several parameters are important in liquid lens performance such as the materials, the volume of the droplet, device structure, surface morphology, actuation mechanism and etc. Here we review two main actuation mechanism including mechanical manipulation and electrical manipulation [65].

1.2.2.2.2.1 Mechanical manipulation

The shape of the droplet and also the pressure inside a droplet can be determined by the volume of the liquid and the liquid chamber design. In order to fabricate a liquid lens, the controllable shape of the liquid, the structure of the container and the material properties which define the optical performance of the lens should be carefully considered. Mechanical manipulation can be performed to adjust the shape and the volume of the droplet. The focal length of a lens can be tuned by changing the design of the liquid chamber, manipulation of the droplet size and the aperture size. Flexible membrane and moving parts are the necessary requirements in mechanical manipulation

of a droplet. Jeong et al reported a tunable lens that can be tuned either by changing the shape of the liquid filled lens or changing the refractive index of filling media [66]. The device structure consists of an elastomeric membrane on top of a container and several microchannels to control the amount of liquid filling the cavity as shown in figure 1.13. Polydimethylsiloxane (PDMS) has been used for fabrication of the microchannel and the cavity. The lens curvature is dynamically modulated by deflecting the PDMS membrane using the pneumatic control via microchannel. Pumping liquid in or out will deflect the membrane as a bio-convex lens or meniscus. Filling cavity with different refractive index can change the focal length.
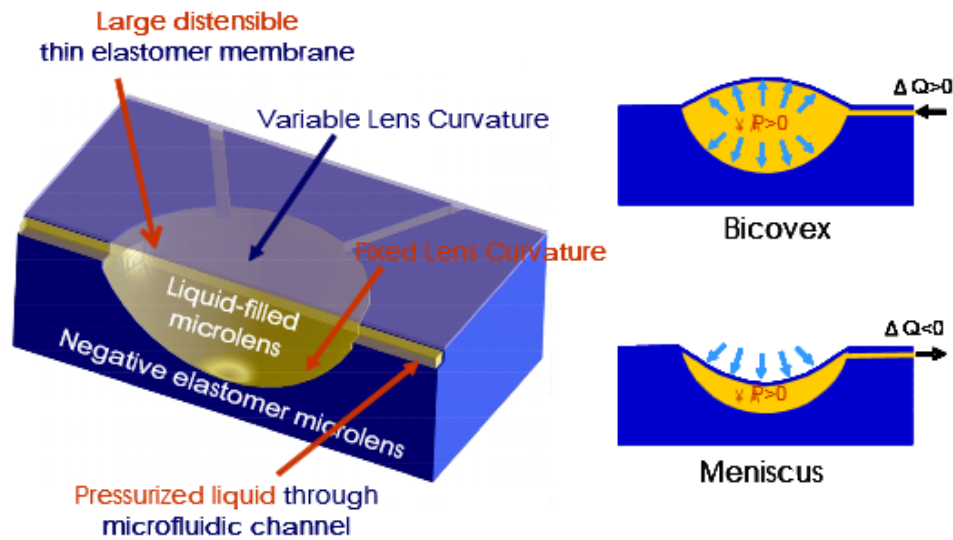
Figure 1.13 A tunable lens with mechanical manipulation [66].

Ren and Wu demonstrated a variable focal liquid lens by changing the aperture [67]. A media with a flexible membrane and a solid plate which is filled with a liquid with fixed volume and a circular periphery define the lens structure as shown in figure 1.14. A

lever actuator with impeller is used for mechanical manipulation that changes the aperture size and the curvature of flexible membrane to vary the focal length.
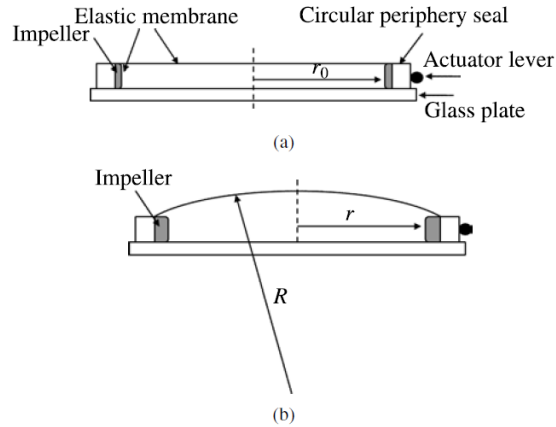
Figure 1.14 tunable lens with tunable aperture a) no focus and b) focus effect.

In pneumatic tuning, the focal length change is due to application of a pressure that in most cases will deform a membrane. There are two different design of pneumatic tuning in terms of electrode design: the out-of-plane design and the in-plane design.

Liquid lenses with out-of-plane design consist of a small chamber with a flexible membrane on the top, figure 1.15. When the pressure is applied to the membrane, the curvature of the membrane changes resulting to focal length change. The out-of-plane design of liquid lens was first reported by Ahn and Kim which was inspired by human eye [68]. In Their lens, they have a chamber between glass diaphragm and a substrate which has been filled with working fluid. Application of a pressure using a pump can change the glass diaphragm and leads to a relatively large focal length change between 30 cm to 60 cm. It is possible to reduce the size of the aperture and the focal length using a soft material such as PDMS, figure 1.15a. Werber and Zappe have replaced the glass diaphragm with a PDMS membrane with a surface roughness of about 9 nm [69]. The

distensible membrane was activated by an applied pressure using microfluidic liquid handling system where changes the focal length. This lens was quiet robust with focal length between 1 to 18 mm. Jeong et al. also reported bioconvex design for liquid lens with two membrane [66]. They could obtain shorter focal length between 0.6 to 3 mm, figure 1.15b. A similar design has been reported by Zhang et al in which two independent chambers control two distinct membranes, figure 1.15c.

In most of the above mentioned design an external source of pressure has been utilized to achieve the focal length change that makes all the process more complicated. A different design in which the liquid is sealed in the chamber has been reported by Ren et al where the pressure is applied using a servo motor [70]. Yu et al. designed a double focus lens with a membrane of different thickness which leads to different radius of curvature [71, 72].
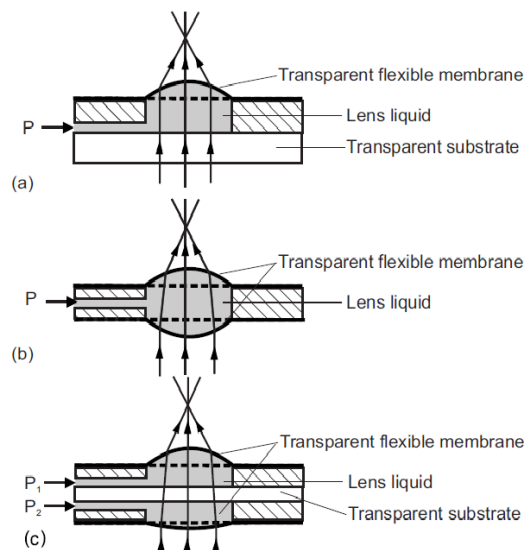
Figure 1.15 Liquid lenses with pneumatic tuning [64].

The second design in pneumatic tuning is in-plane design where the meniscus between two immiscible liquid can change. In these lenses the interface between two immiscible liquids can be utilized as a lens curvature. Lien et al have used this concept to demonstrate a new technique to fabricate spherical micro-mirror using PDMS [73]. Dong and Jiang have used pneumatic manipulation of fluid in micro-channel to form in-plane micro-lenses with liquid/air interface [15]. The liquid lenses are formed in T-shaped junctions within micro-channel. In addition to tunable focal length, these lenses can be repositioned, removed and reformed at the T-shaped junctions. Shi et al. have also utilized liquid/air interface to demonstrate a tunable in-plane micro-lens on a curved surface [74]. The standard soft lithography has been used to fabricate this device. The curvature of the air/liquid interface can be controlled by adjusting the flow rate of the liquid stream in the channel.

1.2.2.2.2.2 Electrical manipulation

In microfluidic systems, several mechanism such as acoustic and electrostatic forces, external pumps and syringes and so on have been applied to manipulate a small droplet for different application (e.g. lab on chip and liquid lenses) [75-79]. Electrical manipulation with internal pumps and no moving part are suitable to replace mechanical manipulation. The electrical actuated liquid lenses without mechanical parts can maintain the optical property while they are very precise and durable.

Here we classify electrical driven liquid lenses in terms of liquid to Conductive and insulating liquids. There are two major forces to electrically manipulate various liquids in microfluidic system, the EWOD [30, 80-82] and Dielectrophoresis [83, 84]. Insulating

liquids and conductive liquids have been successfully driven by DEP and EWOD forces, respectively.

1.2.2.2.2.3 Insulating liquids and liquid crystals

Polarizable particles can be driven by DEP force in a non-uniform electric field. In DEP actuation, the dimension of the device or the liquid channel is an important parameter. The DEP force which exert on polarizable particle by application of a voltage is proportional to the gradient of electric field and describes as [78]:

$$F_{DEP} = \frac{\varepsilon_0(\varepsilon_L - \varepsilon_M)W}{2d}V^2, \hspace{4cm} 1.11$$

Where ε_0 is the permittivity of vacuum, d is the distance between two parallel electrodes, W is the width of the electrodes, ε_L and ε_M are the relative permittivity of the liquid and the surrounding medium, respectively. Cheng and Yeh reported a dielectrically driven liquid lens consists of two immiscible liquid with different dielectric constant [85]. Figure 1.16 shows the structure of the lens in which the sealing droplet has higher dielectric constant. The density of the two immiscible droplets should be almost same to reduce the gravitational effect and maintain the symmetry of the droplet. The liquid lens demonstrated was convex lens with tunable focal length. The concentric design of the electrodes helped to create gradient of electric field where the liquid with higher permittivity attracted to the electrodes rather than the surrounding liquid. Application of voltage from 0 to 200 V demonstrates a focal length between 34 mm to 12 mm for a lens with 3mm aperture. The wettability of the surface on top of electrodes changes to contract the interface of the two liquids where the DEP force is effective [86].
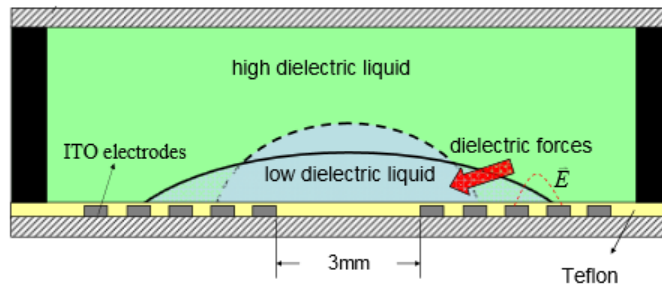
Figure 1.16 DEP driven liquid lens [85].

Liquid crystals can also be driven in a non-uniform electric field by application of a voltage. A non-uniform electric field can be generated by a proper design of the electrodes. Figure 1.17 shows the electrode design that Cheng has reported for DEP driven liquid crystal lens to generate a gradient of electric field [86]. The focal length changed from 1.6 mm to 2.6 mm using AC voltage between 0-200 V with small distance between electrodes, 50 μm.
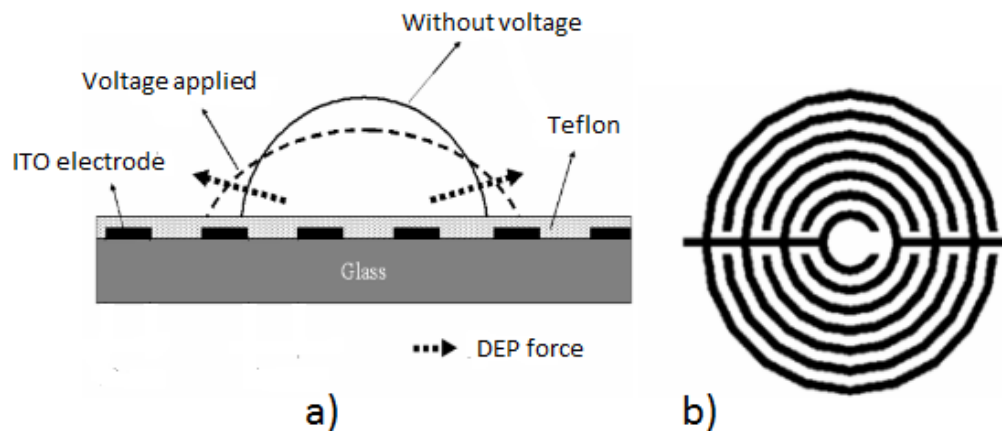
Figure 1.17 Liquid lens with concentric electrode design to generate DEP force [86].

Liquid crystal (LC) molecules which are composed of several different molecules have shown desirable properties in electro-optics. LCs have different refractive indices in

different molecular axis directions that makes them a good candidate for liquid lens applications. Tunable focal length can be achieved by tunable refractive indices of LCs.

1.2.2.2.2.4 Conductive liquids and Electrowetting tuning

Electrowetting and EWOD forces can be used to drive conductive liquids [30, 80-82]. Electrocappilarity which is the basis of Electrowetting has been introduced for the first time by G. Lippmann [1]. The electrical double layer at the interface of the conductive liquid and the solid surface can explain the Electrowetting phenomenon. In EWOD a thin dielectric layer added to decrease the electrolysis and improve the reversibility. The applied AC voltage will drop on dielectric layer rather that the electrical double layer and change the contact angle of the droplet [87]. Thus, EWOD is a powerful tool that can be used to manipulate a conductive liquid. In microscale, the surface tension of the droplet which is the dominant force and also the cohesive force of the droplet can control the shape of the droplet to make a liquid lens or display [4, 88, 89].

Electrochemical, piezoelectric and electromagnetic actuation are the commonly used mechanism for electric tuning of a conductive droplet. Lee and lee used an electromagnetic micro-actuator to apply pressure on a PDMS membrane [90]. A gold layer is patterned underneath the PDMS to generate electromagnetic field for actuation, figure 1.18a. Choi et al used electro-active polymer actuator attached on PDMS membrane to change the lens shape [91, 92]. By application of electric potential polymer actuator (EAP) pushes optical fluid which changes the light pass of the lens. Figure 1.18b shows their micro-lens structure with transparent PDMS membrane. Surface tension can also be controlled using electric field to tune the radius of curvature. Lopez et al. utilized

that application of a voltage can change the surface tension on one capillary surface relative to other which induces a change in focal length [93]. Figure 1.18c shows that the electrodes are designed on both side of the lens.
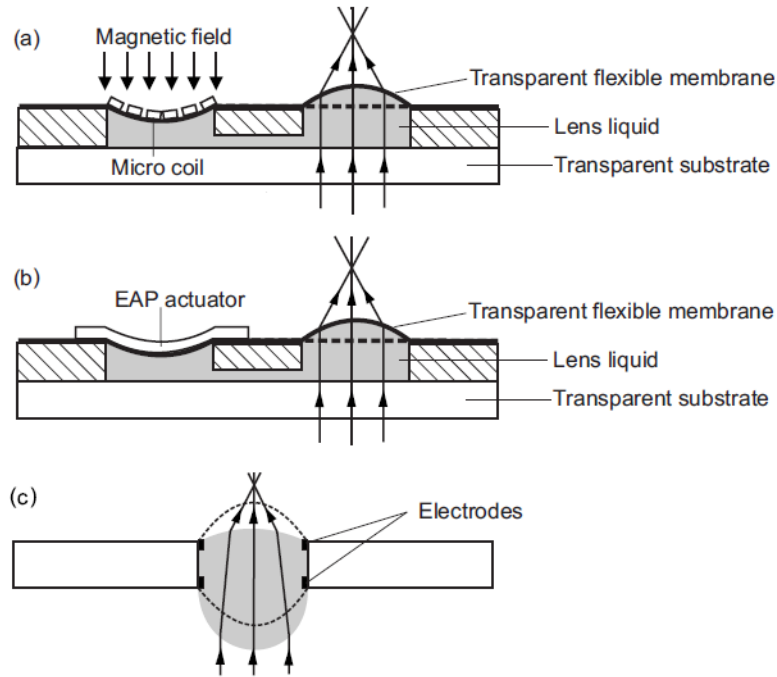
Figure 1.18 Liquid lenses with electric tuning [64].

Electrowetting is one of the fastest and most effective way to achieve a tunable focal length micro-lenses. Application of a voltage generates electrostatic force that moves the molecules of the conductive droplet at three phase contact line to reduce the contact angle. Most of the common liquid lenses that have been reported in the literature are based on EWOD.

Liu et al have reported a liquid lens based on electrowetting using planar electrodes [94]. They have designed double ring electrodes on a planar surface where the outer ring electrode electrowets the area of above it upon applied voltage to change the contact

angle, figure 1.19. However, they need to apply a high DC voltage in their design (around 250 V) and also their electrodes are not transparent.
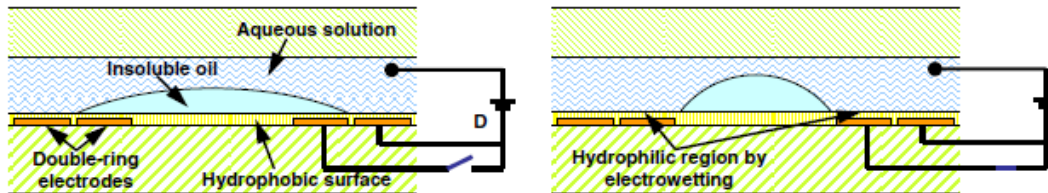
Figure 1.19 Liquid lens with planar electrodes.

Kuiper and Hendriks have demonstrated a tunable lens for miniature cameras by electrowetting of two immiscible liquids [31]. They have designed a cylindrical housing which is coated with a hydrophobic insulator contains two immiscible liquids, figure 1.20. The meniscus of the two liquids can be changed to convex and concave upon applied voltage. The cylindrical chamber design here is problematic and also is not applicable for integrated microfluidics. Similar design has also been reported by Smith et al for arrays of liquid lenses. A tunable focal length lens with coplanar electrode have been demonstrated by An et al [95]. They have made their device on a glass substrate which is coated with ITO. In their design, the conductive droplet is in direct contact with electrode which raises the electrolysis problem at lower voltages. Berge has investigated the principles of electrowetting based lenses and their application to imaging [96]. He has explained the principle of these lenses that emphasis on key feature such as equality of densities of two immiscible liquid, centering of the droplet, choice of choosing insulator materials and etc.
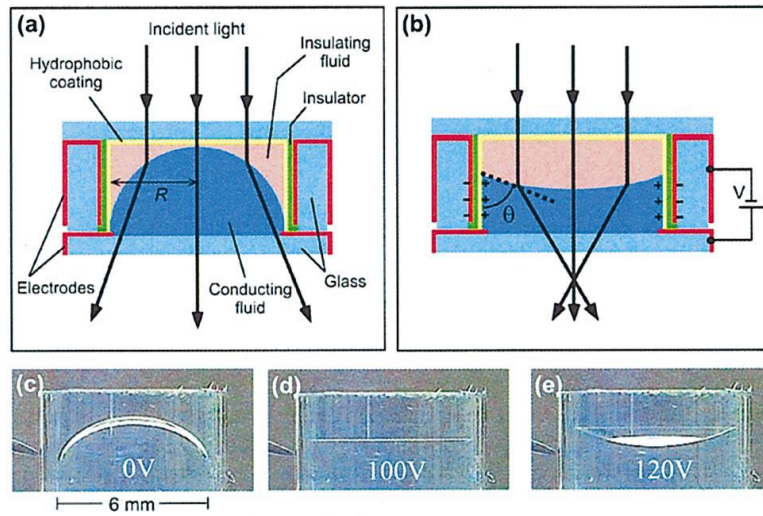
Figure 1.20 EWOD lens with side-wall electrodes.

Li and Jiang have designed a liquid lens based on EWOD on curved substrate [97]. They have used PDMS to build the chamber which contains two immiscible liquids and the process have been developed at low temperature to reduce the stress. Both diverging and converging micro-lens has been achieved at low and high voltages, respectively.

CHAPTER 2 VERSATILE MINIATURE TUNABLE LIQUID LENSES USING TRANSPARENT GRAPHENE ELECTRODES

2.1 Introduction

Microfluidics have been applied in many emerging biomedical applications such as cancer diagnosis using circulating tumor cells (CTC), [98-100] drug screening with organ-on-a-chip systems [101-104] and others [32, 105, 106]. In these applications, it is critical to monitor cell responses over an extended period of time. An autofocusing lens integrated into microfluidics could potentially enhance real-time functional analysis of cells. Nevertheless, a low-cost, tunable and miniaturized lens integrated into microfluidic platforms such as a Quake's valve has not been reported yet [107].

Electrowetting on dielectric (EWOD) is the control of the contact angle/wetting of conducting droplets by applying electrical voltage between the droplet and a counter electrode coated by a hydrophobic dielectric layer [11, 26]. In recent years, EWOD has drawn a lot of interest for use in the development of tunable lenses for optical application thanks to their quick response, low power consumption and robustness in operation [9, 31, 66, 97, 108]. In most designs, two immiscible liquids (silicone oil and water) have been dispensed in a liquid chamber, where the sidewalls are coated with metal and a hydrophobic layer [109]. The geometry of the oil-water interface changes from convex to concave when voltage is applied. Most current EWOD based tunable lenses are fabricated on planar rigid substrates (such as glass). The electrode materials that have been used include metals (gold, platinum, copper, aluminum), semiconductors (silicon, carbon nanotubes) and ceramics (indium tin oxide, ITO) [40, 94, 108]. ITO is optically

transparent in the visible light range; however, it is brittle and lacks flexibility. On the other hand, gold offers more flexibility, but is rather expensive and optically opaque.

Graphene, an atomic layer of carbon, has recently been found to have excellent physical and electrical properties as a transparent electrode, including high optical transparency, maximum strain (12%), high electron mobility and conductivity. Graphene has several advantages as EWOD electrodes. It has very small sheet resistance, as low as only tens of ohms per unit square and also has extraordinary optical transmission (about 97% in the visible light range). Our group has investigated graphene's properties in EWOD [110] as well as actuation of droplets on graphene transparent electrodes [111].

In this chapter, versatile miniature liquid lenses with high resolution for cell visualization have been fabricated. Droplets of ionic liquid and KCl solutions with different volume are used on the top of a flexible membrane made of parylene C (2,8-Dichlorotricyclo[8.2.2.2^{4,7}]hexadeca-1(12),4,6,10,13,15-hexaene) and polydimethylsiloxane (PDMS) to demonstrate the functionality of the liquid lens. The geometry of the droplet meniscus can be controlled using the EWOD phenomenon. For EWOD actuation, transparent planar graphene electrodes are patterned to have both driving and reference electrodes on the same surface which makes it easily integrated with microfluidics. Due to the high degree of flexibility of the PDMS/parylene membrane, both convex and concave curvature can be easily achieved by applying pressure underneath the membrane. Due to their flexibility and strechability, graphene electrodes remain functional when the membrane is deformed. The geometry of the liquid lenses can be tuned to be plano convex, positive meniscus and biconvex to achieve different

applications such as corrective lenses and focusing lenses (figure 2.1). Individual control of lens curvature enables the combination of convex and concave lenses, a way to minimize spherical aberration in lens designs. To the best of the authors' knowledge, this is the first report of a functional graphene-based tunable liquid lens.
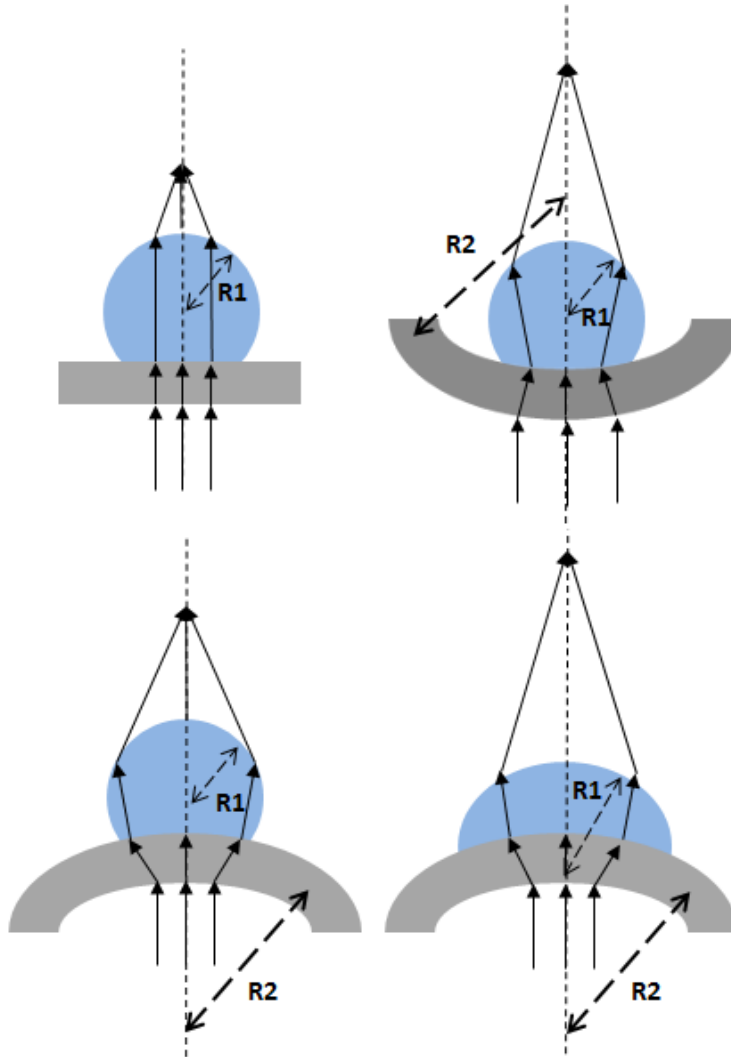
Figure 2.1 The concept of a liquid lens where the curvature can be controlled by EWOD and pneumatic pressure. Due to the flexibility and strechability of the graphene electrode and the parylene/PDMS membrane, the lens can function as plano convex, positive meniscus and biconvex as sketched here.

2.2 Planar graphene electrode design for EWOD applications.

Figure 2.2a shows the planar electrode design for the EWOD lens that is presented in this work. Since graphene is optically transparent, the edges of graphene are marked with dotted lines in the figure. The electrodes consist of a circular driving electrode in the center surrounded by two reference electrodes in a semicircular shape. The large black rings shown in the image are copper metal that was used to connect graphene to external contact pads. Application of a voltage to the electrodes generates an electric field that accumulates charges at the solid-liquid interface which reduces the solid-liquid interfacial tension and decreases the contact angle of the droplet. The modified Lippmann-Young equation has been derived for the planar electrodes [80]

$$cos\theta_V - cos\theta_0 = \frac{\varepsilon_0 \varepsilon_r}{2\gamma_{lv}d}[\frac{A_d}{A_t}\left(\frac{A_r}{A_d+A_r}\right)^2 + \frac{A_r}{A_t}\left(\frac{A_d}{A_d+A_r}\right)^2]V^2 \qquad 2.1$$

where θ_0 is the initial contact angle at 0 V, θ_V is the contact angle upon applied voltage, d is the thickness of the dielectric layer, γ_{lv} is the liquid-vapor surface tension, ε_r is the relative permittivity of the dielectric material and A_d, A_r and A_t are the areas of the driving electrode, reference electrode and droplet contact, respectively.

For the maximum change in contact angle, the areas of the driving and reference electrodes should be equal while the area of the gap is minimized. Here, the radius of the driving electrode (black circle) was 0.7 mm and the radius of the reference electrode (outer white circle) was 3 mm. The gap between the driving and reference electrodes was 0.1 mm. The 0.1 mm gap was chosen for the ease of fabrication. The dynamic behavior of the ionic liquid droplet in the air under 100 V is simulated with COMSOL (figure 2.2b).The model of laminar two phase flow moving mesh was used to take the fluid

movement into consideration. This physics solve the Navier-Stocks equations combined with the continuity equation to describe the fluid motion. The time dependent study was used for this simulation with 1 ms time intervals which studies the droplet movement toward the final contact angle upon applied voltages during time. Equation. 2.1 was used as boundary condition at the contact point to modify the final contact angle following the tutorial model of electrowetting lens provided by COMSOL Multiphysics. The larger semicircle in figure 2.2b is air with a fixed mesh outer boundary condition. The smaller semicircle represents the ionic liquid. Moving mesh boundary condition is considered in the bottom line where the contact point is allowed to move. Figure 2.2b indicates the droplet movement was within a few milliseconds after voltage was switched from 0 V to 100 V. (See supporting information for more details on Comsol simulation).

The simulation results show that the contact angle oscillated around the final position for the case of a KCl droplet (figure 2.3a,b). Also, the KCl droplet responded faster (50 ms response time) compared to ionic liquid (150 ms response time) due to lower viscosity of KCl (figure 2.3b,c). However, the response of the contact angle change became overdamped for an ionic liquid droplet. The differences in transient responses are due to higher viscosity in ionic liquid. The simulation results suggest that the application of ionic liquids as a liquid lens can damp the oscillation out to improve the lens performance.

Based on Lens-maker's equation, the focal length of the liquid lens can be determined as [112]:

$$\frac{1}{f} = (n-1)\left[\frac{1}{R_1} - \frac{1}{R_2} + \frac{(n-1)D}{nR_1R_2}\right] \qquad\qquad 2.2$$

where *n* is the refractive index of liquid, *D* is the thickness of liquid, and R_1 and R_2 are the curvature of the droplet and deformed membrane, respectively.
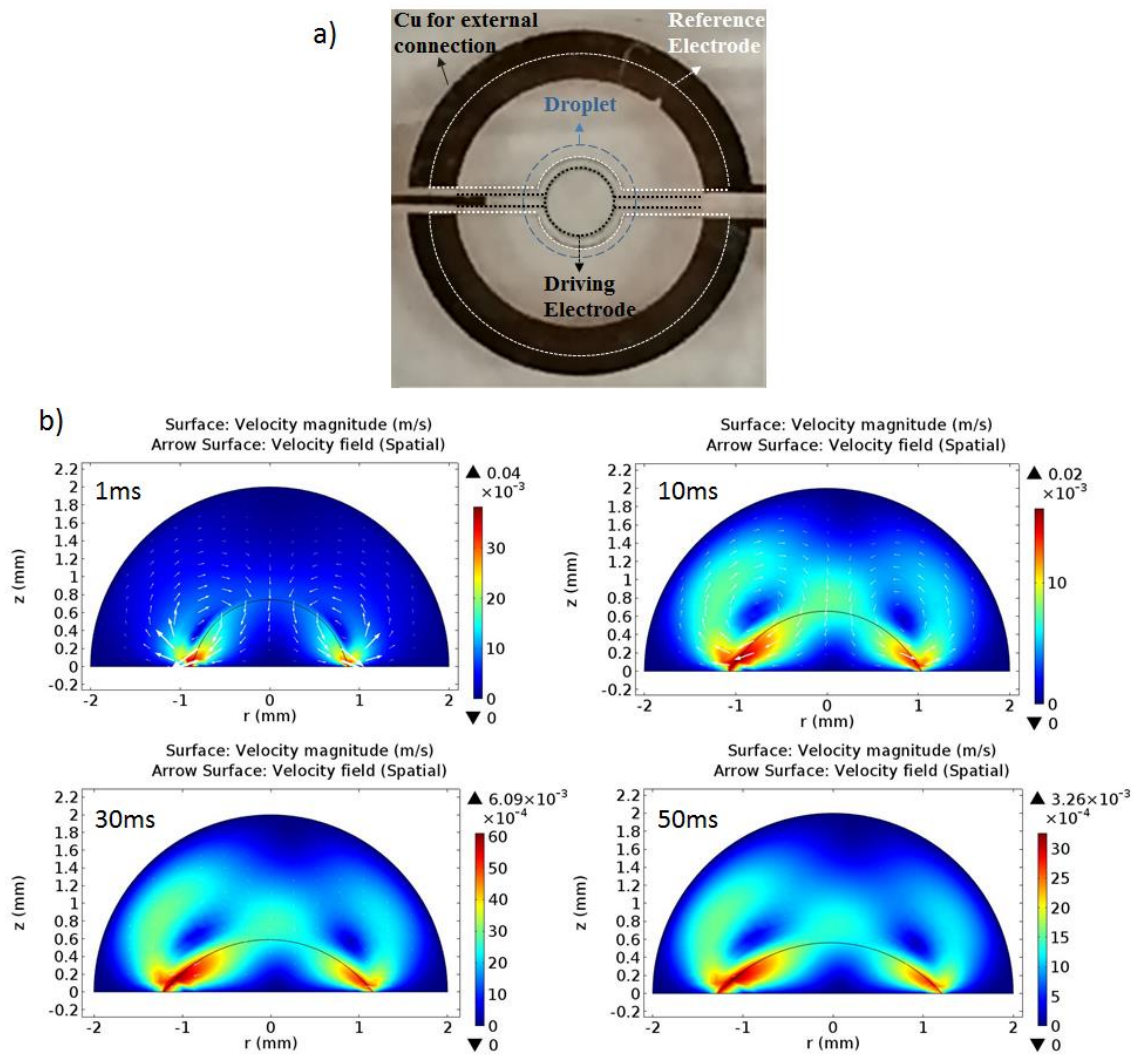
Figure 2.2 (a) The planar graphene electrodes for EWOD actuation of a droplet with two sectors showing that the working area is completely transparent. (b) Comsol simulation of dynamic movement of ionic liquid in the air during time. The parameters include the dynamic viscosity of air18.27 μPa.s, density of air1.225 kg/m³, dynamic viscosity of ionic liquid 0.12 μPa.s and density of ionic liquid1420 kg/m³.
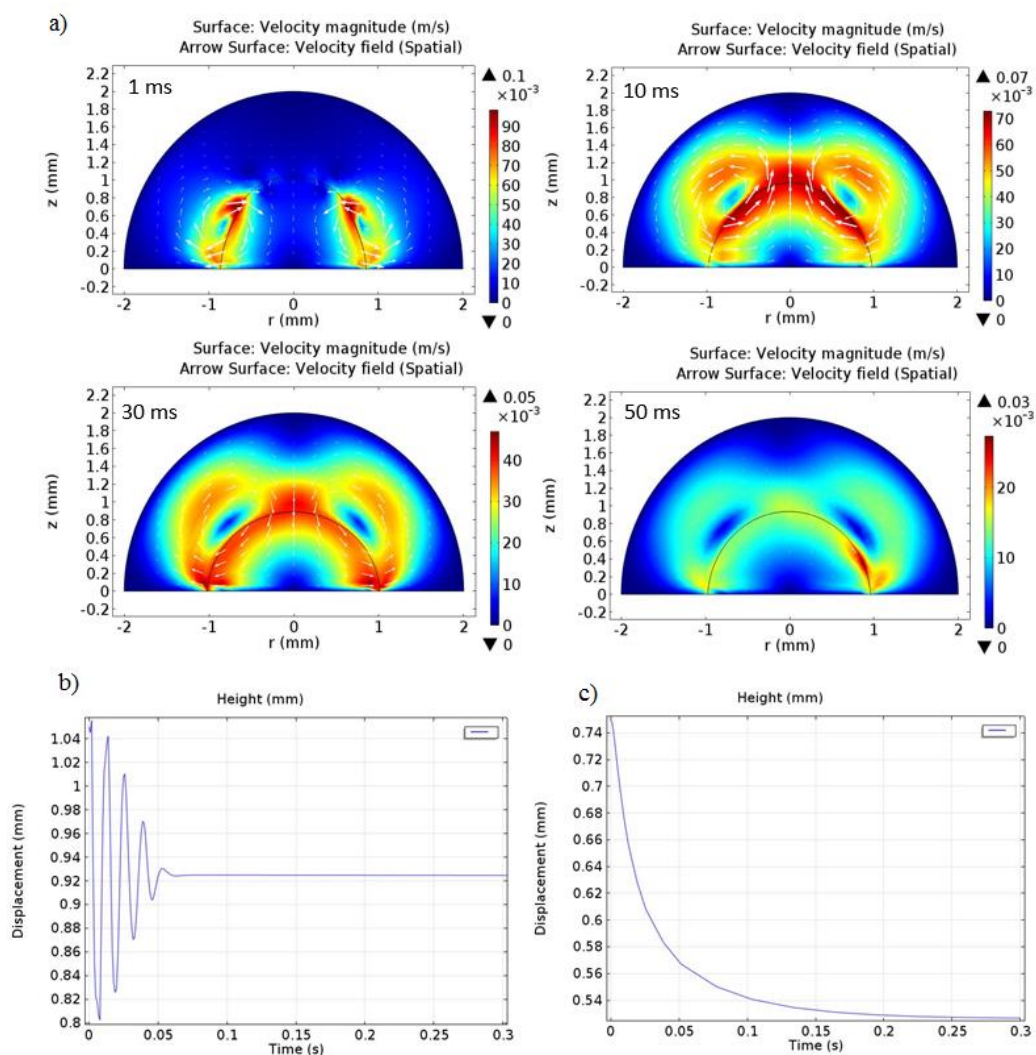
Figure 2.3 (a) COMSOL simulation for KCl solution in the air a few milliseconds after voltage is switched from 0 to 100V. (b) KCl droplet height displacement over time towards the final height (contact angle) a few milliseconds after voltage is switched from 0 to 100V. (c) Ionic liquid droplet height displacement over time towards the final height (contact angle) a few milliseconds after voltage is switched from 0 to 100V.

2.3 Materials and methods

Figure 2.4 is summarized the fabrication process flow. The membrane was made of the flexible, transparent materials PDMS and parylene C. PDMS was prepared by mixing the base to curing agent (Dow Corning SYLGARD 184) with a ratio of 10:1 (in weight).

The prepared PDMS was spin-coated and cured on a silicon wafer (200 µm-300 µm). A thin parylene layer (2 µm) was then deposited on top of PDMS using chemical vapor deposition (CVD, Specialty Coating System). Clean copper foil (Alfa Aesar, 25 µm thick) was used as a substrate to grow graphene using CVD [113]. Briefly, the furnace was filled with 3 sccm H_2 and heated up to 1000°C. Then, 30 sccm CH_4 gas was flown into the furnace for 30 minutes and decomposed to allow the carbon materials to form graphene sheets on the copper surfaces. The transfer of graphene to the membrane started with spin-coating of a thin protection layer of Poly(methylmethacrylate)(Microchem PMMA 495) on top of graphene/copper. After drying in room temperature overnight, the copper foil was etched overnight in ammonium persulfate (Transene APS-100) diluted in DI water with a ratio of (1:10). The released PMMA/graphene sheets were carefully harvested using a glass slide. Prior to graphene/PMMA transfer, parylene surfaces were treated with oxygen plasma for 20 seconds to improve the adhesion between graphene and parylene. PMMA was removed by acetone following the transfer process. Raman spectroscopy of the grown graphene demonstrates that the graphene was single layer (figure 2.4k). The transferred graphene was patterned to form electrodes by photolithography and oxygen plasma. A layer of copper (150 nm) was deposited using electron beam evaporation and patterned for contact pads. Silver conductive epoxy kit (MG Chemicals) was used to bond wires (Micron Meters36 AWG) to the contact pads. A thin parylene layer (0.8 µm) was deposited as a dielectric layer using CVD. A hydrophobic Teflon layer (1-3% DuPont AF 1600 diluted in 3M FC72) was spin-coated and baked on a hot plate at 120 °C for 15 min. The device was released carefully from the

silicon substrate using a solution of potassium hydroxide (0.87 M). A droplet of 3 μl volume (either ionic liquid (N,N-diethyl-N-(2-methoxyethyl)-N-methylammoniumbis-(trifluoromethylsulfonyl)-imide (DEME-TFSI) or 10 mM potassium chloride (KCl) solution) was carefully placed in the center of the graphene electrode to form the liquid lens. A home-built system consisting of a white light illumination source delivered by a semi-flexible fiber optic tube, a Navitar 12x zoom lens, and a USB CCD camera (iSolution) was used to measure contact angles. Typical experimental parameters include AC voltages from 0 V to 130 V with a frequency between 10 Hz and 10 KHz generated by a function generator (Agilent 33120A) and an AC power amplifier. The system was controlled by a Labview program. ImageJ software was used to measure the contact angle of the droplet. The setup for focal length measurements of the droplet is shown in figure 2.4j. The measurement was carried out using an optical microscope equipped with a CCD camera (Infinity 2) to visualize the object through the liquid lens. The object was first placed under the optical microscope and focused to get the optimum image. The size of the image h_0 was measured using ImageJ software. The liquid lens was then mounted on a three-axis stage between the microscope objective and the object. The distance between the object and the liquid lens, d, was adjusted to obtain another optimum image of the object through the liquid lens. The size of the picture (h_I) was measured. The magnification of the image with the liquid lens compared to the one without the liquid lens was calculated by:

$$m = \frac{h_I}{h_0} \hspace{4cm} 2.3$$
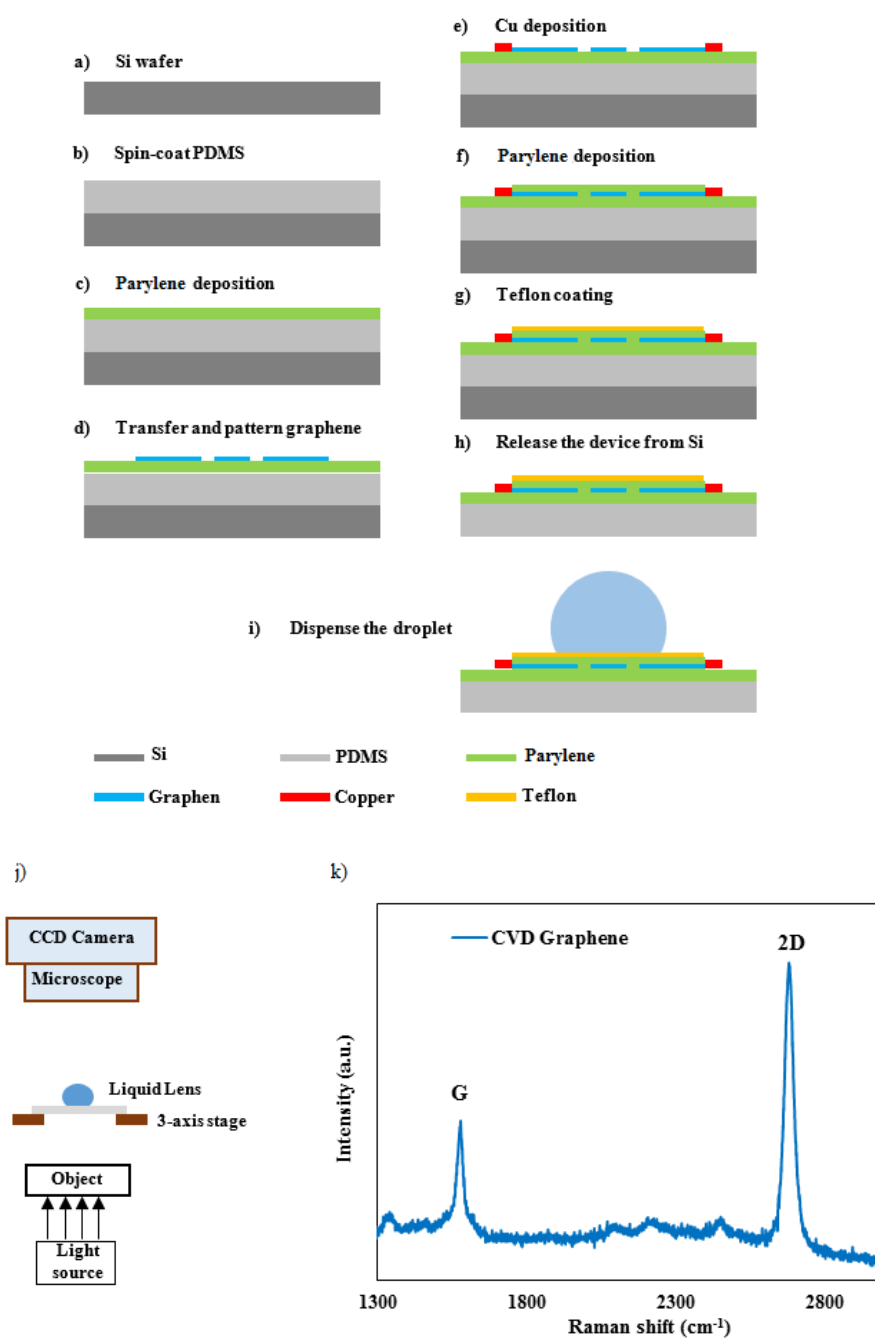
Figure 2.4 General fabrication process of the device. (a) RCA clean of a Si wafer, (b) Spin-coating PDMS on a Si wafer and curing, (c) CVD parylene on top of PDMS, (d) Transfer of graphene on parylene and pattern it, (e) Copper deposition and patterning for external contact pads, (f) Parylene deposition as a dielectric layer, (g) Hydrophobic Teflon coating, (h) Release of the device using KOH solutions, (i) Dispense of a droplet in the center. (j) The optical setup for the focal length measurement where a CCD camera was used to capture images. (k) Raman spectra of CVD grown graphene.

Then, the focal length of the liquid lens was calculated using the formula $f = md / (m+1)$

for the case of the real image [94].

Experimental results

The prototype of the liquid lens is shown in figure 2.5. The device was flexible and

could be deformed on any curved objects. Since the diameter of the KCl droplet (around

1.8mm) is less than the capillary length (around 2mm), surface tension is the dominant

force that maintain the droplet [114]. This picture shows that the liquid lens and its

underlying electrodes were transparent. The droplet shape was symmetric about its center.

The diameter of the droplet could range from 1.5 mm to 6 mm in our design. In order to

demonstrate the functionality of the device on a deformed substrate, the contact angle

measurement was performed on a curved substrate.
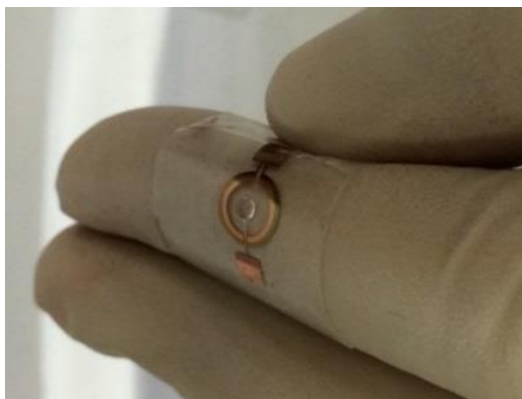
Figure 2.5 A picture of a device prototype. The center part of the membrane was clear
and transparent. The outer copper ring was used to connect the graphene to the external
contact pads.

Figure 2.6 illustrates the responses of a 3 µl KCl droplet to AC voltages from 0 V to

120 V when the substrate was deformed with a 3 mm radius of curvature. As the applied

voltage increased, the contact angle decreased in response to the electric fields generated

inside the droplet (figure 2.6a). No water hydrolysis was observed at higher voltages. Figure 2.6b shows the voltage dependent contact angle change for a droplet on a curved substrate with 3 mm radius of curvature which can be well described by a modified Lippmann-Young equation (Equation. 2.1). According to Wang and Zhao, [115] the radius of the curvature of the membrane plays a minor role in the contact angle change when the radius is much larger than the thickness of the substrate. The experimental results were consistent with the theory. Ionic liquid has also been investigated as a liquid lens. Ionic liquid has been studied due to its high thermal stability and non-volatility that can be used for long term applications [116]. Ionic liquid consists of ions instead of neutral particles. These ions accumulate in the solid-liquid interface upon applied voltage, decreasing the contact angle of the droplet. Due to lower surface tension [117] and higher viscosity, i.e. low ionic mobility of ionic liquids which make them more stable with respect to hydrolysis, larger contact angle change can be achieved in ionic liquids compared to KCl droplets resulting to wider range of tunable focal lengths.

The optical performance was studied for both the KCl droplet and the ionic liquid droplet. The initial diameters for 3 µl KCl and ionic liquid droplets were 1.8 mm and 2.34 mm, respectively. Figure 2.7a shows images of a 1951 USAF resolution chart through the KCl liquid lens under different applied voltages. The center of the object was in focus initially (at zero volts). When voltage was applied, the image became blurrier due to the increased focal length of the lens and decreased curvature of the droplet.
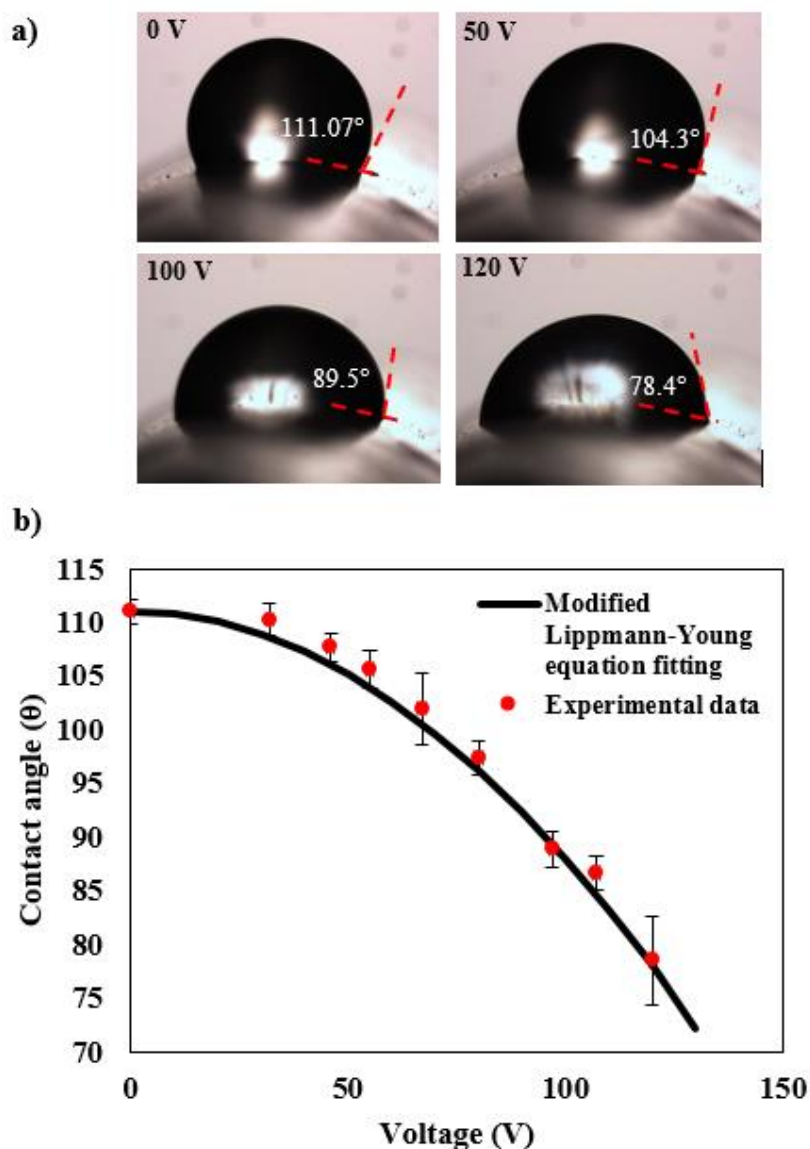
Figure 2.6 (a) The measured contact angle change for a 3 μl KCl droplet with planar graphene electrodes on top of a curved parylene/PDMS substrate observed at different voltages. (b) The contact angle change vs applied voltage for a 10 mM KCl droplet on a curved surface with a 3mm radius of curvature. The black line is the fitting curve using modified Lippmann-Young equation. The error bars represent the standard deviation from mean contact angle. The fitting parameters are: initial contact angle, $\theta_0 = 111.07$, relative dielectric constant of Teflon $\varepsilon = 3.1$, $\varepsilon_0 = 8.85 \times 10^{-12}$ F/m and surface tension $\gamma = 72.7$ dyn/cm, the dielectric thickness $d = 0.8$ μm.

Figure 2.7b shows the focal length and contact angle changes of the 3 μl KCl droplet when the voltages were applied from 0 V to 130 V on a flat substrate. In this experiment, the focal length did not change much at voltages below 50 volts as a result of small contact angle change. A large change of focal lengths was observed at around 70 V which corresponded to a contact angle around 95 degrees. In addition, a larger focal length could be observed with larger volume droplets due to a larger radius of the curvature.
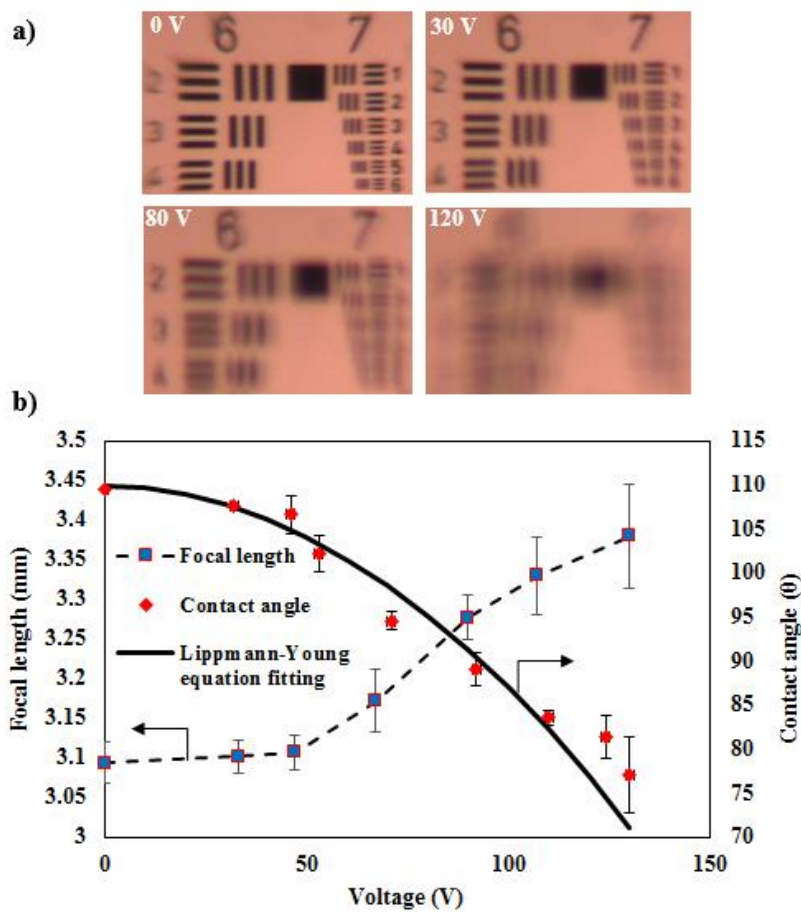
Figure 2.7 (a) The optical performance of the liquid lenses (a 10mM 3 μl KCl droplet) at different voltages. The elements of group 6 and 7 of the 1951 USAF resolution chart were in focus at zero volts. The images of the object became out of focus with increasing voltage. (b) The corresponding focal length and contact angle change for applied voltages from 0 V to 130 V.

Figure 2.8a shows the focal length and contact angle of 3 µl ionic liquid droplet. Since there was no report on surface tension of DEME-TFSI, the surface tension of [N(4)113][Tf2N] ionic liquid is used which has similar structure to the one that is used in this work [118]. At 0 V, the focal length of the ionic liquid lens was larger compared to a KCl droplet with the same volume due to a smaller initial contact angle which contributed to a larger radius of curvature. Also, the tunable focal length range was larger for ionic liquid due to the smaller surface tension of ionic liquid compared to KCl solution. Here, the focal length and contact angle started to change at 25 V compared to KCl solution at 35 V. The lower actuation voltage was due to higher fluid conductivity that affected the apparent relative permittivity of droplets [119]. The electrical conductivity of the ionic liquid is 0.35 S/m [116] compared to a 10 mM KCl droplet which is 0.1408 S/m [120] in room temperature. Further focal length changes are limited with saturation of contact angle that happens at higher voltages. A 1951 USAF resolution chart was used to determine the maximum resolution of the liquid lens system with a 3 µL ionic liquid droplet. Figure 2.8b demonstrates that the finest line pair that could be resolved was element 6 in the group 8 which corresponded to a resolution of 456.1 lp/mm. The widths of the lines in group 8 and 9 were in the range of 1.1-3.91 µm which showed the feasibility of imaging small objects such as cellular structures or tissues. The appearance of shadows and minor distortions on the right edge of the image were caused by light illumination and the thickness (1.1mm) of the glass chart. The incidence of a fiber optic white light source was obliquely from upper left to lower right corners above the glass chart.
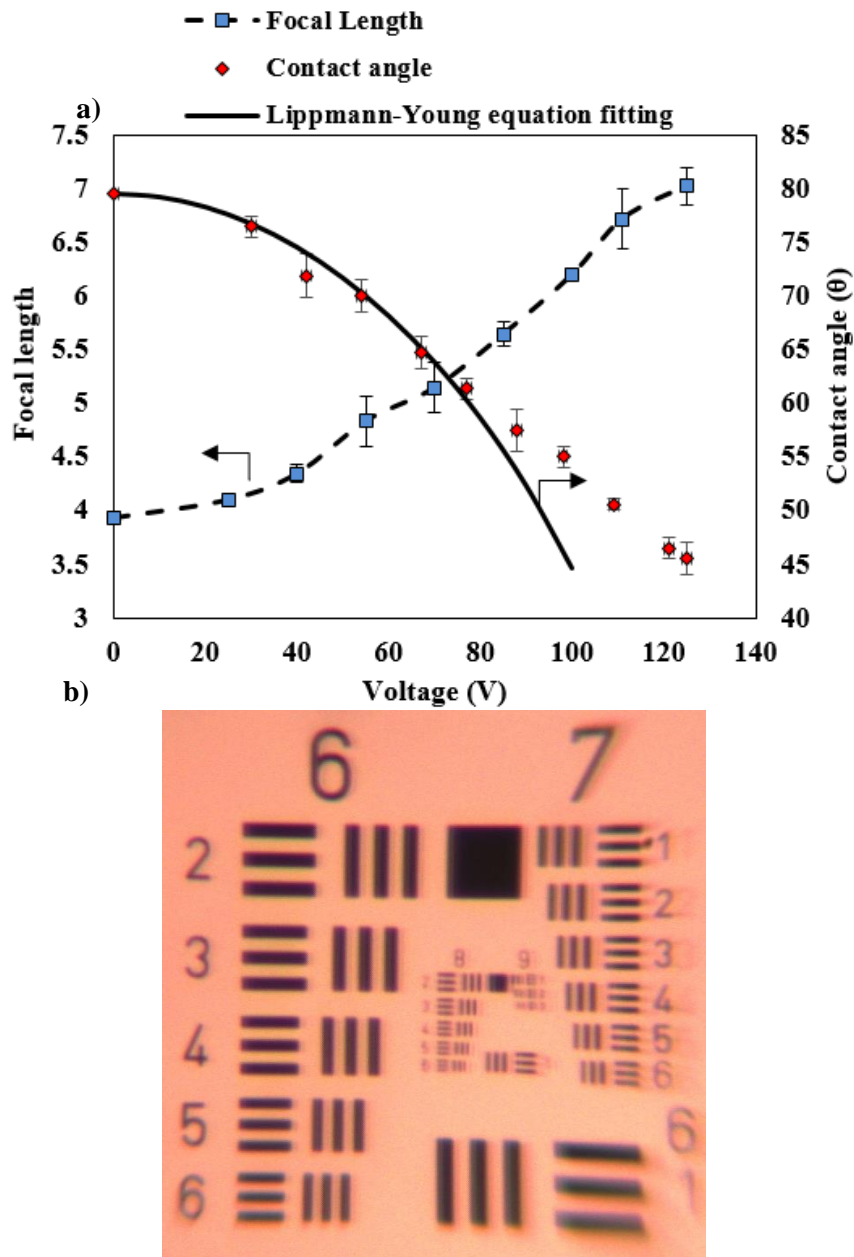
Figure 2.8 (a) The focal length and contact angle change versus voltage for a 3 μL ionic liquid lens. The focal length of the ionic liquid was larger compared to KCl solutions due to its larger initial contact angle. The fitting parameters are: initial contact angle $\theta_0 = 79.6$, relative dielectric constant of Teflon $\varepsilon = 3.1$, $\varepsilon_0 = 8.85 \times 10^{-12}$ F/m, surface tension $\gamma = 38.38$ mN/m [118]**,** and the dielectric thickness $d = 0.8$ μm. The error bars represent the standard deviation from mean contact angle. (b) The test of imaging quality using a resolution chart. Element 6 of group 8 could be observed.

Contact angle hysteresis is a phenomenon that the observed contact angle depends on whether the liquid is advancing or receding on the surfaces [121]. Figure 2.9 shows a typical curve of contact angle hysteresis for a 3µl DEME-TFSI ionic liquid droplet. This figure demonstrates that the contact angle hysteresis which is the difference between advancing and receding contact angle is around 2.5 degree. Contact angle saturation is another challenge in EWOD systems in which the contact angle change does not follow the Lippmann Young formula at higher voltages. Although, several studies have been carried out to understand the actual physics of this phenomenon, it is still not clear.
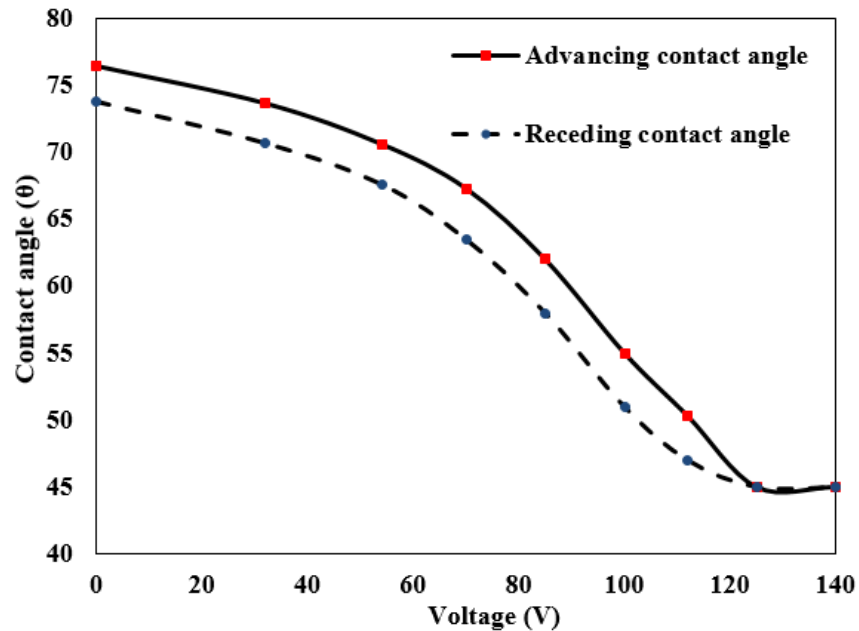
Figure 2.9 The contact angle hysteresis for 3 µl DEME-TFSI. The difference between advancing and receding contact angle was about 2.5 degree. Saturation of contact angle was observed above 130 V.

Charge trapping in the dielectric layer at the contact line, microdroplet ejection from the main droplet or air ionization are some proposed mechanisms to explain contact angle saturation [27, 28, 122]. At higher voltages (above 130V), the saturation of contact angle

was observed which prevents further contact angle change. This experiment shows that ionic liquid-based lenses can work in a large range of voltage without electrolysis and with low contact angle hysteresis. Figure 2.10 shows an image of bone marrow dendritic cells (BMDCs) captured through a 3 μl ionic liquid lens. In this experiment, the BMDCs were cultured in a growth medium RPMI 1640 supplied with 10% FBS for 7 days. Some of the BMDCs were attached to the bottom of Petri dish while others were floating in the liquid. The BMDCs were clearly visible under the lens. Early stages of the "dendrites" formation were observed on BMDCs surfaces, indicating the typical morphological features of the loosely adherent BMDCs. At different applied voltages, sharply resolved cell walls could be clearly observed. Colony formation with large cells clumps was also observed at different sites. The virtual imaging procedure is used for this measurement using setup shown in figure 2.4j.
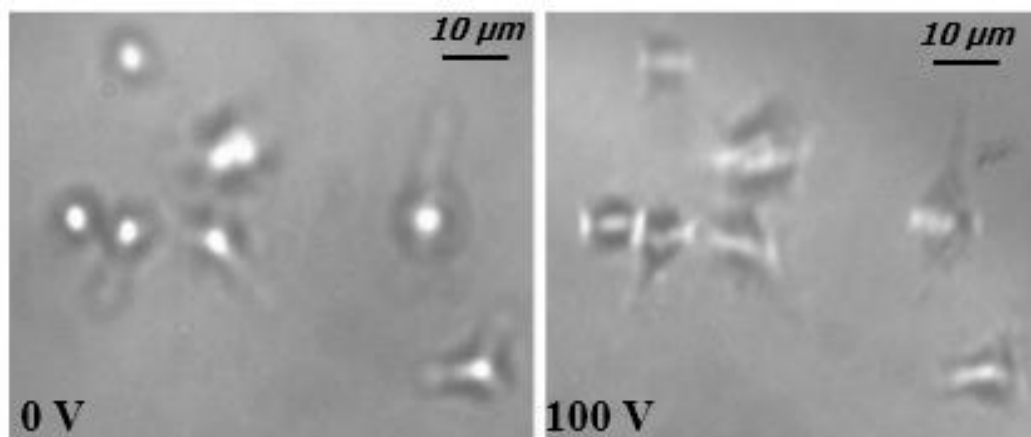
Figure 2.10 The images of the BMDCs captured through an ionic liquid lens. At zero volts, the cells were not well focused. At higher applied voltages, cells were focused and a sharp image of cells could be acquired.

The flexible lens can be mounted on curved substrates with different radii of curvature to tune the field of view. Figure 2.11 demonstrates the concept of increasing the

field of view by imaging English letters in an alphabetic order. The device was initially on flat polyethylene terephthalate (PET) sheet where the letters from H to P could be observed clearly through the lens representing a 15 mm field of view (figure 2.11a). Application of a mechanical force to the PET sheet changed the radius of curvature of the substrate, creating a positive meniscus lens. As a result, the letters from F to Q were brought into focus when the radius of curvature of the substrate was changed to 5 mm in figure 2.11b, representing a 21 mm field of view. The field of view increased about 6 mm. In figure 2.11a, the focused area was in the center and in figure 2.11b the edges of the image were brought into focus. Because of the large field of view, the image was a little blurred and distorted within the out of focus area caused by the curvature and distortion aberration.
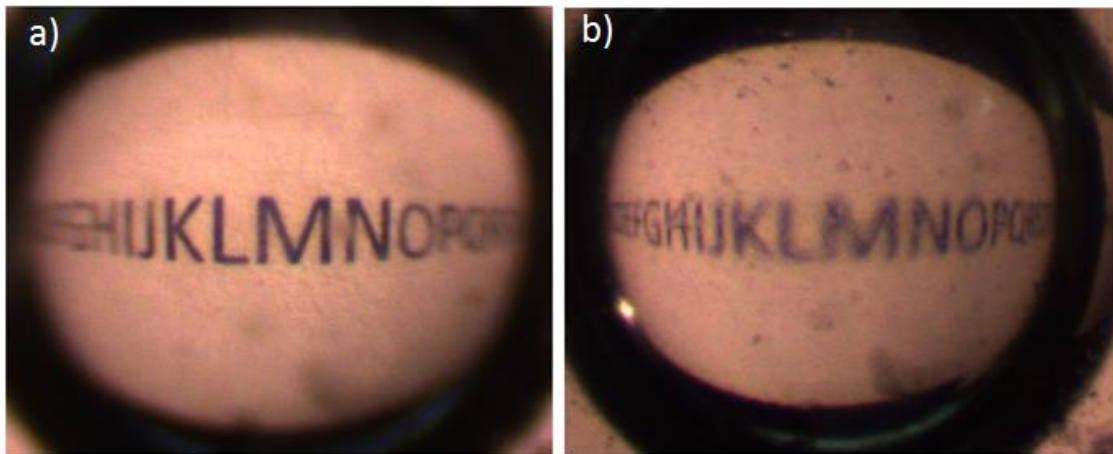
Figure 2.11 Demonstration of enlarged field of view of the lens. (a) The initial state where no mechanical force was applied and the substrate was flat, (b) with applied mechanical force where the radius of curvature of the substrate was about 5mm.

Table 2.1 summarizes selected liquid lenses that have been demonstrated in literature. Krupenkin et al have reported a liquid lens made of an aqueous solution of potassium

sulphate actuated by a set of planar ITO electrodes [40]. A liquid lens consisting of a droplet of silicone oil in an aqueous 1% KCl solution actuated by co-planar electrodes has also been demonstrated by Liu et al [94]. In these lenses the substrate is glass which is rigid. Benh-Kheim et al have proposed a variable focal length lens based on electrostatic force with a thin parylene layer that encapsulated the droplet [123]. Nevertheless, a thin gold electrode on the top of parylene decreased the optical transparency of the lens. Kim et al have developed a tunable liquid lens with hydraulic manipulation for confocal endoscopy applications [124]. Due to the required mechanical manipulation, the device was large and the range of tunable focal length was small (around 280 µm). Kuiper and Hendriks have demonstrated a glass chamber with two immiscible liquids for camera applications [31]. ITO was deposited on the sidewalls of the glass chamber which made the fabrication process complicated. An EWOD based liquid lens on flexible substrate with Al electrodes has also been presented by Li and Jiang [97]. In most of liquid lenses listed above, the lenses were made by rigid substrates with gold or ITO as electrodes. The liquid lens demonstrated here is made of flexible polymers as a substrate which allows its implementation in most microfluidic platforms. Graphene has been used as a transparent electrode which has higher optical transmission (97.7% [125]) compared to ITO (80% [126]) and gold (<20% [127]). Also, the electrical conductivity of graphene (9.6×10^5 S/cm)[128] is higher compared to gold (4.52×10^5 S/cm)[129] and ITO (1×10^4 S/cm)[130]. Graphene sheets can be easily transferred to a flat substrate and patterned to define electrodes for the actuation of a tunable lens.

Table 2.1 Comparison between different liquid lenses

Paper	Electrodes	Actuation	Voltage	Focal length change	Resolution (lp/mm)
Berge (2000)[9]	Not	EWOD	230	~9	Not
Krupenkin(2003)[4	ITO	EWOD	100	~ 0.6	Not
Liu (2008)[94]	Al	EWOD	250	~25	Not
Kheim (2008)[123]	ITO/Au	Electrowettin	300	~2	Not
Kim (2014)[124]	-	Pneumatic	-	~0.28	228
Kuiper (2004)[31]	ITO	EWOD	120	~10	Not
Li (2012)[97]	ITO	EWOD	150	~28	25.39
This work (2015)	Graphene	EWOD	120	~4	456.1

2.4 Conclusions

Development of versatile miniature liquid lenses has been reported in this chapter. Lenses made of a droplet of ionic liquid and KCl solutions have been demonstrated on a flexible and transparent PDMS/parylene membrane which enables the generation of different radii of curvature. Variable focal length of the liquid lens is achieved based on EWOD phenomena using planar graphene electrodes. The high optical transmission of graphene makes it an ideal material for EWOD lenses, while its high electrical conductivity could enhance EWOD performance. Based on the type of liquid (ionic liquid or a KCl solutions) and the size of droplets, variable focal lengths can be achieved ranging from 3 mm to 7 mm. Apart from the small size and high degree of transparency, the resolution of the lens system is surprisingly high which makes it ideal for cell visualization. These excellent characteristics combined with its high chemical and

mechanical stability, enable it to be utilized for future endoscopic applications. Since the liquid lens can be assembled on a curved transparent substrate, compound lenses can also be fabricated. This provides an opportunity for aberration correction by fine tuning of the substrate curvatures to reduce spherical and chromatic aberrations. In addition, the curved substrate design makes the liquid lenses useful for larger field of view imaging. Also, arrays of liquid lenses on a curved substrate can be used to image 3D effect visualization.

CHAPTER 3 TOWARD ALL GRAPHENE INDIVIDUALLY TUNABLE COMPOUND EYE

3.1 Introduction

Compound eyes of the insects have drawn a lot of researcher's attention in recent years due to their exceptionally wide field of view (FOV), low aberration, high acuity to motion and infinite depth of field [131, 132]. These features have inspired researchers to develop sophisticated imaging systems for applications including display technologies, endoscopy and security surveillance cameras [133-135]. Currently, most of the biomimetic compound eyes are built using PDMS with hemispherical shapes which consist of a fixed curvature of both supporting and lens material, but lacks tunability [136-138]. The challenge in the current compound eye with fixed lenses is the limited viewing angle. The distance between the object and the lenses farther from the central axis increases beyond a certain angle (gap mismatch) resulting to out of focus images. Compound eyes that exploit tunable lenses could overcome the gap mismatch by adjusting the focal length of the lenses close to the edge. However, tunable lenses demand a change in curvature of image acquisition sensors supporting (R) to match the focal length change, renders them incompatible with the fixed R. Here we have demonstrated a lens system capable of changing both curvatures of the lens (R_1) and the curvature of lenses supporting membrane (R_2) to address this issue. Our motivation in this chapter is to propose a system of lens that afford scalable pathway to working artificial compound eye with tunable lenses.

Electrowetting on dielectric (EWOD), changing the contact angle (focal length) of a conductive droplet by applying voltage, has been widely used in the tunable focal lens design. Tunable lenses based on EWOD consist of a chamber with two liquids and sidewall electrodes have been developed [9, 31, 109, 139]. EWOD system with planar electrodes have also been implemented for liquid lens application [80, 94]. Unfortunately, the current EWOD lenses are capable of tuning only R_1 which is not suitable for application where high quality imaging is required, due to the enhanced spherical aberration. Spherical aberration results from the geometry of the lens in which the lens curvature deviates from ideal sphere. The aberration could be corrected by carefully designing and addition of other lens elements [140]. Another strategy to correct aberration is by precise control of the second curvature, a procedure that is implemented in wearable glasses (lens).

Here we have demonstrated a means of auto focusing lenses realized by both curvatures change using pressure and voltage. A free-standing circular polydimethylsiloxane PDMD/parylene membrane was prepared as flexible supporting with perimeter mounted on Si wafer. Applying pressure to the membrane deforms it to semi-hemispherical shape which is suitable for compound eye application [141-143]. In addition, the membrane deformation with reversible fashion changes the second curvature of the lens resulting to higher optical quality. The lens exploits well-established graphene electrodes with planar processing approaches for EWOD actuation [110, 111, 144]. The unique design of the electrodes implemented on 3D deformable membrane

enables realization of tunable compound eye. High optical transparency of graphene provides larger optical aperture compared to the non-transparent electrodes.

3.2 Theory and simulation

Autofocusing could be achieved by either changing R_1 or R_2 using applied voltage or pressure, respectively as shown in ray tracing diagram (figure 3.1). The lens-maker's equation correlate the focal length to R_1 and R_2 is [112]

$$\frac{1}{f} = (n-1)[\frac{1}{R_1} - \frac{1}{R_2} + \frac{(n-1)D}{nR_1R_2}] \qquad 3.1$$

Where n is the refractive index of liquid and D is the thickness of liquid. Figure 3.1 shows the ray tracing diagram for a compound eye configuration using COMSOL. The physics of geometrical optics along with ray tracing study was used for this simulation. By analogy to imaging system in the insect eye, each microlens on a compound eye corresponds to an image acquisition sensor located in the focal point of the lens. In figure 3.1a all the lenses have identical focal length as a result of identical geometry. The image sensors are placed on a curved surface correspond to the focal point of each lens. Figure 3.1b demonstrates a compound eye configuration in which the lenses are actuated. The challenge in this figure is that, the R should be adjusted to overcome the focal length change. Thus, by fine tuning of both R_1 and R_2, tunable compound eye could be achieved without changing R (figure 3.1c). This simulation illustrates that by apposition of the tunable lenses on a dynamically tunable curved surface (e.g. PDMS supporting membrane) a tunable compound eye system with fixed R could be designed.
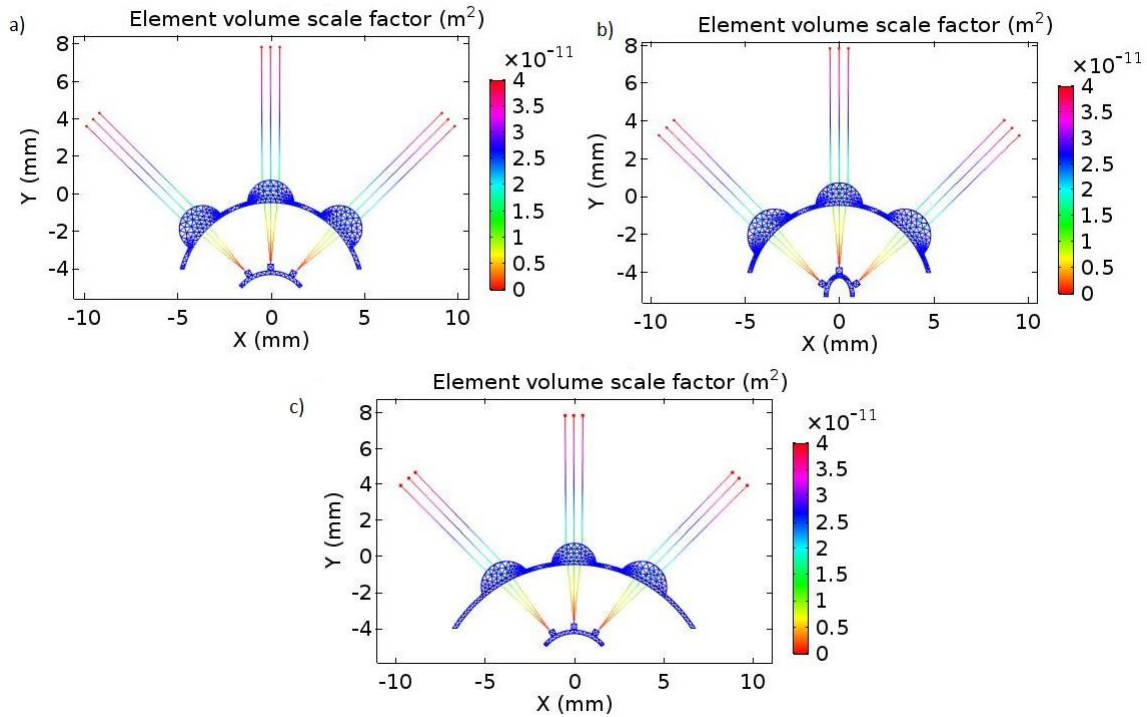
Figure 3.1 COMSOL simulation of ray tracing diagram for compound eye with individual image sensors for (a) All the lenses have identical geometry (b) Individually actuated droplets which needs changing R and (c) Tuning both curvature of the lenses and the supporting membrane prevents from changing R.

One of the limitations in optical lenses is the spherical aberration due to the non-perfect geometry of the lens. Spherical aberration is more crucial in EWOD liquid lenses due to the dynamic behavior of the liquid under applied voltage [139]. In ideal lenses, all the rays pass the exit pupil will focus at one point on the optical axis (focal point) of the lens. However, in most of the optical lenses the rays coming from the lens focus at different points resulting to degradation of image quality. Any deviation of the wavefront formed by lens from ideal spherical wavefront results optical aberration. The difference between the reference ideal sphere and the actual lens curvature is called wavefront error (aberration). A standard way to quantify the wavefront error is to calculate the optical

pass difference among all rays at the focal point. Figure 3.2 shows COMSOL simulation of spherical aberration for the liquid lens geometry that is presented in this study to analyze the performance of our lens system. The physics of geometrical optics under ray optics module was used for this simulation with ray tracing study. This physics uses a linear least-squares fit to express the optical path difference as a linear combination of a standard set of orthogonal polynomials on the unit circle, called Zernike polynomials. The 3D geometry of the lens was first created for four different R_1 and R_2 correspond to our lens geometry. An intersection point 3D data set with hemispherical surface type at focal point was used pointing from the focus toward the center of the exit pupil. Each term in normalized Zernike polynomials represent a specific aberration and $Z(4,0)$ was used for spherical aberration. This simulation demonstrates that the spherical aberration increased for a droplet on a flat substrate under applied voltage (figure 3.2b) compared to 0 V (figure 3.2a). The enhanced aberration corresponds to larger optical pass difference of the rays coming from the lens. Applying pressure to the lens changes the second lens curvature resulting to either better or worse aberration. Figure 3.2c illustrates that by precise control over the R_2, the aberration could be reduced for a lens under applied voltage. Applying higher pressure decreased the R_2 resulting to more aberration (figure 3.2d). All the simulation results correspond to the experimental result presented in figure 3.5.
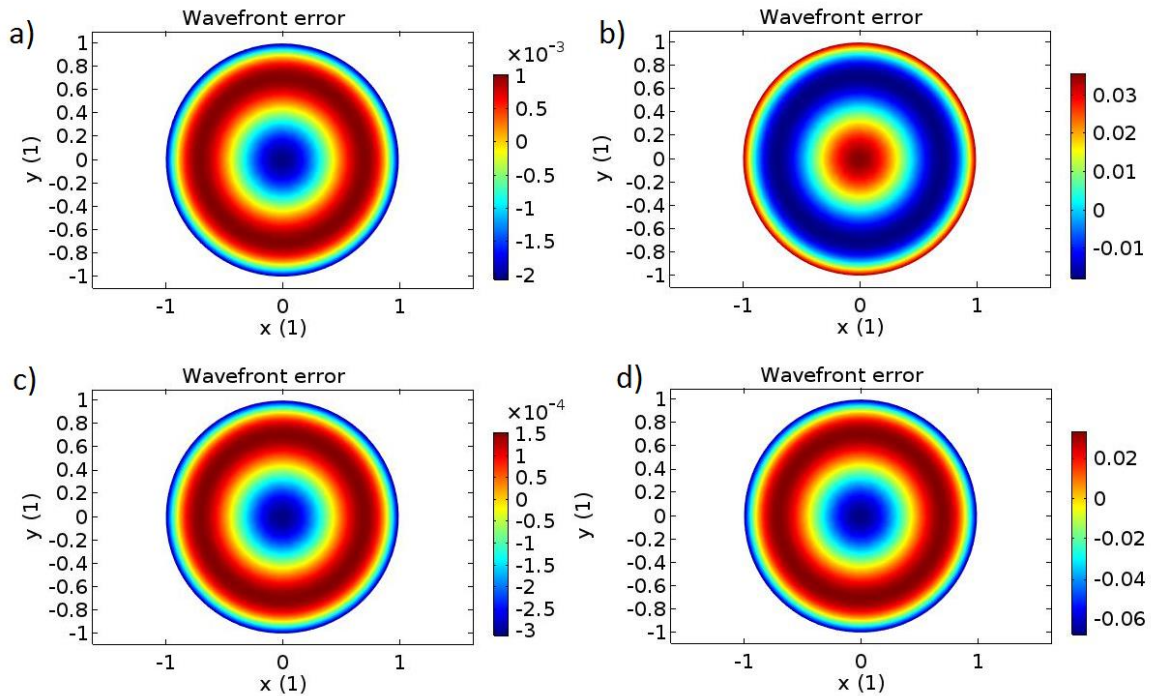
Figure 3.2 COMSOL simulation of spherical aberration for droplet geometries (a) $R_1 = 1.25$ mm, $R_2 = \infty$ (0 V, 0 mmHg) (b) $R_1 = 1.31$ mm, $R_2 = \infty$ (50 V, 0 mmHg) (c) $R_1 = 1.31$ mm, $R_2 = 65$ mm, (50 V, 30 mmHg) (d) $R_1 = 1.31$ mm, $R_2 = 40$ mm, (50 V 80 mmHg).

3.3 Experimental results

The detailed fabrication process of the liquid lens is described in section 2.3 of this thesis. Briefly, a single-layer graphene (grown by chemical vapor deposition) was transferred to the 100 µm PDMS/parylene coated Si wafer and patterned to form the planar electrodes. As dielectric and hydrophobic layer parylene and Teflon were used, respectively (1µm). Finally, the back side of the wafer was removed by deep reactive ion etching (DRIE, PlasmaTherm Bosch process) to generate free standing membrane. As a lens material, ionic liquids, with low vapor pressure and desired properties, were good candidates for EWOD application [116, 145-147]. DEME-TFSI (N,N-diethyl-N-(2-

methoxyethyl)-N-methyl-ammoniumbis(trifluoromethylsulfonyl) imide ionic liquid was used as liquid lens in this work. The height of the droplet (the lens thickness) decreased by increasing the applied voltage due to decreased contact angle (black curve in figure 3.3). Application of voltage to the droplet moved the outer edges of the droplet and spread it on the substrate resulting to smaller thickness. The outer diameter of the lens (the optical aperture diameter) changed from 2.4 mm (for 0 V) to 2.74 mm (for 100 V) corresponding to 3 µl DEME-TFSI. The center part of the membrane deflects by applying positive pressure. The membrane deflection increased by increasing the pressure changing the lens structure from plano-convex to positive meniscus (blue curve). Applying pressure to this membrane deflected the center linearly at smaller pressure while it followed the shape of a parabola at higher pressure following membrane deflection theory.

Figure 3.4 illustrates the effect of pressure on the focal length and radius of curvature of the membrane. The circular elastomer membrane deformed from plano-convex to positive meniscus under applied positive pressure. The associated focal length of the lens increased, owing to the larger curvature of the membrane. Our lens is capable of changing 0.5% focal length at 10 mmHg pressure indicating its capability for aberration correction.
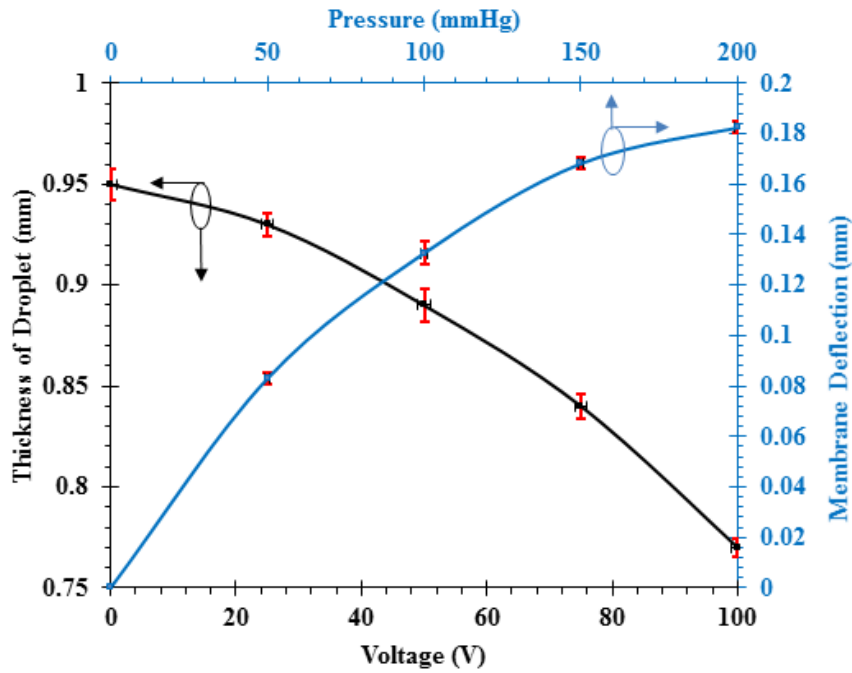
Figure 3.3 Thickness of ionic liquid droplet (black) vs voltage (left-bottom axis). The deflection of the center of membrane (blue) under pressure (right-top axis).
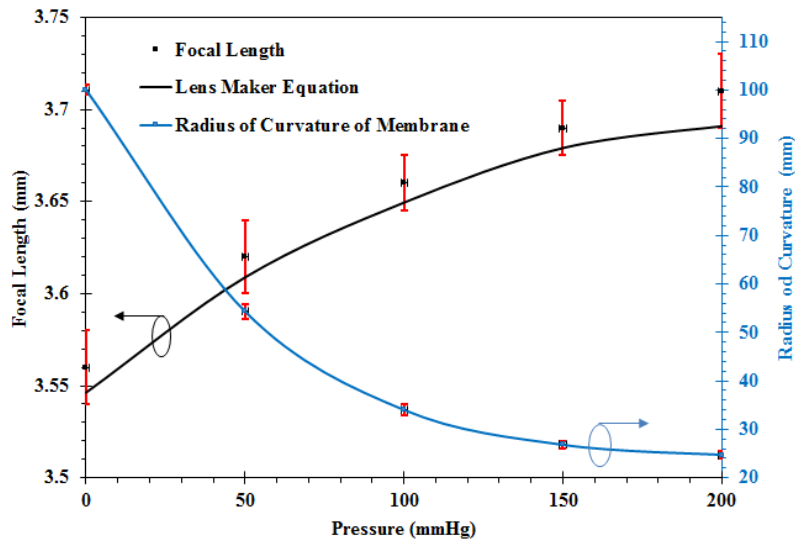
Figure 3.4 Focal length (black) and radius of curvature of membrane (blue) vs pressure. Focal length increased by increasing pressure due to the change of lens from plano-convex to positive meniscus following lens maker equation. R_2 decreased by increasing pressure resulting to more curvature of the lens following membrane deflection theory.

The imaging ability of our lens system was validated by acquiring images of 1951 USAF resolution chart through the liquid lens (figure 3.5a-d). Figure 3.5a shows the image captured through the plano-convex lens while no voltage and pressure was applied to the system. The R_1 was 1.25 mm and the focal length was 3.57 mm resulting to a magnification of 1.33. Elements 8 and 9 were tried to be in best focus in this picture. The image became dim by applying 50 V to the droplet, owing to the larger focal length associated with the larger R_1 (figure 3.5b). The R_1 was 1.31 mm and the focal length was 3.74 mm resulting to a magnification of 1.35. Although a demagnified image was expected to be observed, the image was magnified, owing to the exceeded distance between the lens and the primary principle plane (d_0) which is dominant in determining the image compared to focal length. The object were focused again by changing the lens geometry to positive meniscus by applying 30 mmHg pressure (figure 3.5c). The R_1 was 1.31 mm and the R_2 was 65 mm, the focal length was 3.78 mm resulting to a magnification of 1.326. Applying pressure to the system decreased d_0 while increasing the focal length of the lens by increasing the R_2 resulting to demagnification of the image. Figure 3.5d shows that by applying higher pressure, the resolution of the device were improved and the elements could be clearly resolved (by comparing the numbers 8 and 9 in the resolution chart). This attribute enables exceptionally high resolution images (greater than 456.1 lp/mm) associated with the positive meniscus geometry (figure 3.5e).
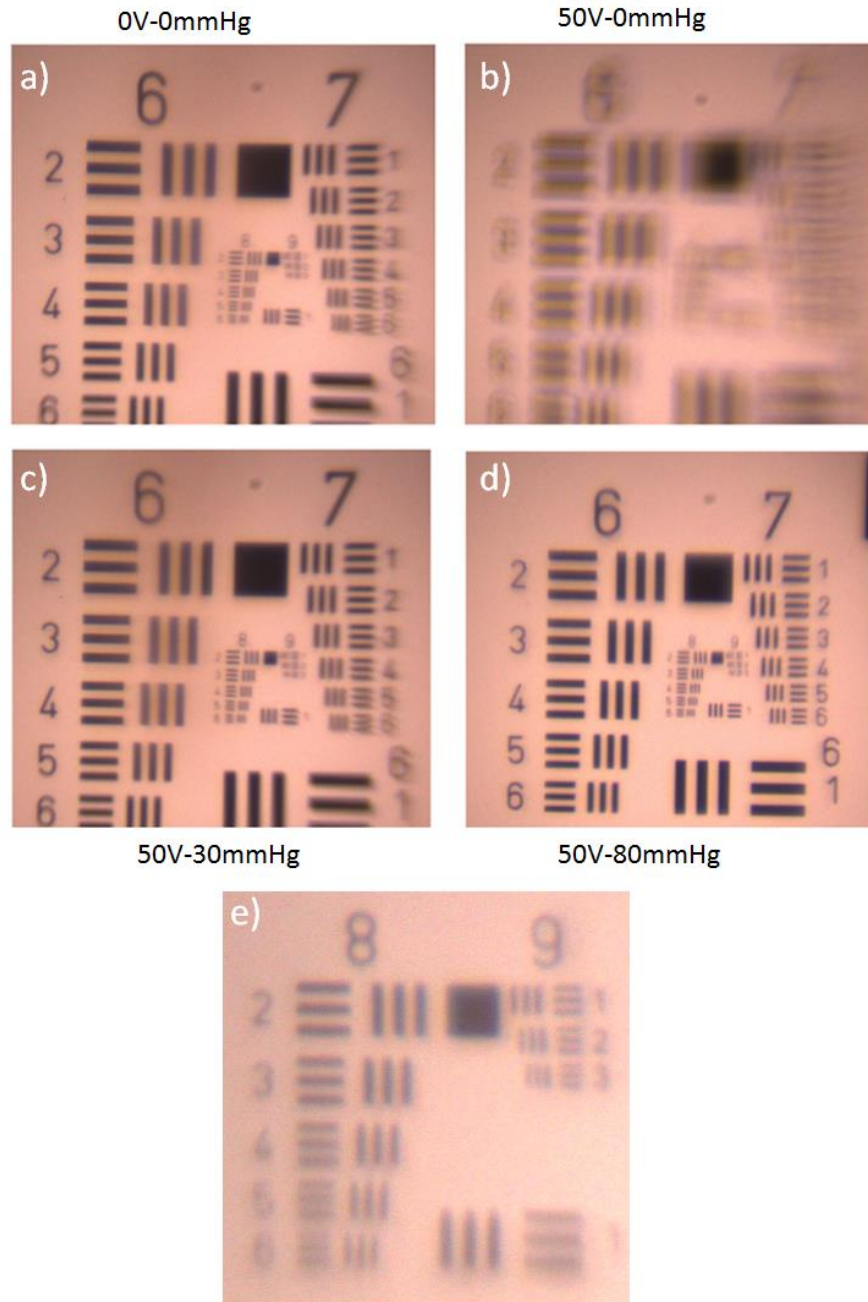
Figure 3.5 Image of object taken by liquid lens under different voltages and pressures. (a) Under no voltage and no pressure (b) Under 50 V and no pressure which increased the focal length and blurred the image. (c) Under 50 V and 30 mmHg which brought the object back in focus. (d) Under 50 V and 80 mmHg which changed the magnification and improved the resolution. (e) Magnified image of resolution chart showing elements of group 8 and 9 captured by our lens.

The focusing power of the lens was examined by real imaging configuration using a Lego structure with a smiley face as object. The Lego had two steps with 10 mm separation and the lens was placed 20 mm above the Lego. In figure 3.6 left where no voltage was applied to the droplet, the top smiley face was in focus while the bottom one was blur. Applying voltage to the electrodes increased the focal length of the lens and brought the bottom smiley face into the focus (figure 3.6 right). In this experiment the distance between objective lens and the liquid lens was fixed (90 mm) and the voltage was changed from 0 V to 100 V. The response time for this lens was 150 ms without any oscillation around the final contact angle.
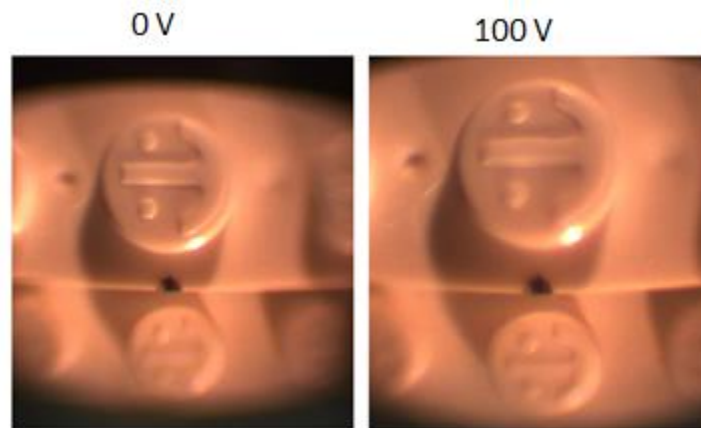
Figure 3.6 Focal length tunability of our lens examined by acquiring images of the Lego object at different distance from lens. At 0 V (left) the top smiley face is clear and the bottom one is dim. At 100 V (right) the bottom smiley face came into focus and the top one became dim.

Figure 3.7a demonstrates the prototype of the tunable compound eye with nine elemental lenses. The electrodes had a unique design in which all the elements share the same driving electrode while the reference electrodes were separated. This design allowed us to apply voltage to the elemental lenses individually. Figure 3.7b shows that

the bottom left lens (white dashed circle) was actuated while the other lenses remain constant. The number 1 in the figure was magnified at 100 V owing to the larger focal length compared to the 0 V. The dark lines in the figure are copper which was used for external connection. The key features of this design (individually control of the focal length) along with the simulation in figures 3.1 and 3.2 allow us to design a tunable compound eye with minimum aberration and no change in curvature of the sensors supporting.
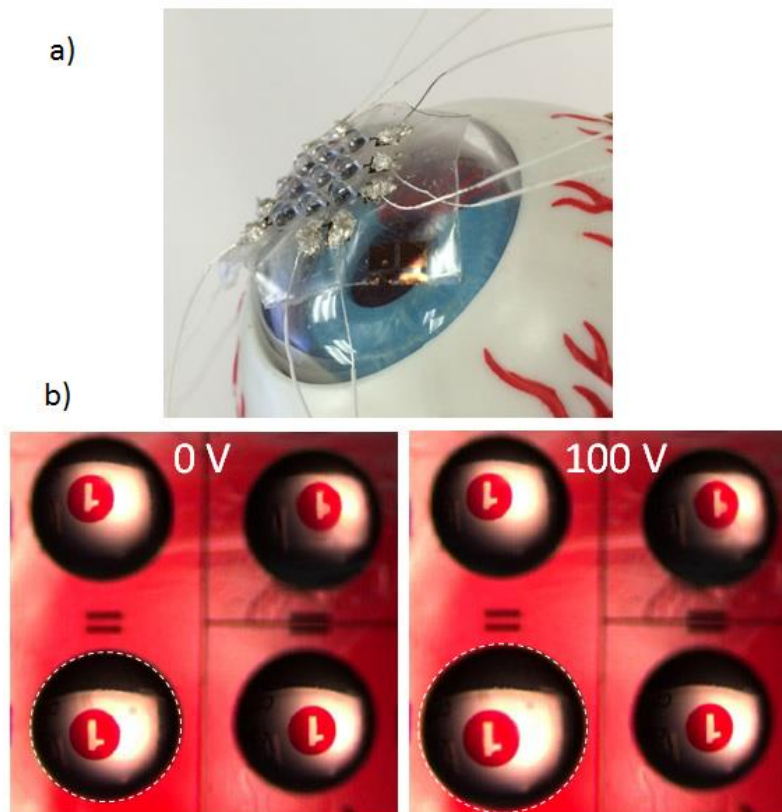
Figure 3.7 (a) Prototype of compound eye with 9 elemental lenses. (b) Individually tuning the lenses using applied voltage. At 100 V the bottom left droplet was changed and the image was magnified while the other lenses remain constant.

Table 3.1 summarizes selected tunable lenses that have been reported in the literature.

EWOD has used to change the droplet curvature in liquid lenses inside a chamber [9, 97].

Variable fluidic lenses have been fabricated using controlled deformation of liquid interface by applying pressure [148]. Elastomeric lenses have been introduced by controlling the strain on flexible elastomer [149]. Tunable lenses based on electroactive elastomer were introduced by Shian et al capable of changing both lens curvatures [150]. Pneumatic actuation can also be used to build a variable focal length for confocal endoscopy [124]. However, in all above lenses either one curvature of the lens was changed or both curvatures changed simultaneously. The liquid lens that is presented in this chapter has the advantage of changing both curvatures individually.

Table 3.1 Comparison between different tunable lenses with different materials and actuation mechanism.

Paper	Curvature change	Actuation	Lens Materials	Focal length range (mm)	Resolution (lp/mm)
Berge [9]	R_1	EWOD	Water/Oil	9	-
Li [97]	R_1	EWOD	Water oil	28	25.39
Moran [148]	R_1 & R_2	Pressure	Water	4.6	-
Liebetraut	R_1 & R_2	Strain	PDMS	2.3	-
Shian [150]	R_1 & R_2	Electrical	Electroactive	>100%	-
Kim [124]	R_1	Pneumatic	PDMS/Water	0.28	228
This work	R_1 & R_2	EWOD	Ionic liquid	4	>456.1

3.4 Conclusion

In summary, the single lens system studied here demonstrates a simple example of how changing R_2 enabled us to acquire high image quality. A key defining attribute of the single lens system is its applicability in artificial compound eyes with larger numbers

of auto focusing lenses. This design can open up new avenue in flexible technologies on transparent platform for imaging and detection purposes. Compatibility of graphene with the flexible and transparent elastomer provides the possibility of other applications to address some limitations associated with the materials. The proposed all graphene liquid lens has several unique advantages including high transparency, light weight, high flexibility, high resolution, low spherical aberration and large optical aperture. A promising topic for future work is to explore the application of this device in other area such as biology.

CHAPTER 4 INDIVIDUALLY TUNABLE LIQUID LENS ARRAYS USING TRANSPARENT GRAPHENE FOR COMPOUND EYE

4.1 Introduction

Considerable efforts have been made to develop biomimetic compound eyes [137]. The replica of 3D structures using PDMS is commonly used [134]. In recent years, MEMS have been applied to tune the focal length of the lenses, including electroactive polymer, pneumatic/hydraulic pressure or thermal actuation [141, 142, 151, 152]. The designs were effective, but typically all the lenses were actuated simultaneously.

Electrowetting on dielectric (EWOD) is the control of wettability of a conducting droplet on an electrode coated with a dielectric layer using electrical potential. EWOD has been widely used to control the shape of individual droplets on a planar rigid substrate, but it has not been applied to the droplets on a 3D curved substrate [109, 153]. Traditional transparent electrode such as indium tin oxide (ITO) lacks flexibility. Recently, graphene, a single atomic layer of carbon, has been found with excellent electrical and physical properties that are adequate for transparent and flexible electrode.

The motivation of this work is to apply graphene electrodes to a new lens design, which controls the radius of curvature of liquid droplets on a flexible membrane using both EWOD and pneumatic pressure. The graphene electrodes consist of a circular driving electrode in the center surrounded by four reference electrodes of a quadrant shape. A small gap between two electrodes functions as a dielectric layer. Miniature liquid lenses can be selectively driven by applying voltage based on EWOD. An electric field accumulates charges at the solid-liquid interface and reduces the interfacial tension

between the droplet and substrate. Graphene is highly transparent in visible light, and all the images can be visualized through the liquid lens and graphene. Because of its high optical transparency, high mechanical strength and flexibility, graphene enables a new design for fine tuning of radius of curvatures of liquid lens.

Figure 4.1 shows a schematic view of a biomimetic compound eye based on tunable liquid lens arrays in order to achieve different field of view (FOV) by adjusting individual lenses. The radius of curvature of the membrane and the droplet can be tuned by pneumatic pressure and EWOD, respectively. The pressure changes the curvature of the PDMS/parylene membrane (R_2), which increases FOV. The focal length of individual lens can be adjusted individually by applying voltage to each graphene electrode. Graphene is the only transparent electrode that is adequate for this design due to high degree of flexibility and mechanical strength.
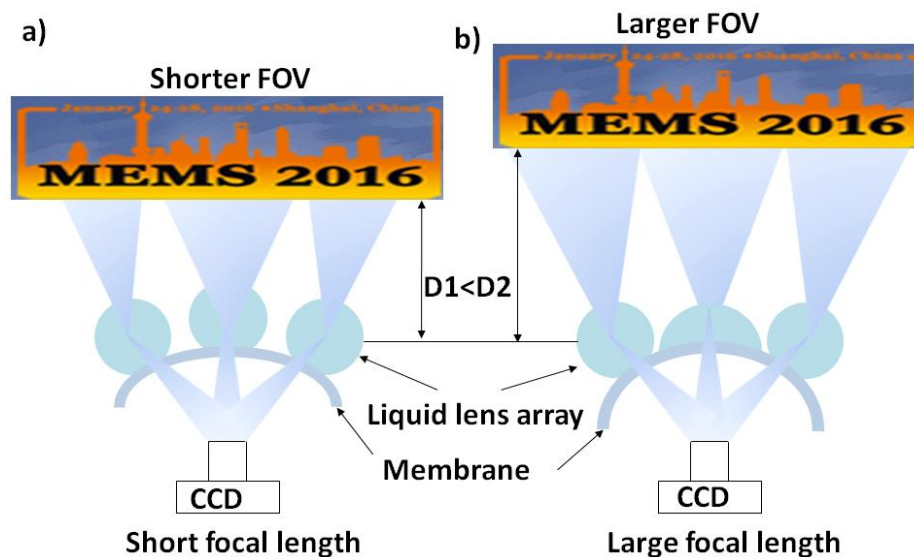
Figure 4.1 A schematic view of the device that mimics the compound eye of the insect (a) No voltage and a larger radius of curvature of the membrane result in shorter FOV and (b) With applied voltage and membrane deformation, larger FOV is expected.

4.2 Experiment

The process flow of the device fabrication is shown in figure 4.2. PDMS (200 µm) was first spin coated to a silicon wafer and cured. A thin parylene layer (2.5 µm) was then deposited on the top of PDMS to form a hybrid membrane for the lens array. Graphene was grown by a chemical vapor deposition (CVD) method using a copper foil (Alfa Aesar) as catalyst [113]. The CVD grown graphene was covered with a thin PMMA layer. Then the copper was etched using a solution of 1M ferric chloride (FeCl$_3$) and deionized water (with ratio of 1:10 in volume) overnight. The floating graphene/PMMA sheets were carefully transferred to the membrane following the PMMA removal using acetone. The surface of the parylene was treated with oxygen plasma for 20s right before the transfer in order to improve the adhesion between parylene and graphene. Both driving and reference electrodes were formed by patterning graphene with a special concentric design in which all the driving electrodes were connected to each other. A thin copper (150 nm) was deposited using electron beam evaporation and patterned as external contact pads. Parylene (1µm) was deposited using CVD as dielectric layer. Teflon (DuPont AF 1600 1% in 3M FC 72) was then coated to the whole device as hydrophobic layer. Finally, the droplets were carefully dispensed to the center of each driving electrodes. A prototype of a 3x3 array of liquid lenses on a curved substrate is shown in bottom right of figure 4.2. The advantage of this design is the droplet was separated from both reference and driving electrodes with parylene which prevents the hydrolysis.
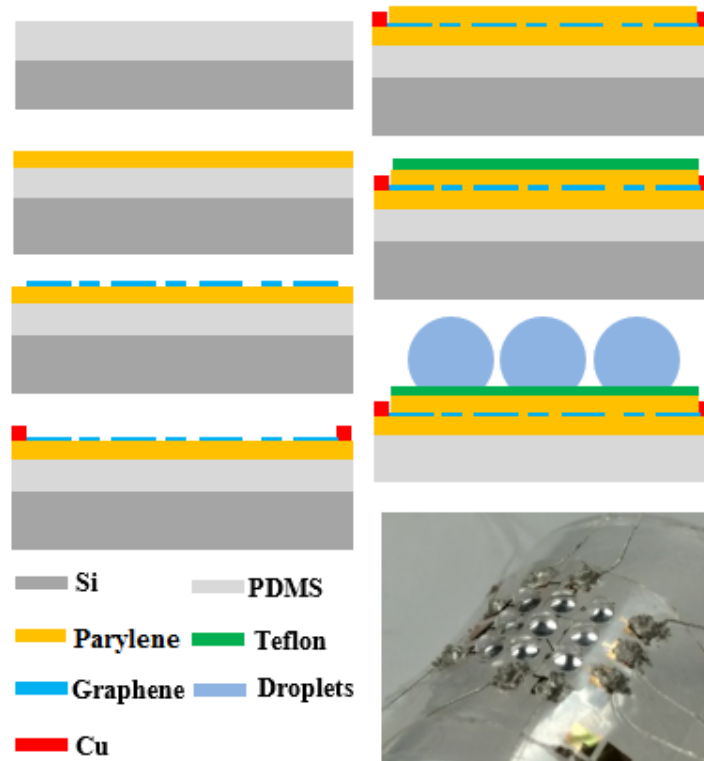
Figure 4.2 The fabrication process flow. Parylene was deposited on top of a PDMS-coated Si wafer. The graphene was transferred and patterned. Cu was deposited for external contact pads and a thin parylene was coated as a dielectric layer. Teflon was spin-coated as a hydrophobic layer. (Bottom right) the final fabricated device.

The optical setup for focal length measurement and imaging consists of an optical microscope with different zoom lenses, a USB CCD camera (Infinity), a three-axis stage and a flexible optical fiber light source. The image of the object was first captured without liquid lenses and the size of the image (h_0) was recorded. Then, the device was mounted on the three-axis stage and a focused image of the object (h_I) was captured through the liquid lens by adjusting the distance between the device and the object (d). Finally, the focal length was calculated using $f = Md / (M+1)$, in which M (h_I / h_0) was the magnification. An AC voltage was applied to the device using a function generator

(Agilent 33120A) connected to a power amplifier. The system could generate AC voltages from 0~130V with a frequency from 10 Hz to 10 kHz. Droplets of ionic liquid (N,N-diethyl-N-(2-methoxyethyl)-N-methylammoniumbis-(trifluoromethylsulfonyl)-imide (DEME-TFSI) and 10 mM KCl solution with 3 µl volume were used as liquid lenses.

4.3 Result and discussion

Figure 4.3 demonstrates the feasibility to control lens individually. Application of a voltage decreased the contact angle at the three phase contact line. The figure shows the lens array consists of 3 droplets on top of object (alphabetic letters ABC and H). The letters A and B were in focus through the central lens at 0 V. Application of a voltage (100 V) to the middle droplet brought the letter C in FOV in addition to A and B (bottom figure).
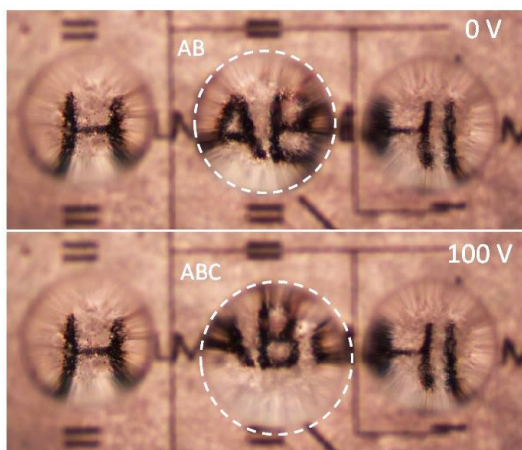
Figure 4.3 The actuation of an individual lens. The center lens was actuated to get both larger FOV and longer focal length using EWOD.

The response of an aqueous droplet (10 mM KCl) to the applied AC voltages (1 kHz) from 0V to 130 V is shown in figure 4.4a. The initial contact angle at zero volt was

around 110° due to the hydrophobic Teflon layer. The droplet analysis tool of the ImageJ software was used to measure contact angle. When the voltage was gradually increased, the contact angle of the droplet started to change at around 30 V. Further reduction of contact angle was observed at higher applied voltages. Meanwhile, the contact angle saturation was observed at voltages above 130 V which limited the further contact angle change. Matlab simulation was performed to depict the expected contact angle versus voltage using the modified Lippmann-Young equation for planar electrodes [80]. The fitting parameters include: the initial contact angle (θ_0) of 110.7^o, the surface tension (γ) 72.7 dyn/cm and the dielectric thickness of 1 μm. Our experimental results show that the KCl droplets responded faster to electric potential compared to ionic liquid which was due to higher viscosity of the ionic liquids. The focal length vs voltage is plotted in figure 4.4b for the droplets (10 mM KCl) of three different sizes. The focal length measurements were carried out based on the above mentioned method. The small contact angle of the droplets with applied voltage resulted in a higher radius of curvature and a higher focal length. Furthermore, increasing the volume of the droplet enlarged the initial radius of the curvature resulting to a larger initial focal length. The experiment shows that for the same volume of the ionic liquid, the focal length was larger compared to KCl due to lower surface tension of ionic liquids where the initial contact angle was smaller. However, the droplet oscillation was damped out in ionic liquid compared to KCl due to higher viscosity of the ionic liquids.
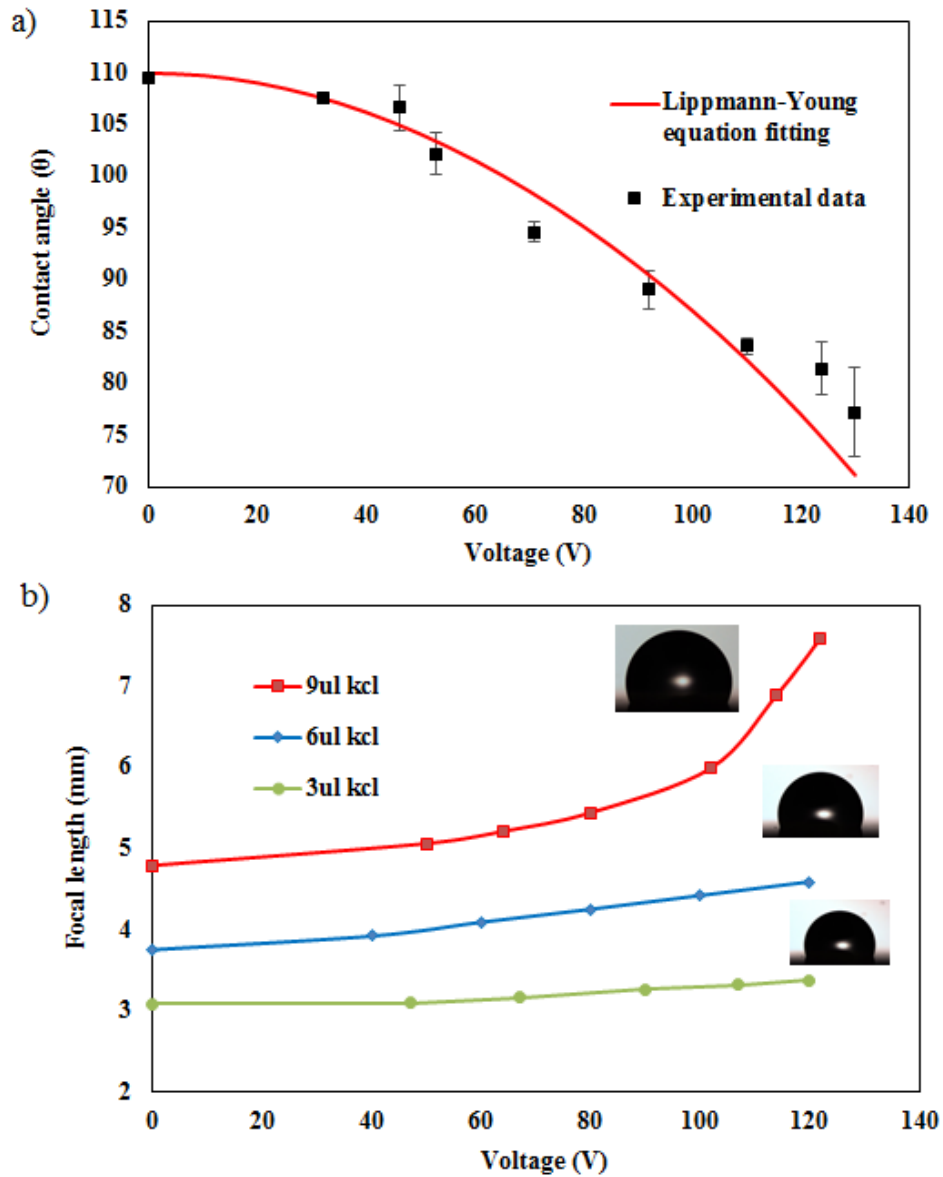
Figure 4.4 (a) Contact angle change vs applied voltage. The contact angle reduced upon applied voltages. Contact angle saturation was observed at voltages above 130 V. The error bars shows standard deviation about the mean contact angle. (b) The focal length change vs voltage for 3 different sizes of the droplets. The larger volumes of droplets have a larger focal length due to a larger radius of curvature.

Since the membrane was flexible, the radius of curvature of the membrane could be

tuned using mechanical forces or pneumatic pressure in order to increase the FOV. Figure

4.5a compares the images of an object under flat and curved membranes. The magnified image under curved membrane illustrates that the FOV could be enlarged by adjusting the curvature of the membrane. In most literature of lens design, tuning the membrane has been applied to reduce the spherical aberration which exists in liquid lenses. Figure 4.5b shows the concept of FOV enlargement with 3 lenses. The logo of MEMS 2016 conference was used as an object for this experiment. This figure shows that different part of "MEMS 2016" could be visualized in every single lens. The compound eye of the insect follows the same principle for visualization of the large object. Each single lens of the eye captures a part of the object and then the whole image of the object can be reconstructed.
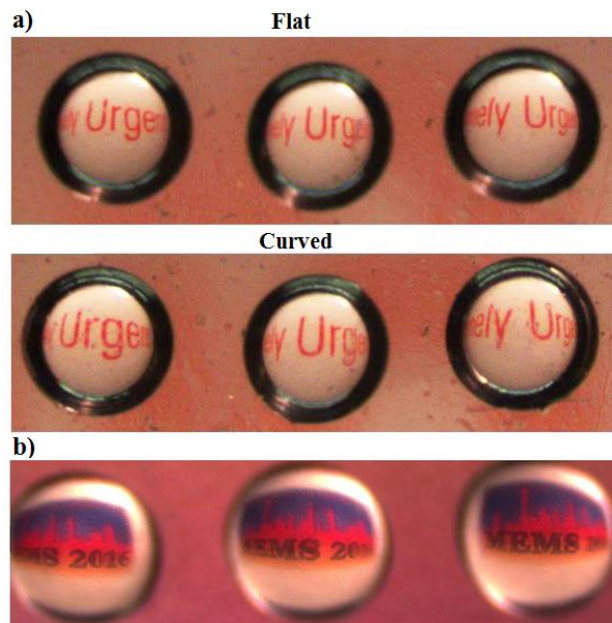
Figure 4.5 (a) Increasing field of view by tuning the membrane curvature. (b) Increasing field of view using lens array.

Table 4.1 summarizes some of the liquid lens arrays in the literature. Most of the liquid lens arrays were fabricated on flat substrates and ITO and gold have been widely

used as electrodes. ITO is transparent but mechanically brittle which limits its application where tuning substrate curvature is required. In contrast, gold is flexible but not transparent and rather expensive. The liquid lens array that is presented in this work was made on highly flexible membrane which is capable of adjustment of both the radius of curvature of the lens and the membrane. Graphene is the only transparent and flexible electrode which is utilized for the first time for liquid lens applications. Furthermore, our lens arrays are capable of selective actuation of individual lenses by a specific planar electrode design.

Table 4.1 Comparison between previous works with the present work.

Paper	Actuation voltage (V)	Focal length (mm)	Diameter of the lens (mm)	Substrate
Nguyen [151]	0-250	0.8-3.8	0.02-10	Flat
Smith [109]	0-25	-2.77-4.34	0.3	Flat
Murade [153]	0-150	2.5-8.5 (single lens)	0.2(array)-1.2(single)	Flat
Wei [141]	-	2.1-74.2	2	Flexible
This work	0-130	3-8	0.5-3	Flexible

4.4 Conclusion

An array of liquid lenses was designed and fabricated on a transparent and highly flexible membrane. Single layer graphene was grown and transferred to PDMS/parylene membrane. Flexible graphene electrodes with specific planar design enable switchable actuation of liquid lenses. Every single lens can be actuated by EWOD and mechanical pressure. Tunable range of focal length between 3-8 mm has been achieved upon applied

voltages between 0-130 V without hydrolysis. The focal length can be further increased by increasing the volume of the droplets. Furthermore, larger FOV has been observed by tuning the radius of the curvature of the membrane. One of the potential applications of this device is a compound eye camera where a lens array is arranged on a flexible supporting.

CHAPTER 5 Self-Powered and Transparent All-Graphene Biosensor

5.1 Introduction

With the advent of microsystem engineering and wireless communications, the wireless health and wearable sensors have emerged as an active area of research. The passive and chipless radio frequency identification (RFID) sensing tags have gained considerable attention, due to their simplicity and low fabrication cost. The success of harmonic radar in tracing tiny objects with vanishingly small radar cross sections has inspired the development of interference-free harmonic sensors that has recently generated a lot of interest among the RFID and sensor community. This wireless sensor receives a fundamental tone and re-transmits a modulated signal at the orthogonal frequency, e.g. second harmonic, in such a way that the unwanted clutter echoes and back-scattered noise can be suppressed, enabling much higher sensitivity and detectivity compared with conventional backscatter-RFID tags. Here, we propose a new paradigm of all-graphene harmonic sensor for the wireless diagnosis of molecular, bacterial, and infectious agents [154, 155], as illustrated in figure 1a. Graphene is known as the first ever discovered 2D material that comprises single or few layers of carbon atoms. Thanks to its extreme thinness, graphene can be optically transparent, flexible and stretchable. In addition, the conductivity of graphene can be readily tuned by chemical and electrostatic gating [156, 157]. It has been demonstrated that a sensor based on the graphene field-effect transistor (GFET) can have a molecular-level sensitivity to certain gases, chemical, and bimolecular agents, offering a feasible way for the practical realization of highly-sensitivity implantable nanosensors. Figure 1b schematically shows the all-graphene

harmonic sensor that comprises (1) a GFET-based circuit that monolithically integrates the sensing and the frequency modulation functions, and (2) a transparent, ultrabroad-band (UWB) graphene monopole antenna connected to the circuit through a RF diplexer. The excellent physical flexibility and optical transparency of graphene may make this nanomaterial-based harmonic sensor, particularly desired for eye-wearable devices that detect, for instance, the pathogen and infectious keratitis of interest in real time, as shown in figure 1a.
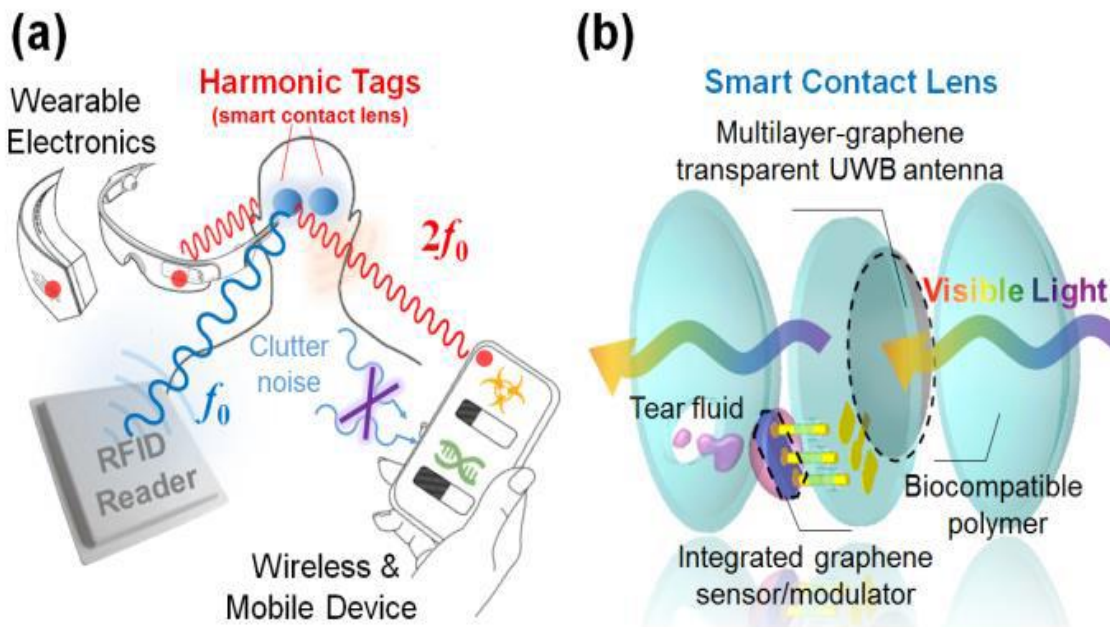
Figure 5.1 (a) Schematics of the battery-free and transparent harmonic sensor designed for various point-of-care monitoring and wireless sensing applications, such as smart contact lenses and microscope slides. (b) All-graphene harmonic sensors comprising a GFET-based sensing-modulator and a transparent graphene antenna on a biocompatible soft polymer.

5.2 Self-powered, chemical-offset frequency modulator based on graphene transistors

Figure 2a shows the fabricated back-gate GFET and the measured drain current–gate voltage (I_{DS}-V_{GS}) characteristics, which shows the unique "V-shape" curve resulted from the ambipolar charge transport [157, 158]. Such symmetric I_{DS}-V_{GS} characteristic has been proposed to realize an efficient frequency modulator (doubler), converting the input RF signal into its second harmonic [158], without any need for filters. This is, however, not available with the conventional solid-state transistors. In addition, a GFET shows an interesting self- gating effect: when n-/p-type chemical agents (e.g. bacteria) bind to the surface of graphene channel, a shift in Dirac point (or charge neutral point Vcnp) may alter the bias point and thus the nonlinear conversion gain. Figure 2a reports the measured the IDS-VGS characteristics for a GFET functionalized with the E.Coli tail-specific protease (TSP) (which serves as a specific binding site for the bacteria under detection) before and after the attachment of E.Coli bacteria. It is clearly seen that when the E.Coli bacteria is attached on the GFET, the Vcnp experiences a p-type shift.

Combining the chemical sensitivity of graphene and the RF frequency doubling effect in a GFET may achieve a wireless biosensor that can detect the bacterial exposure, by launching a monotone RF input signal and detecting the amplitude variation in the output second harmonic. We note that the sensing and frequency modulation functions, typically requires two individual components if realized with the traditional semiconductor circuit, can be realized within a single GFET. This significantly reduces the integration complexity, cost, and size of a harmonic sensor. Figure 2b shows the RF setup of such

single-GFET harmonic sensor, and the simulated results for the output second-harmonic signals with and without the binding of E.Coli bacteria; the circuit simulation was based on the physics-based drift-diffusion model for a back-gate GFET [157]. It is seen that the amplitude of second harmonic generated by the GFET biosensor is modulated by the bacterial binding. By choosing the suitable biomolecular binding site, selective to specific molecular agents, the GFET wireless sensor may be applicable for versatile biosensing platforms
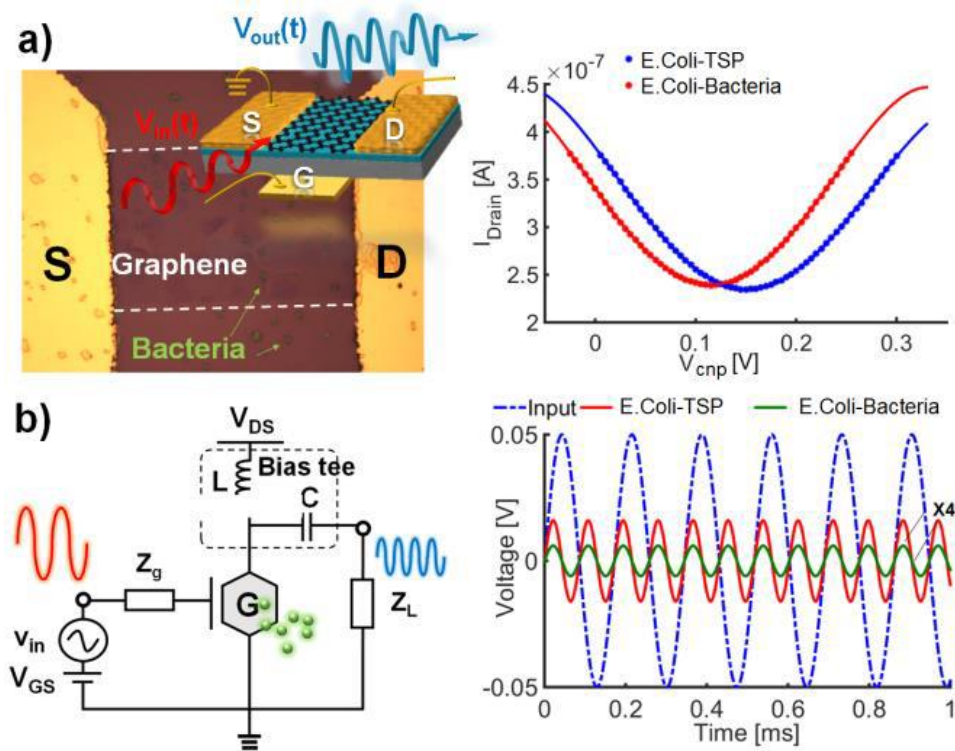
Figure 5.2 (a) Microscopic image of the back-gate graphene field-effect transistor and its measured drain current-gate voltage characteristics with (red line) and without (blue line) the bacterial binding. (b) A frequency-modulated sensor based on a single graphene transistor (left) and the simulated second-harmonic output for different surface conditions of graphene channel.

Although a single GFET can already combine multiple functions in a compact size, it still requires a drain-to-source dc bias to operate properly. For ubiquitous wireless sensor

network applications, fully passive sensor nodes that need no battery or power-harvesting module are preferred, in order to minimize the cost and simplifying the maintenance. Here, we also propose a self-powered harmonic sensor based on four GFETs constituted into a quad-ring-mixer topology, as shown in figure 3a. In this RF circuit, the cross-coupled GFETs, acting as biochemical receptors, constitute a fully passive nonlinear frequency doubler. The onset voltage of each GFET is varied when it is exposed to the specific biomolecular agents. This implies that the magnitude of second-harmonic output is modulated by the absorption of biomolecular agents onto the graphene surface (figure 2a). This GFET-based ring balancing circuit can be self-biased, without any need for battery or continuous wave as extra power source. Figure 3a also shows the simulated waveforms for the fundamental tone and the second-harmonic output for the proposed self-powered GFET circuit, with and without the bacterial binding. We find that the self-frequency-modulation for a RF signal is possible even without the dc bias, and the second-harmonic conversion gain is quite sensitive to V_{cnp}, reflecting the exposure condition of biochemical surface dopants. In practice, V_{cnp} can be tuned chemically over a wide range in a back-gate GFET, depending on the concentration of bacteria. Figures 3b show the system block diagram for the self-powered all-graphene harmonic sensor, in comparison with the traditional harmonic sensor. A diplexer comprising the UWB antenna and microfabricated low-pass filter (LPF) and high-pass filter (HPF) can couple the received fundamental tone into the GFET circuit and outcouple the modulated second harmonic signal back to free space (readers). A properly designed diplexer can eliminate possible RF interference and intermodulation between different harmonic tones. When

compared to a conventional wireless sensor (figure 3b), our all-graphene sensor circuit may remove the need for frequency modulator and/or rectifying component (energy harvesting circuit), thus significantly reducing size and integration complexity of the device.
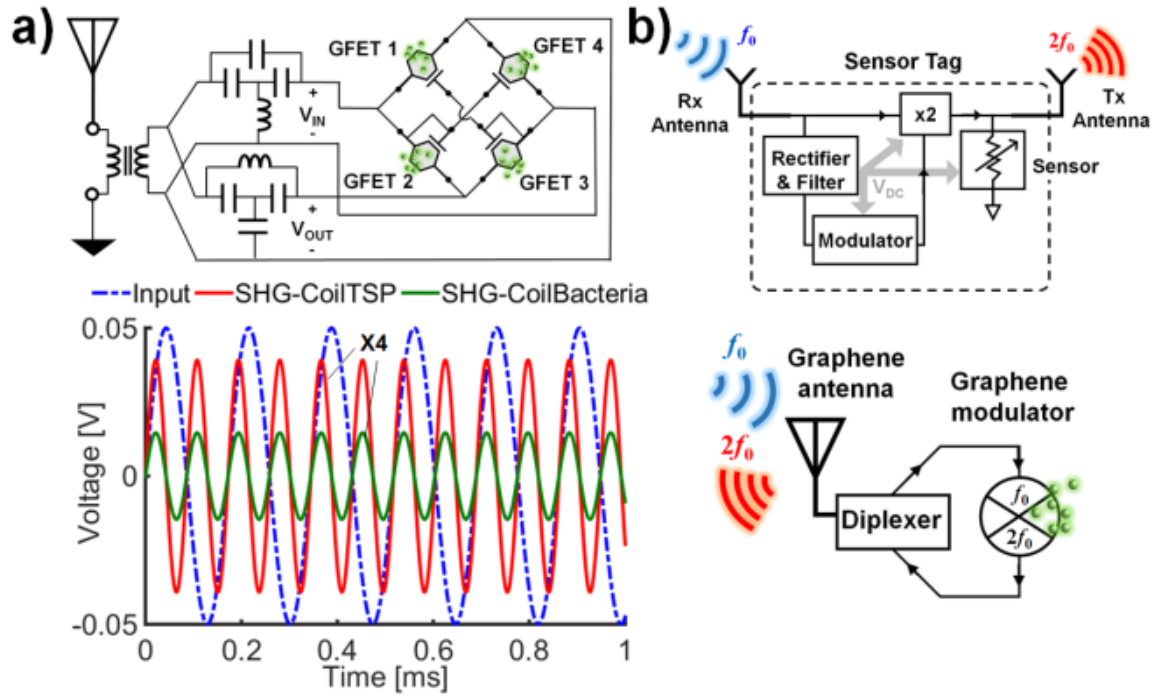
Figure 5.3 (a) Circuit designs for a self-powered, all-graphene harmonic sensor (top) and the simulated second-harmonic output waveform with and without the bacterial binding on graphene transistors (bottom). (b) System diagram of the traditional harmonic sensor that requires sensor, frequency modulator, two antennas, and possibly ac-to-dc rectifier (top), and the proposed compact, low-cost graphene harmonic sensor, realized with a single sensor-frequency modulator circuit and a shared UWB antenna for both fundamental tone and second harmonic (bottom).

5.3 Design of transparent graphene antenna

With the aim of making the whole sensor system compact and light-weight, we have designed and fabricated a broadband graphene monopole antenna, which is connected to a lumped-element-based diplexer (figure 3a). We have designed a coplanar waveguide

(CPW)-fed graphene monopole antenna on a flexible, transparent and biocompatible polyethylene terephthalate (PET) substrate. Here the graphene monolayer was prepared by the chemical vapor deposition (CVD). The CVD grown graphene was then transferred to the PET substrate, followed by the photolithographic patterning and the (Oxygen plasma) dry etching. The transfer process was repeated several times to make the multi-layered graphene. Finally, copper was deposited by E-beam evaporation and lithographically patterned as the CPW feed. In the RF regime, although a graphene antenna offers advantages of lightweight and optical transparency, it may be less efficient compared with the printed metallic antennas, due to its relatively high electrical resistance. In order to mitigate the low radiation efficiency and the difficulty in impedance matching, we investigate here the RF antenna made of multi-layered graphene, whose conductivity would increase with increasing the number of graphene layers. Figure 4a shows the fabricated transparent graphene antenna with different number of stacked monolayers. As expected, when a multilayered graphene is used, the opacity is somewhat sacrificed. Still, a high transparency can be obtained, even with 8 graphene monolayers.
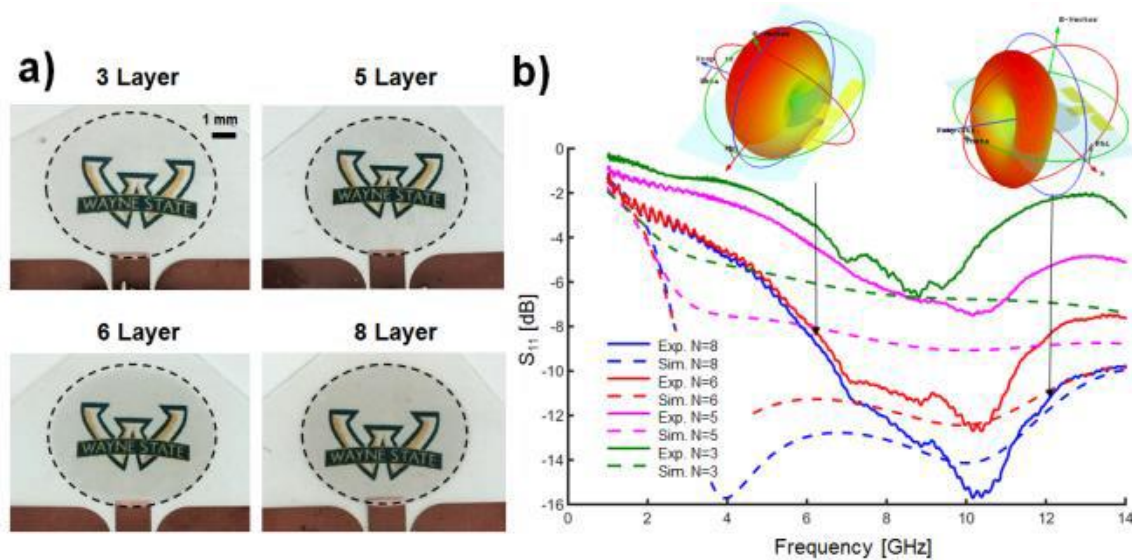
Figure 5.4 (a) Photography for multi-layered graphene UWB antennas with different number of stacked graphene monolayers. (b) Measured (solid lines) and simulated (dashed lines) return loss for different graphene antennas in (a).

Figure 4b shows the experimental and numerical results for return loss (S11) of the graphene antenna in figure 4a. In our numerical modeling, the full-wave electromagnetic simulation was conducted, with the dynamic conductivity of graphene being modeled by the semiclassical Kubo formula [159, 160]. Here an elliptical graphene sheet has a long-axis diameter of 7 mm, short-axis diameter 5.9 mm, a Fermi energy of 0.25 eV, and a phenomenological scattering rate of 41.3 meV. It is evident from figure 4b that the return loss can be improved by increasing the number of graphene layer, which is verified both experimentally and theoretically. The measured return loss shows a moderately broadband bandwidth of operation, which may find potential applications in UWB communication systems that require a high transparency. For a 8-layer-graphene antenna, the calculated radiation efficiency is 40 % ~ 55 % in the frequency range 3 GHz to 15 GHz. For a 3-layer graphene antenna, although being almost invisible in the visible light

spectrum, shows a high reflection (S11) and a low radiation efficiency of 10% ~ 20% in the same frequency range. We expect that the radiation efficiency and return loss of the graphene antenna can be further improved by increasing the number of graphene monolayers, which is experimentally feasible. This transparent, broadband monopole antenna, when used in the harmonic sensor system, allows for receiving the RF carrier frequency of 5.8 ± 0.75 GHz (C band) and re-transmitting the modulated signal at 10.7-12.2 GHz (X band), which are compatible with the FCC protocol. The inset of figure 4b also shows the simulated radiation pattern for this graphene antenna, showing a satisfactory radiation directivity comparable to a linear monopole antenna.

5.4 Conclusion

We have proposed a new class of wireless, self-powered and transparent biosensor, comprising monolithically integrated graphene antenna and a graphene (quad-ring) circuits with dual sensing-frequency modulation functions. The unique ambipolar charge transport in graphene transistors and their constituted circuit may allow efficient frequency multiplication with the conversion gain varied by the biomolecular and chemical exposures. The proposed harmonic-based wireless sensing scheme may be resilient to the background clutters and multiple-scattering noises. This all-graphene wireless sensor can be light-weight, flexible, and optically transparent, thanks to the excellent mechanical and optical properties of graphene. We have also demonstrated the applicability of the multilayered graphene to the realization of a transparent UWB antenna. We believe that this all-graphene wireless sensor may benefit a variety of

wireless health and wearable technologies on transparent platforms, sensing PH/gas/molecular/chemical adhesions.

CHAPTER 6 CONCLUSION AND FUTURE WORKs

6.1 Conclusion

In this work, we developed liquid lenses based on EWOD using CVD graphene as electrodes. Compared to traditionally EWOD lenses inside the chamber, we have used planar electrode design where no sidewall electrode deposition is required resulting to easier fabrication process. The focus of this work was mostly on applying graphene in liquid lenses where transparent and flexible electrodes are required. The advantage of graphene compared to non-transparent electrodes is the larger optical aperture in graphene devices where planar electrodes are implemented. Moreover, the flexibility of graphene enabled us to implement the lenses on curved structure to increase the field of view. Compared to previous EWOD lenses on planar electrodes where an opening was created on both electrodes and the dielectric layer, parylene was used as dielectric in our device without opening that enabled us to apply higher voltages without hydrolysis.

In chapter two, we developed an EWOD lens using both salt solution and ionic liquids. We first used COMSOL software to study the droplet dynamic behavior toward the final contact angle a few miliseconds after voltage was applied. We found the differences between ionic liquid and KCl solution in which the KCl solution responded faster to the applied voltage while oscillating toward the final contact angle. This was due to the higher viscosity of the ionic liquid compared to KCl solution. Then, we investigated the droplet response for both droplets experimentally. We demonstrated that for 3µl droplet, the contact angle change was larger for ionic liquid compared to the KCl solution. This resulted to higher focal length change for ionic liquid solution. The optical

performance of the device was also performed using the liquid lens. Based on the experiments, the image of the object became blur under applied voltages owning to the larger focal length of the lens. This attributes resulted from the larger radius of the curvature of the lens under applied voltage. In addition, the lens device show small contact angle hysteresis in the case of ionic liquid compared to KCl solution. The device was further investigated on a curved structure showing higher field of view. In order to evaluate the resolution of device in a real application, we utilized the liquid lens to visualize BMDCs. We demonstrated that the device was capable of focusing on the cells under applied voltages. Thus, the device is promising in applications where a flexible lens with high resolution is required.

In chapter three, we reported a lens capable of changing both curvatures (R_1 and R_2). R_1 was manipulated using EWOD phenomenon while applied pressure was used to change R_2. The motivation of this work was to reduce the spherical aberration and propose a system for future compound eye. We first utilized COMSOL to demonstrate the concept of tunable compound eye using an array of tunable lenses on a tunable curved structure. We showed that the tunable compound eye enable us to manipulate both R_1 and R_2 so no change in curvature of the sensors supporting is required. The spherical aberration was then investigated by using device geometries under applied voltage and pressure. We demonstrated that by fine tuning both curvature of the lens, the spherical aberration could be significantly reduced. The radius of the curvature of the membrane was altered using applied pressure. For the first time, we proposed a device that is capable of changing the R_2 in a liquid lens resulting to higher focal length. The imaging

performance of the lens was also validated by using both voltage and pressure. We demonstrated that the image of the object beneath the lens could be further improved by changing R_2 while the droplet curvature was altered. In addition, the resolution of the device was increased applying higher pressure to the membrane compared to the device on a flat surface. The imaging ability of the device for the object farther than the focal point was also shown in this work. Finally, a prototype of the compound eye was proposed capable individually tuning the lenses.

In chapter four, we proposed an array of tunable liquid lenses on a flexible membrane. We demonstrated that with specific design of the electrodes, liquid lenses could be individually tuned, a feature that is useful to solve the gap mismatch for the lenses close to the edge. We have shown that the range of focal length could be altered by manipulating the size of the droplet for different applications. Individually tuning the lenses provides freedom in designing compound eye lenses with wider field of view.

6.2 Future works

This thesis has demonstrated tunable liquid lenses utilizing both flexibility and transparency of graphene. Although this work gives proof of concept for EWOD lenses using graphene, this is not the end and there are number of challenges that need to be addressed. The liquid lenses that we have demonstrated here don't have housing which is required in applications where movement is unavoidable. One can work on the housing of this lens to make a system that is more robust. One suggestion for this is to use parylene deposition directly on top of the liquid. However, the liquid should low vapor pressure that can tolerate the high vacuum during the deposition. In addition, two immiscible

liquids could be also used for the lens with carefully designing electrodes and appropriate size of the liquids. Then thin layer of parylene could be deposited to cover the lens. A chamber can be used for the case of two immiscible liquids where no sidewall electrode deposition is required. For this case, despite the current EWOD lenses inside the chamber where the contact angle moves on the sidewalls, the contact angle moves on the bottom surface. Moreover, a compound eye lenses with individual sensors could be manufactured capable of image reconstruction. This could be implemented inside a camera for larger field of view and low aberration. It would also be interesting if one can find some other applications using EWOD actuation mechanism in display technology, biology, and everything that needs both transparency and flexibility.

Graphene is promising nanomaterial for future MEMS RF Antenna. Transparent and flexible sensors could be exploited based on graphene radio frequency components. These sensors could be designed to be self-powered wirelessly which is beneficial in wireless health and wearable technologies on transparent platforms.

REFERENCES

[1]   G. Lippmann, "Relations entre les phénomènes électriques et capillaires," Gauthier-Villars, 1875.

[2]   G. Beni, S. Hackwood, and J. Jackel, "Continuous electrowetting effect," *Applied Physics Letters,* vol. 40, pp. 912-914, 1982.

[3]   G. Beni and S. Hackwood, "Electro‑wetting displays," *Applied Physics Letters,* vol. 38, pp. 207-209, 1981.

[4]   R. A. Hayes and B. Feenstra, "Video-speed electronic paper based on electrowetting," *Nature,* vol. 425, pp. 383-385, 2003.

[5]   J. Heikenfeld and A. Steckl, "High-transmission electrowetting light valves," *Applied Physics Letters,* vol. 86, p. 151121, 2005.

[6]   P. Sen and C.-J. Kim, "A fast liquid-metal droplet microswitch using EWOD-driven contact-line sliding," *Microelectromechanical Systems, Journal of,* vol. 18, pp. 174-185, 2009.

[7]   J. Crassous, C. Gabay, G. Liogier, and B. Berge, "Liquid lens based on electrowetting: a new adaptive component for imaging applications in consumer electronics," in *Photonics Asia 2004*, 2004, pp. 143-148.

[8]   G. Beni and M. Tenan, "Dynamics of electrowetting displays," *Journal of applied physics,* vol. 52, pp. 6011-6015, 1981.

[9]   B. Berge and J. Peseux, "Variable focal lens controlled by an external voltage: An application of electrowetting," *The European Physical Journal E,* vol. 3, pp. 159-163, 2000.

[10] H. Dahms, "Electrocapillary Measurements at the Interface Insulator‐Electrolytic Solution," *Journal of The Electrochemical Society,* vol. 116, pp. 1532-1534, 1969.

[11] W. C. Nelson and C.-J. C. Kim, "Droplet actuation by electrowetting-on-dielectric (EWOD): a review," *Journal of Adhesion Science and Technology,* vol. 26, pp. 1747-1771, 2012.

[12] J. Lee, H. Moon, J. Fowler, T. Schoellhammer, and C.-J. Kim, "Electrowetting and electrowetting-on-dielectric for microscale liquid handling," *Sensors and Actuators A: Physical,* vol. 95, pp. 259-268, 2002.

[13] H. Moon, S. K. Cho, and R. L. Garrell, "Low voltage electrowetting-on-dielectric," *Journal of applied physics,* vol. 92, pp. 4080-4087, 2002.

[14] N.-T. Nguyen and S. T. Wereley, *Fundamentals and applications of microfluidics*: Artech House, 2002.

[15] L. Dong and H. Jiang, "Selective formation and removal of liquid microlenses at predetermined locations within microfluidics through pneumatic control," *Microelectromechanical Systems, Journal of,* vol. 17, pp. 381-392, 2008.

[16] M. Vallet, B. Berge, and L. Vovelle, "Electrowetting of water and aqueous solutions on poly (ethylene terephthalate) insulating films," *Polymer,* vol. 37, pp. 2465-2470, 1996.

[17] M. G. Pollack, R. B. Fair, and A. D. Shenderov, "Electrowetting-based actuation of liquid droplets for microfluidic applications," *Applied Physics Letters,* vol. 77, pp. 1725-1726, 2000.

[18]   S.-K. Fan, T.-H. Hsieh, and D.-Y. Lin, "General digital microfluidic platform manipulating dielectric and conductive droplets by dielectrophoresis and electrowetting," *Lab on a Chip,* vol. 9, pp. 1236-1242, 2009.

[19]   H. A. Pohl, "The motion and precipitation of suspensoids in divergent electric fields," *Journal of Applied Physics,* vol. 22, pp. 869-871, 1951.

[20]   M. Ahmadi Zeidabadi, "2D Liquid Lens Based on EWOD."

[21]   T. Young, "An essay on the cohesion of fluids," *Philosophical Transactions of the Royal Society of London,* pp. 65-87, 1805.

[22]   S. Chevalliot, "Advancing the Frontiers of Low Voltage Electrowetting on Dielectrics through a Complete Understanding of Three Phases System Interactions," University of Cincinnati, 2012.

[23]   B. Berge, "Electrocapillarité et mouillage de films isolants par l'eau," *Comptes rendus de l'Académie des sciences. Série 2, Mécanique, Physique, Chimie, Sciences de l'univers, Sciences de la Terre,* vol. 317, pp. 157-163, 1993.

[24]   F. Mugele, "Fundamental challenges in electrowetting: from equilibrium shapes to contact angle saturation and drop dynamics," *Soft Matter,* vol. 5, pp. 3377-3384, 2009.

[25]   S. Chevalliot, S. Kuiper, and J. Heikenfeld, "Experimental validation of the invariance of electrowetting contact angle saturation," *Journal of Adhesion Science and Technology,* vol. 26, pp. 1909-1930, 2012.

[26]   F. Mugele and J.-C. Baret, "Electrowetting: from basics to applications," *Journal of Physics: Condensed Matter,* vol. 17, p. R705, 2005.

[27]   H. Verheijen and M. Prins, "Reversible electrowetting and trapping of charge: model and experiments," *Langmuir,* vol. 15, pp. 6616-6620, 1999.

[28]   M. Vallet, M. Vallade, and B. Berge, "Limiting phenomena for the spreading of water on polymer films by electrowetting," *The European Physical Journal B-Condensed Matter and Complex Systems,* vol. 11, pp. 583-591, 1999.

[29]   M. Pollack, A. Shenderov, and R. Fair, "Electrowetting-based actuation of droplets for integrated microfluidics," *Lab Chip,* vol. 2, pp. 96-101, 2002.

[30]   S. K. Cho, H. Moon, and C.-J. Kim, "Creating, transporting, cutting, and merging liquid droplets by electrowetting-based actuation for digital microfluidic circuits," *Microelectromechanical Systems, Journal of,* vol. 12, pp. 70-80, 2003.

[31]   S. Kuiper and B. Hendriks, "Variable-focus liquid lens for miniature cameras," *Applied physics letters,* vol. 85, pp. 1128-1130, 2004.

[32]   V. Srinivasan, V. K. Pamula, and R. B. Fair, "An integrated digital microfluidic lab-on-a-chip for clinical diagnostics on human physiological fluids," *Lab on a Chip,* vol. 4, pp. 310-315, 2004.

[33]   P. Paik, V. K. Pamula, and R. B. Fair, "Rapid droplet mixers for digital microfluidic systems," *Lab on a Chip,* vol. 3, pp. 253-259, 2003.

[34]   D. G. Castner and B. D. Ratner, "Biomedical surface science: Foundations to frontiers," *Surface Science,* vol. 500, pp. 28-60, 2002.

[35]   J.-Y. Yoon and R. L. Garrell, "Preventing biomolecular adsorption in electrowetting-based biofluidic chips," *Analytical Chemistry,* vol. 75, pp. 5097-5102, 2003.

[36]   D. S. Ginger, H. Zhang, and C. A. Mirkin, "The Evolution of Dip‑Pen Nanolithography," *Angewandte Chemie International Edition,* vol. 43, pp. 30-45, 2004.

[37]   P. Belaubre, M. Guirardel, G. Garcia, J. Pourciel, V. Leberre, A. Dagkessamanskaia*, et al.*, "Fabrication of biological microarrays using microcantilevers," *Applied Physics Letters,* vol. 82, pp. 3122-3124, 2003.

[38]   D. Huh, A. H. Tkaczyk, J. H. Bahng, Y. Chang, H.-H. Wei, J. B. Grotberg*, et al.*, "Reversible switching of high-speed air-liquid two-phase flows using electrowetting-assisted flow-pattern change," *Journal of the American Chemical Society,* vol. 125, pp. 14678-14679, 2003.

[39]   J.-Y. Cheng and L.-C. Hsiung, "Electrowetting (EW)-based valve combined with hydrophilic Teflon microfluidic guidance in controlling continuous fluid flow," *Biomedical microdevices,* vol. 6, pp. 341-347, 2004.

[40]   T. Krupenkin, S. Yang, and P. Mach, "Tunable liquid microlens," *Applied Physics Letters,* vol. 82, pp. 316-318, 2003.

[41]   M. Kang and R. Yue, "Variable-focus liquid lens based on EWOD," *Journal of Adhesion Science and Technology,* vol. 26, pp. 1941-1946, 2012.

[42]   M. Im, K. Choi, D.-H. Kim, J.-H. Lee, J.-B. Yoon, and Y.-K. Choi, "Adhesion Force Change by Electrowetting on a Polymer Microlens Array," *Journal of Adhesion Science and Technology,* vol. 26, pp. 2079-2086, 2012.

[43]   T. Roques-Carmes, R. A. Hayes, B. Feenstra, and L. Schlangen, "Liquid behavior inside a reflective display pixel based on electrowetting," *Journal of applied physics,* vol. 95, pp. 4389-4396, 2004.

[44] H. You and A. Steckl, "Electrowetting on flexible substrates," *Journal of Adhesion Science and Technology,* vol. 26, pp. 1931-1939, 2012.

[45] E. C. Tam, "Smart electro-optical zoom lens," *Optics letters,* vol. 17, pp. 369-371, 1992.

[46] G. J. Woodgate and J. Harrold, "LP‑1: Late‑News Poster: High Efficiency Reconfigurable 2D/3D Autostereoscopic Display," in *SID symposium digest of technical papers*, 2003, pp. 394-397.

[47] S. Larcombe, J. Stern, P. Ivey, and N. Seed, "An ultra-miniature camera and processing system," in *Integrated Imaging Sensors and Processing, IEE Colloquium on*, 1994, pp. 4/1-4/6.

[48] E. I. Assia, "Accommodative intraocular lens: a challenge for future development," *Journal of Cataract & Refractive Surgery,* vol. 23, pp. 458-460, 1997.

[49] H. J. Tiziani, M. Wegner, and D. Steudle, "Confocal principle for macro-and microscopic surface and defect analysis," *Optical Engineering,* vol. 39, pp. 32-39, 2000.

[50] R. Völkel, M. Eisner, and K. Weible, "Miniaturized imaging systems," *Microelectronic Engineering,* vol. 67, pp. 461-472, 2003.

[51] M. Wakaki, Y. Komachi, and G. Kanai, "Microlenses and Microlens Arrays Formed on a Glass Plate by Use of a CO< sub> 2</sub> Laser," *Applied optics,* vol. 37, pp. 627-631, 1998.

[52] M. E. a. K. J. W. R. V¨olkel, "Miniaturized imaging systems," *Microelectron.. Eng,* vol. 67-68, pp. 461-472, 2003.

[53]   N. R. Smith, D. C. Abeysinghe, J. W. Haus, and J. Heikenfeld, "Agile wide-angle beam steering with electrowetting microprisms," *Optics Express,* vol. 14, pp. 6557-6563, 2006.

[54]   H. Okayama, "Design criterion for micro-machine scanner optical switch based on beam steering angle error analysis," *Optical Review,* vol. 8, pp. 294-300, 2001.

[55]   Y.-A. Peter, H.-P. Herzig, and R. Dandliker, "Microoptical fiber switch for a large number of interconnects: optical design considerations and experimental realizations using microlens arrays," *Selected Topics in Quantum Electronics, IEEE Journal of,* vol. 8, pp. 46-57, 2002.

[56]   R. Irawan, C. M. Tay, S. C. Tjin, and C. Y. Fu, "Compact fluorescence detection using in-fiber microchannels—its potential for lab-on-a-chip applications," *Lab on a chip,* vol. 6, pp. 1095-1098, 2006.

[57]   M. Yamauchi, M. Tokeshi, J. Yamaguchi, T. Fukuzawa, A. Hattori, A. Hibara*, et al.*, "Miniaturized thermal lens and fluorescence detection system for microchemical chips," *Journal of Chromatography A,* vol. 1106, pp. 89-93, 2006.

[58]   A. Tuantranont, V. Bright, J. Zhang, W. Zhang, J. Neff, and Y. Lee, "Optical beam steering using MEMS-controllable microlens array," *Sensors and Actuators A: Physical,* vol. 91, pp. 363-372, 2001.

[59]   H. Ren, Y.-H. Lin, and S.-T. Wu, "Flat polymeric microlens array," *Optics communications,* vol. 261, pp. 296-299, 2006.

[60]   G. F. Elliott and S. A. Hodson, "Cornea, and the swelling of polyelectrolyte gels of biological interest," *Reports on Progress in Physics,* vol. 61, p. 1325, 1998.

[61] W. S. Trimmer, "Microrobots and micromechanical systems," *Sensors and actuators,* vol. 19, pp. 267-287, 1989.

[62] D. Erickson, X. Heng, Z. Li, T. Rockwood, T. Emery, Z. Zhang*, et al.*, "Optofluidics," in *Optics & Photonics 2005*, 2005, pp. 59080S-59080S-12.

[63] D.-Y. Zhang, N. Justis, and Y.-H. Lo, "Fluidic adaptive zoom lens with high zoom ratio and widely tunable field of view," *Optics communications,* vol. 249, pp. 175-182, 2005.

[64] N.-T. Nguyen, "Micro-optofluidic Lenses: A review," *Biomicrofluidics,* vol. 4, p. 031501, 2010.

[65] C.-P. Chiu, T.-J. Chiang, J.-K. Chen, F.-C. Chang, F.-H. Ko, C.-W. Chu*, et al.*, "Liquid lenses and driving mechanisms: A review," *Journal of Adhesion Science and Technology,* vol. 26, pp. 1773-1788, 2012.

[66] K.-H. Jeong, G. Liu, N. Chronis, and L. Lee, "Tunable microdoublet lens array," *Optics Express,* vol. 12, pp. 2494-2500, 2004.

[67] H. Ren and S.-T. Wu, "Variable-focus liquid lens by changing aperture," *Applied Physics Letters,* vol. 86, p. 211107, 2005.

[68] S.-H. Ahn and Y.-K. Kim, "Proposal of human eye's crystalline lens-like variable focusing lens," *Sensors and Actuators A: Physical,* vol. 78, pp. 48-53, 1999.

[69] A. Werber and H. Zappe, "Tunable microfluidic microlenses," *Applied optics,* vol. 44, pp. 3238-3245, 2005.

[70] H. Ren, D. Fox, P. A. Anderson, B. Wu, and S.-T. Wu, "Tunable-focus liquid lens controlled using a servo motor," *Optics express,* vol. 14, pp. 8031-8036, 2006.

[71]   Y. Hongbin, Z. Guangya, C. F. Siong, L. Feiwen, and W. Shouhua, "A tunable Shack–Hartmann wavefront sensor based on a liquid-filled microlens array," *Journal of Micromechanics and Microengineering,* vol. 18, p. 105017, 2008.

[72]   H. Yu, G. Zhou, F. Chau, F. Lee, S. Wang, and H. Leung, "A liquid-filled tunable double-focus microlens," *Optics express,* vol. 17, pp. 4782-4790, 2009.

[73]   V. Lien, Y. Berdichevsky, and Y.-H. Lo, "Microspherical surfaces with predefined focal lengths fabricated using microfluidic capillaries," *Applied physics letters,* vol. 83, pp. 5563-5565, 2003.

[74]   J. Shi, Z. Stratton, S.-C. S. Lin, H. Huang, and T. J. Huang, "Tunable optofluidic microlens through active pressure control of an air–liquid interface," *Microfluidics and Nanofluidics,* vol. 9, pp. 313-318, 2010.

[75]   T. M. Squires and S. R. Quake, "Microfluidics: Fluid physics at the nanoliter scale," *Reviews of modern physics,* vol. 77, p. 977, 2005.

[76]   G. M. Whitesides, "The origins and the future of microfluidics," *Nature,* vol. 442, pp. 368-373, 2006.

[77]   H. Craighead, "Future lab-on-a-chip technologies for interrogating individual molecules," *Nature,* vol. 442, pp. 387-393, 2006.

[78]   S.-K. Fan, W.-J. Chen, T.-H. Lin, T.-T. Wang, and Y.-C. Lin, "Reconfigurable liquid pumping in electric-field-defined virtual microchannels by dielectrophoresis," *Lab on a Chip,* vol. 9, pp. 1590-1595, 2009.

[79]   S. K. Tang, C. A. Stan, and G. M. Whitesides, "Dynamically reconfigurable liquid-core liquid-cladding lens in a microfluidic channel," *Lab on a Chip,* vol. 8, pp. 395-401, 2008.

[80]   U.-C. Yi and C.-J. Kim, "Characterization of electrowetting actuation on addressable single-side coplanar electrodes," *Journal of Micromechanics and Microengineering,* vol. 16, p. 2053, 2006.

[81]   S.-K. Fan, H. Yang, and W. Hsu, "Droplet-on-a-wristband: Chip-to-chip digital microfluidic interfaces between replaceable and flexible electrowetting modules," *Lab on a Chip,* vol. 11, pp. 343-347, 2011.

[82]   J. Gong, "All-electronic droplet generation on-chip with real-time feedback control for EWOD digital microfluidics," *Lab on a Chip,* vol. 8, pp. 898-906, 2008.

[83]   J. A. Schwartz, J. V. Vykoukal, and P. R. Gascoyne, "Droplet-based chemistry on a programmable micro-chip," *Lab on a Chip,* vol. 4, pp. 11-17, 2004.

[84]   O. D. Velev, B. G. Prevo, and K. H. Bhatt, "On-chip manipulation of free droplets," *Nature,* vol. 426, pp. 515-516, 2003.

[85]   C.-C. Cheng and J. A. Yeh, "Dielectrically actuated liquid lens," *Optics Express,* vol. 15, pp. 7140-7145, 2007.

[86]   C.-C. Cheng, C. A. Chang, and J. A. Yeh, "Variable focus dielectric liquid droplet lens," *Optics Express,* vol. 14, pp. 4101-4106, 2006.

[87]   S.-K. Fan, P.-W. Huang, T.-T. Wang, and Y.-H. Peng, "Cross-scale electric manipulations of cells and droplets by frequency-modulated dielectrophoresis and electrowetting," *Lab on a Chip,* vol. 8, pp. 1325-1331, 2008.

[88]   F. Gindele, F. Gaul, and T. Kolling, "Optical systems based on electrowetting," in *Photonics Europe*, 2004, pp. 89-100.

[89]   Z. Wan, H. Zeng, and A. Feinerman, "Area-tunable micromirror based on electrowetting actuation of liquid-metal droplets," *Applied physics letters,* vol. 89, p. 201107, 2006.

[90]   S. W. Lee and S. S. Lee, "Focal tunable liquid lens integrated with an electromagnetic actuator," *Applied physics letters,* vol. 90, p. 121129, 2007.

[91]   J.-Y. Lee, S.-T. Choi, S.-W. Lee, and W. Kim, "Microfluidic design and fabrication of wafer-scale varifocal liquid lens," in *SPIE Optical Engineering+ Applications*, 2009, pp. 742603-742603-11.

[92]   S. T. Choi, J. Y. Lee, J. O. Kwon, S. Lee, and W. Kim, "Liquid-filled varifocal lens on a chip," in *SPIE MOEMS-MEMS: Micro-and Nanofabrication*, 2009, pp. 72080P-72080P-9.

[93]   C. A. López, C.-C. Lee, and A. H. Hirsa, "Electrochemically activated adaptive liquid lens," *Applied Physics Letters,* vol. 87, p. 134102, 2005.

[94]   C.-X. Liu, J. Park, and J.-W. Choi, "A planar lens based on the electrowetting of two immiscible liquids," *Journal of Micromechanics and Microengineering,* vol. 18, p. 035023, 2008.

[95]   J. Y. An, J. H. Hur, S. Kim, and J. H. Lee, "Spherically encapsulated variable liquid lens on coplanar electrodes," *Photonics Technology Letters, IEEE,* vol. 23, pp. 1703-1705, 2011.

[96]   B. Berge, "Liquid lens technology: principle of electrowetting based lenses and applications to imaging," in *Micro Electro Mechanical Systems, 2005. MEMS 2005. 18th IEEE International Conference on*, 2005, pp. 227-230.

[97]   C. Li and H. Jiang, "Electrowetting-driven variable-focus microlens on flexible surfaces," *Applied physics letters,* vol. 100, p. 231105, 2012.

[98]   S.-B. Huang, M.-H. Wu, Y.-H. Lin, C.-H. Hsieh, C.-L. Yang, H.-C. Lin*, et al.*, "High-purity and label-free isolation of circulating tumor cells (CTCs) in a microfluidic platform by using optically-induced-dielectrophoretic (ODEP) force," *Lab on a Chip,* vol. 13, pp. 1371-1383, 2013.

[99]   L. Yu, S. R. Ng, Y. Xu, H. Dong, Y. J. Wang, and C. M. Li, "Advances of lab-on-a-chip in isolation, detection and post-processing of circulating tumour cells," *Lab on a Chip,* vol. 13, pp. 3163-3182, 2013.

[100]   J. H. Kang, S. Krause, H. Tobin, A. Mammoto, M. Kanapathipillai, and D. E. Ingber, "A combined micromagnetic-microfluidic device for rapid capture and culture of rare circulating tumor cells," *Lab on a Chip,* vol. 12, pp. 2175-2181, 2012.

[101]   S. N. Bhatia and D. E. Ingber, "Microfluidic organs-on-chips," *Nature biotechnology,* 2014.

[102]   A. Agarwal, J. A. Goss, A. Cho, M. L. McCain, and K. K. Parker, "Microfluidic heart on a chip for higher throughput pharmacological studies," *Lab on a Chip,* vol. 13, pp. 3599-3608, 2013.

[103]   D. Huh, B. D. Matthews, A. Mammoto, M. Montoya-Zavala, H. Y. Hsin, and D. E. Ingber, "Reconstituting organ-level lung functions on a chip," *Science,* vol. 328, pp. 1662-1668, 2010.

[104]   D. Huh, Y.-s. Torisawa, G. A. Hamilton, H. J. Kim, and D. E. Ingber, "Microengineered physiological biomimicry: organs-on-chips," *Lab on a chip,* vol. 12, pp. 2156-2164, 2012.

[105]   P. S. Dittrich and A. Manz, "Lab-on-a-chip: microfluidics in drug discovery," *Nature Reviews Drug Discovery,* vol. 5, pp. 210-218, 2006.

[106]   Q. Hamid, C. Wang, Y. Zhao, J. Snyder, and W. Sun, "A three-dimensional cell-laden microfluidic chip for in vitro drug metabolism detection," *Biofabrication,* vol. 6, p. 025008, 2014.

[107]   M. A. Unger, H.-P. Chou, T. Thorsen, A. Scherer, and S. R. Quake, "Monolithic microfabricated valves and pumps by multilayer soft lithography," *Science,* vol. 288, pp. 113-116, 2000.

[108]   F. Krogmann, W. Moench, and H. Zappe, "A MEMS-based variable micro-lens system," *Journal of Optics A: Pure and Applied Optics,* vol. 8, p. S330, 2006.

[109]   N. R. Smith, L. Hou, J. Zhang, and J. Heikenfeld, "Fabrication and demonstration of electrowetting liquid lens arrays," *Journal of Display Technology,* vol. 5, pp. 411-413, 2009.

[110]   X. Tan, Z. Zhou, and M. M.-C. Cheng, "Electrowetting on dielectric experiments using graphene," *Nanotechnology,* vol. 23, p. 375501, 2012.

[111]   X. Tan, J. Yang, P. Zeng, E. Kim, C. Huard, and M. Cheng, "Electrowetting on flexible, transparent and conducting single-layer graphene," in *Micro Electro Mechanical Systems (MEMS), 2012 IEEE 25th International Conference on*, 2012, pp. 1037-1040.

[112] E. Hecht, "Optics 2nd edition," *Optics 2nd edition by Eugene Hecht Reading, MA: Addison-Wesley Publishing Company, 1987,* vol. 1, 1987.

[113]   X. Li, W. Cai, J. An, S. Kim, J. Nah, D. Yang*, et al.*, "Large-area synthesis of high-quality and uniform graphene films on copper foils," *Science,* vol. 324, pp. 1312-1314, 2009.

[114]   G. K. Batchelor, *An introduction to fluid dynamics*: Cambridge university press, 2000.

[115]   Y. Wang and Y.-P. Zhao, "Electrowetting on curved surfaces," *Soft Matter,* vol. 8, pp. 2599-2606, 2012.

[116]   T. Sato, G. Masuda, and K. Takagi, "Electrochemical properties of novel ionic liquids for electric double layer capacitor applications," *Electrochimica Acta,* vol. 49, pp. 3603-3611, 2004.

[117]   S. Zhang, N. Sun, X. He, X. Lu, and X. Zhang, "Physical properties of ionic liquids: database and evaluation," *Journal of physical and chemical reference data,* vol. 35, pp. 1475-1517, 2006.

[118] P. Kilaru, G. A. Baker, and P. Scovazzo, "Density and surface tension measurements of imidazolium-, quaternary phosphonium-, and ammonium-based room-temperature ionic liquids: data and correlations," *Journal of Chemical & Engineering Data,* vol. 52, pp. 2306-2314, 2007.

[119]   C.-H. Chen, S.-L. Tsai, M.-K. Chen, and L.-S. Jang, "Effects of gap height, applied frequency, and fluid conductivity on minimum actuation voltage of electrowetting-on-dielectric and liquid dielectrophoresis," *Sensors and Actuators B: Chemical,* vol. 159, pp. 321-327, 2011.

[120]   W. Pratt, "Proposed new electrolytic conductivity primary standards for KCl solutions," *J. Res. Natl. Inst. Stand. Technol,* vol. 96, pp. 191-201, 1991.

[121]   L. Gao and T. J. McCarthy, "Contact angle hysteresis explained," *Langmuir,* vol. 22, pp. 6234-6237, 2006.

[122]   A. Quinn, R. Sedev, and J. Ralston, "Contact angle saturation in electrowetting," *The journal of physical chemistry B,* vol. 109, pp. 6268-6275, 2005.

[123]   N. Binh-Khiem, K. Matsumoto, and I. Shimoyama, "Polymer thin film deposited on liquid for varifocal encapsulated liquid lenses," *Applied Physics Letters,* vol. 93, p. 124101, 2008.

[124]   M. Kim, D. Kang, T. Wu, N. Tabatabaei, R. W. Carruth, R. V. Martinez*, et al.*, "Miniature objective lens with variable focus for confocal endomicroscopy," *Biomedical optics express,* vol. 5, pp. 4350-4361, 2014.

[125]   A. Kuzmenko, E. Van Heumen, F. Carbone, and D. Van Der Marel, "Universal optical conductance of graphite," *Physical review letters,* vol. 100, p. 117401, 2008.

[126]   L. Hu, G. Gruner, J. Gong, and B. Hornbostel, "Electrowetting devices with transparent single-walled carbon nanotube electrodes," *Applied Physics Letters,* vol. 90, p. 093124, 2007.

[127]   J. Beermann, T. Søndergaard, S. M. Novikov, S. I. Bozhevolnyi, E. Devaux, and T. W. Ebbesen, "Field enhancement and extraordinary optical transmission by tapered periodic slits in gold films," *New Journal of Physics,* vol. 13, p. 063029, 2011.

[128]   K. S. Novoselov, A. K. Geim, S. Morozov, D. Jiang, Y. Zhang, S. Dubonos*, et al.*, "Electric field effect in atomically thin carbon films," *science,* vol. 306, pp. 666-669, 2004.

[129]   G. Elert, "The physics hypertextbook," *Online at http://hypertextbook. com/physics/about. shtml,* 2006.

[130]   C. Granqvist and A. Hultåker, "Transparent and conducting ITO films: new developments and applications," *Thin solid films,* vol. 411, pp. 1-5, 2002.

[131]   R. Dudley, *The biomechanics of insect flight: form, function, evolution*: Princeton University Press, 2002.

[132]   E. Warrant and D.-E. Nilsson, *Invertebrate vision*: Cambridge University Press, 2006.

[133]   L. Li and Y. Y. Allen, "Development of a 3D artificial compound eye," *Optics express,* vol. 18, pp. 18125-18137, 2010.

[134]   Y. M. Song, Y. Xie, V. Malyarchuk, J. Xiao, I. Jung, K.-J. Choi*, et al.*, "Digital cameras with designs inspired by the arthropod eye," *Nature,* vol. 497, pp. 95-99, 2013.

[135]   Z. Li and J. Xiao, "Mechanics and optics of stretchable elastomeric microlens array for artificial compound eye camera," *Journal of Applied Physics,* vol. 117, p. 014904, 2015.

[136] D. Floreano, R. Pericet-Camara, S. Viollet, F. Ruffier, A. Brückner, R. Leitel, *et al.*, "Miniature curved artificial compound eyes," *Proceedings of the National Academy of Sciences,* vol. 110, pp. 9267-9272, 2013.

[137] K.-H. Jeong, J. Kim, and L. P. Lee, "Biologically inspired artificial compound eyes," *Science,* vol. 312, pp. 557-561, 2006.

[138] D. Radtke, J. Duparré, U. D. Zeitner, and A. Tünnermann, "Laser lithographic fabrication and characterization of a spherical artificial compound eye," *Optics express,* vol. 15, pp. 3067-3077, 2007.

[139] B. Hendriks, S. Kuiper, M. V. As, C. Renders, and T. Tukker, "Electrowetting-based variable-focus lens for miniature systems," *Optical review,* vol. 12, pp. 255-259, 2005.

[140] W. L. Wolfe, *Optics made clear: the nature of light and how we use it* vol. 163: SPIE Press, 2007.

[141] K. Wei and Y. Zhao, "A three-dimensional deformable liquid lens array for directional and wide angle laparoscopic imaging," in *Micro Electro Mechanical Systems (MEMS), 2013 IEEE 26th International Conference on*, 2013, pp. 133-136.

[142] D. Zhu, X. Zeng, C. Li, and H. Jiang, "Focus-tunable microlens arrays fabricated on spherical surfaces," *Microelectromechanical Systems, Journal of,* vol. 20, pp. 389-395, 2011.

[143] A. Shahini, P. Zeng, Y. Zhao, and M. M.-C. Cheng, "Individually tunable liquid lens arrays using transparent graphene for compound eye applications," in *2016 IEEE*

29th International Conference on Micro Electro Mechanical Systems (MEMS), 2016, pp. 597-600.

[144]   A. Shahini, J. Xia, Z. Zhou, Y. Zhao, and M. M.-C. Cheng, "Versatile Miniature Tunable Liquid Lenses Using Transparent Graphene Electrodes," *Langmuir,* vol. 32, pp. 1658-1665, 2016.

[145]   M. Armand, F. Endres, D. R. MacFarlane, H. Ohno, and B. Scrosati, "Ionic-liquid materials for the electrochemical challenges of the future," *Nature materials,* vol. 8, pp. 621-629, 2009.

[146]   B. Garcia, S. Lavallée, G. Perron, C. Michot, and M. Armand, "Room temperature molten salts as lithium battery electrolyte," *Electrochimica Acta,* vol. 49, pp. 4583-4588, 2004.

[147]   O. N. Starovoytov, H. Torabifard, and G. A. s. Cisneros, "Development of amoeba force field for 1, 3-dimethylimidazolium based ionic liquids," *The Journal of Physical Chemistry B,* vol. 118, pp. 7156-7166, 2014.

[148]   P. M. Moran, S. Dharmatilleke, A. H. Khaw, K. W. Tan, M. L. Chan, and I. Rodriguez, "Fluidic lenses with variable focal length," *Applied Physics Letters,* vol. 88, p. 041120, 2006.

[149]   P. Liebetraut, S. Petsch, J. Liebeskind, and H. Zappe, "Elastomeric lenses with tunable astigmatism," *Light: Science & Applications,* vol. 2, p. e98, 2013.

[150]   S. Shian, R. M. Diebold, and D. R. Clarke, "Tunable lenses using transparent dielectric elastomer actuators," *Optics express,* vol. 21, pp. 8669-8676, 2013.

[151] B.-K. Nguyen, E. Iwase, K. Matsumoto, and I. Shimoyama, "Electrically driven varifocal micro lens fabricated by depositing parylene directly on liquid," in *Micro Electro Mechanical Systems, 2007. MEMS. IEEE 20th International Conference on*, 2007, pp. 305-308.

[152] L. Dong, A. K. Agarwal, D. J. Beebe, and H. Jiang, "Variable-focus liquid microlenses and microlens arrays actuated by thermoresponsive hydrogels," *ADVANCED MATERIALS-DEERFIELD BEACH THEN WEINHEIM-,* vol. 19, p. 401, 2007.

[153] C. Murade, D. Van Der Ende, and F. Mugele, "High speed adaptive liquid microlens array," *Optics express,* vol. 20, pp. 18180-18187, 2012.

[154] H. Huang, P.-Y. Chen, C.-H. Hung, R. Gharpurey, and D. Akinwande, "A zero power harmonic transponder sensor for ubiquitous wireless μL liquid-volume monitoring," *Scientific reports,* vol. 6, 2016.

[155] F. Schedin, A. Geim, S. Morozov, E. Hill, P. Blake, M. Katsnelson*, et al.*, "Detection of individual gas molecules adsorbed on graphene," *Nature materials,* vol. 6, pp. 652-655, 2007.

[156] H. Wang, D. Nezich, J. Kong, and T. Palacios, "Graphene frequency multipliers," *IEEE Electron Device Letters,* vol. 30, pp. 547-549, 2009.

[157] H. Huang, L. Tao, F. Liu, L. Ji, Y. Hu, M. M.-C. Cheng*, et al.*, "Chemical-sensitive graphene modulator with a memory effect for internet-of-things applications," *Microsystems & Nanoengineering,* vol. 2, 2016.

[158] H. Wang, A. Hsu, K. K. Kim, J. Kong, and T. Palacios, "Gigahertz ambipolar frequency multiplier based on CVD graphene," in *Electron Devices Meeting (IEDM), 2010 IEEE International*, 2010, pp. 23.6. 1-23.6. 4.

[159] P.-Y. Chen and A. Alù, "Atomically thin surface cloak using graphene monolayers," *ACS nano,* vol. 5, pp. 5855-5863, 2011.

[160] P.-Y. Chen, C. Argyropoulos, and A. Alu, "Terahertz antenna phase shifters using integrally-gated graphene transmission-lines," *IEEE Transactions on Antennas and Propagation,* vol. 61, pp. 1528-1537, 2013.

ABSTRACT

ACTUATION OF DROPLETS USING TRANSPARENT GRAPHENE ELECTRODES FOR TUNABLE LENSES AND BIOMEDICAL APPLICATIONS

by

ALI SHAHINI

December 2016

Advisor: Dr. Mark. Ming-Cheng Cheng

Major: Electrical Engineering

Degree: Doctor of Philosophy

Variable focal length liquid microlenses are the next candidate for a wide variety of applications. Driving mechanism of the liquid lenses can be categorized into mechanical and electrical actuation. Among different actuation mechanisms, EWOD is the most common tool for actuation of the liquid lenses. In this dissertation, we have demonstrated versatile and low-cost miniature liquid lenses with graphene as electrodes. Tunable focal length is achieved by changing both curvature of the droplet using electrowetting on dielectric (EWOD) and applied pressure. Ionic liquid and KCl solution are utilized as lens liquid on the top of a flexible Teflon-coated PDMS/parylene membrane. Transparent and flexible, graphene allows transmission of visible light as well as large deformation of the polymer membrane to achieve requirements for different lens designs and to increase the field of view without damaging of electrodes. Another advantage of graphene compared to non-transparent electrodes is the larger lens aperture. The tunable range for the focal

length is between 3 and 7 mm for a droplet with a volume of 3 μL. The visualization of bone marrow dendritic cells is demonstrated by the liquid lens system with a high resolution (more than 456 lp/mm). The Spherical aberration analysis is performed using COMSOL software to investigate the optical properties of the lens under applied voltages and pressure. We propose a prototype of compound eye with specific design of the electrodes using both tunable lenses and tunable supporting membrane. The design has many advantages including large field of view, compact size and fast response time. This work maybe applicable in the development of the next generation of cameras, endoscopes, cell phones on flexible platform. We also proposed here the design and concept of self-powered wireless sensor based on the graphene radio-frequency (RF) components, which are transparent, flexible, and monolithically integrated on biocompatible soft substrate. We show that a quad-ring circuit based on graphene transistors may simultaneously offer sensing and frequency modulation functions. This battery-free and transparent sensors based on newly discovered 2D nanomaterials may benefit versatile wireless sensing and internet-of-things applications, such as smart contact lenses/glasses and microscope slides.

AUTOBIOGRAPHICAL STATEMENT

ALI SHAHINI

Education

2012-2016 Doctor of Philosophy, Electrical Engineering, Wayne State University, Detroit, MI, USA

2008-2011 Master Degree in Nanotechnology Engineering, University of Tabriz, Tabriz, Iran.

2002-2007 Bachelor Degree in Electrical Engineering, University of Tabriz, Tabriz, Iran.

Honors and Awards

2016~Best paper award, IEEE SENSORS 2016.

2012~Iranian Nanotechnology Initiative Council Award For M.Sc. Thesis.

Selected Publications

1. **A. Shahini,** J. Xia, Z. Zhou, Y. Zhao and M. M. C. Cheng, "Versatile Miniature Tunable Liquid Lenses Using Transparent Graphene Electrodes," Langmuir, 2016.

2. **A. Shahini,** P. Zheng, Y. Zhao and M. M. C. Cheng, "Individually Tunable Liquid Lens Arrays Using Transparent Graphene for Compound Eye Applications," The 29th IEEE International Conference on Micro Electro Mechanical Systems (MEMS) 2016.

3. H. Huang, M. Sakhdari, M. Hajizadegan, **A. Shahini**, D. Akinwande, P-Y. Chen, "Toward Transparent and Self-Activated Graphene Harmonic Transponder Sensors," Applied Physics Letters, 2016.

4. **A. Shahini**, M. Hajizadegan, M. Sakhdari, H. Huang, M. M. C. Cheng and P-Y. Chen, "Self-Powered and Transparent All Graphene BioSensors," Accepted, IEEE SENSORS 2016.

5. **A. Shahini**, Z. Zhou, Y. Zhao and M. M. C. Cheng, "Toward all graphene individually tunable compound eyes," Submitted, Applied Physics Letters, 2016.